Gesellschaft für Anlagen- und Reaktorsicherheit (GRS) mbH

Modelling of Corrosion-Induced Processes in Emplacement Boreholes and Drifts

GRS - 232

Gesellschaft für Anlagen- und Reaktorsicherheit (GRS) mbH

Modelling of Corrosion-Induced Processes in Emplacement Boreholes and Drifts

Rolf-Peter Hirsekorn
Dirk-Alexander Becker

March 2008

Remark:

This report was prepared under the contract No. 02 E 9844 with the Bundesministerium für Wirtschaft und Technologie (BMWi) and under contract No. FI6W-CT-2003-02389.

The work was conducted by the Gesellschaft für Anlagen- und Reaktorsicherheit (GRS) mbH.

The authors are responsible for the content of this report.

GRS - 232
ISBN 978-3-939355-06-9

Deskriptoren:
Blockade, Endlager, EU, Gas, Geomechanik, Gestein, Grundwasser, Internationale Zusammenarbeit, Labor, Modell, Permeabilität

Kurzfassung

Es gibt eine Anzahl verschiedener physikalischer und chemischer Effekte, die im Nahfeld eines untertägigen Endlagers mit Stahlbehältern auftreten können. Solche Behälter korrodieren unter dem Einfluss von Feuchtigkeit sowohl in Anwesenheit als auch in Abwesenheit von gasförmigem Sauerstoff. Während bei einer Tonformation die Wiederaufsättigung des Wirtsgesteins mit Wasser die normale Entwicklung darstellt, wird von einem Endlager im Salz erwartet, dass es trocken bleibt. Ein Lösungszutritt kann jedoch auch hier nicht völlig ausgeschlossen werden. Darüber hinaus gibt es immer eine gewisse Restfeuchte im Salzversatz. Deshalb sollte angenommen werden, dass in allen Fällen genügend Wasser für die Eisenkorrosion verfügbar ist.

Es gibt zwei Arten von Eisenkorrosion. Der aerobe Eisenkorrosionsprozess läuft in Anwesenheit von Wasser ab, ohne dieses zu verbrauchen. Bei der anaeroben Eisenkorrosion wird Wasser verbraucht und Wasserstoffgas erzeugt, dabei entsteht Magnetit.

Korrosionsprozesse können einen mechanischen Einfluss auf das umgebende Gestein ausüben, da sich die Volumina der Korrosionsprodukte von denen der Ausgangssubstanzen unterscheiden und außerdem eine beträchtliche Menge Gas produziert wird. Dadurch können hohe Drücke im Porenraum des Versatzes in der Nähe der Behälter entstehen. Das entstehende Gas kann Flüssigkeiten aus dem Nahbereich verdrängen und diesen schließlich selbst verlassen. Im Salzgestein gibt es zusätzlich den Effekt der Konvergenz, der zu einer Reduktion des Porenraums im Versatz und weiterer Lösungsverdrängung führt. Es ist möglich, dass die Korrosion zum Stillstand kommt, weil das verfügbare Wasser verbraucht ist und aufgrund zu geringer Porosität in der Umgebung der Behälter auch nicht ersetzt werden kann. In diesem Fall werden die Behälter vollständig eingeschlossen und isoliert.

Die folgenden miteinander wechselwirkenden Effekte, die durch Korrosion verursacht werden und einen erheblichen Einfluss auf die weitere Systementwicklung haben können, werden in diesem Bericht betrachtet:

- Gaserzeugung: Durch anaerobe Eisenkorrosion wird Wasserstoffgas erzeugt. Es kann Wasser oder Lösung aus den Hohlräumen im Behälter oder den Porenräumen im Versatz verdrängen. Der Gasdruck kann hohe Werte erreichen und die mechanische Entwicklung des Systems beeinflussen.

- Wasserverbrauch: Im Gegensatz zur aeroben Korrosion wird bei der anaeroben Korrosion Wasser verbraucht. Dies kann dazu führen, dass Flüssigkeit aus anderen Bereichen nachfließt.

- Salzausfällung: Wenn das Wasser gelöste Stoffe enthält, werden diese beim korrosionsbedingten Wasserverbrauch ausgefällt. Daraus kann eine Reduktion der Versatzporosität in den Einlagerungsbereichen resultieren. Der Effekt ist besonders bei Endlagern im Salz von Interesse, weil die dort auftretende Flüssigkeit normalerweise gesättigte NaCl-Lösung ist.

- Volumenzunahme fester Substanzen: Bei der anaeroben Korrosion wird Eisen in Magnetit umgewandelt, der ein größeres Volumen einnimmt als das ursprüngliche Eisen. Hieraus kann eine Reduktion des Porenraums resultieren und den Druck im Einlagerungsort beeinflussen.

Die genannten Nahfeldprozesse sind gekoppelt. Im Rahmen der hier beschriebenen Arbeiten wurden sie durch Modellrechnungen in drei Schritten untersucht. Im ersten Schritt werden Massen- und Volumenbilanzen ohne Berücksichtigung der Zeitabhängigkeit und der Kopplungen zwischen den Prozessen betrachtet. Zwei vereinfachte Einlagerungskonzepte werden untersucht, die Bohrloch- und die Streckenlagerung von Behältern für abgebrannte Brennelemente. Sowohl Steinsalz- als auch Tonformationen werden dabei betrachtet. Im zweiten Schritt wird ein numerisches Modell vorgestellt, welches eine Berechnung der Zeitentwicklung eines Einlagerungsbohrlochs oder einer Einlagerungsstrecke erlaubt. Das Modell wurde in das Nahfeldmodul LOPOS integriert, das zum Programmpaket EMOS für integrierte Langzeitsicherheitsanalysen gehört. Es wurde auf die gleichen einfachen Strukturen angewandt, die im ersten Schritt betrachtet worden sind. Die Ergebnisse beider Untersuchungen wurden verglichen und gegeneinander verifiziert. Im dritten Schritt wird das Modell auf eine komplexere generische Endlagerstruktur im Steinsalz angewandt.

Die in diesem Bericht beschriebenen Arbeiten wurden im Rahmen des europäischen Forschungsprojekts NF-PRO durchgeführt und von der Europäischen Kommission sowie vom Bundesministerium für Wirtschaft und Technologie gefördert.

Abstract

There are a number of physical and chemical effects occurring in the near field of an underground repository with steel containers. Such containers tend to corrode under the influence of humidity, both in the presence and the absence of gaseous oxygen. While in clay the re-saturation of the host rock with liquid water is the normal evolution, a repository in salt is expected to remain dry, but a brine intrusion can never be completely ruled out. Moreover, there is always some residual humidity in the salt backfill. Therefore, it should be assumed, that in all cases there is enough water available for corrosion.

There are two kinds of iron corrosion. The aerobic iron corrosion process in the presence of elementary oxygen requires the presence of water without consuming it. The anaerobic iron corrosion process consumes water and produces hydrogen gas, transforming iron to magnetite.

Corrosion processes may exert a mechanical impact to the surrounding environment since the volumes of the corrosion products are different from those of the original substances and a considerable amount of gas is produced. This can lead to a high pressure in the pore space around the containers. The gas can also displace liquids from the near field and finally escape itself. In salt host rock, there is additionally the effect of convergence by creep which leads to a reduction of the pore space within the backfill and further brine displacement. It is possible that the corrosion stops because the available water is exhausted and cannot be replaced due to lack of void space near the canisters. In this case the canisters are totally included and isolated.

The following interacting corrosion-induced effects, which can have an essential influence on the further evolution of the system, are considered in this report:

- Gas production: Hydrogen gas is generated by iron corrosion. It can displace water or brine from void volumes inside the canister or from pores in the backfill. The gas pressure can reach considerable values and influence the mechanical evolution of the system.

- Water consumption: As opposed to the aerobic corrosion, the anaerobic corrosion does not only require the presence of water but also consumes it. This may lead to the possibility of water being replenished.

- Salt precipitation: If the water contains solutes, these are precipitated when water is consumed by corrosion. A consequence of this may be the reduction of backfill porosity. This effect is of specific interest in the case of a repository in rock salt, where the fluid is normally expected to be saturated NaCl solution.

- Solid volume increase: During anaerobic corrosion, iron is transformed to magnetite which has a lower density and occupies a higher volume than the original iron. This can lead to a reduction of pore space, which has an effect on the fluid pressure inside the borehole or drift.

The mentioned near field effects are coupled. In the work described here, they have been investigated by means of model calculations in three steps. In the first step, total mass and volume balances are considered without taking account of the time dependence of the processes and their various couplings. Two simplified disposal concepts are considered, borehole and drift disposal of Spent Fuel canisters. Both rock salt and clay formations are taken into account. In the second step a numerical model is described that allows one to calculate the time-development of a disposal borehole or drift in rock salt under consideration of all of the mentioned processes. The model is implemented in the LOPOS code, which is part of the EMOS package for integrated performance assessment, and applied to the same simplified model structures that have been investigated in the first step. The results are compared with those of the first step in order to verify both approaches against each other. In the third step the model applied to a more complex generic repository structure in rock salt.

The work described in this report was performed in the context of the European research project NF-PRO and funded by the European Commission as well as by the German Federal Ministry for Economics and Technology.

Contents

1 Mass and volume balances

In this chapter the first step of investigations, consisting of estimations of total mass and volume balances in the disposal boreholes or drifts is described and some conclusions are drawn that can be used as a basis for the further steps.

1.1 Disposal concepts

1.1.1 Concept-independent aspects

For both host rock formations considered here, borehole disposal is contemplated as well as drift disposal. The general approach to these two ways of disposal is independent of the host rock: lightweight SF containers are piled up in vertical boreholes, large and heavy containers are emplaced in a row parallel to the drift axis. The geometric dimensions of the waste containers in question are compiled in Tab. 1.1. Access galleries and disposal drifts will be excavated at about 500 m depth. For the salt case it is assumed that there are 300 m of rock salt above the repository. Therefore, the fluid column above the repository near field is 500 m of fresh water in clay, but 200 m of water plus 300 m of NaCl brine in salt. With the density of NaCl saturated brine being 1193 kg/m^3, the hydrostatic pressure at the depth of 500 m can be calculated to be 5.47 MPa, while in clay it is only 4.91 MPa.

Tab. 1.1 SF Container data

	Pollux	BSK3-BE
Outer length [m]	6.0	4.9
Inner length [m]		4.8
Outer diameter [m]	1.583	0.43
Inner diameter [m]	1.275	0.37
Steel mass (including container contents) [kg]	60000	1544
Void volume [m^3]	3.0	0.15

1.1.2 Borehole disposal

The disposal boreholes in salt are envisaged to be about 300 m deep with a diameter of 0.6 m. BSK-3-BE containers will be used for storage. The annulus between the borehole wall and the containers will be filled with crushed salt. Along with the fast convergence of the heated rock salt this limits the weight load of the canister column on the lower canisters. In order to redistribute the weight load even further, stacks of a not yet specified number of canisters may be separated by a larger layer of crushed salt. The borehole seal has a length of about 10 m and consists of crushed salt, too. Cementitious material will not be used in the borehole.

Disposal boreholes in clay stone will have the same diameter as in rock salt but the depth will be only some 50 m. The same types of containers with the same geometrical dimensions will be used. Due to temperature limitations less fuel rods per container are foreseen and the containers will be placed with more clearance than in the borehole disposal concept for rock salt. The space between containers is about 0.4 m in rock salt and 8.0 m in clay. Fig. 1.1 shows a simplified borehole concept which is used for the estimations and calculations in this report. Where values for the clay concept differ from those for the salt concept, they are given in parentheses.

1.1.3 Drift disposal

The large and heavy Pollux containers for spent fuel will be brought into the drift by rail-based vehicles and finally lowered between the rails. The drifts in rock salt have a length of about 250 m and a cross-section of 15 m^2, each offering space for 20 Pollux casks. The distance between drifts is 28 m. The remaining space between container and drift wall will be completely filled with blown-in crushed salt. A lining of the drift is not envisaged.

Drifts in clay, however, will be supported by concrete and steel lining. Due to temperature reasons, the distance between the containers has to be larger than in salt, therefore, the drift distance is 40 m and only 8 Pollux casks are foreseen to be emplaced in a 250-m drift. Blocks of highly compacted bentonite installed at the bottom will bear the weight of the waste containers. The backfill consists of bentonite powder, bentonite pellets or bentonite-sand mixtures. Fig. 1.2 shows the simplified drift disposal concept used in this report. Again, values in parentheses refer to the clay concept.

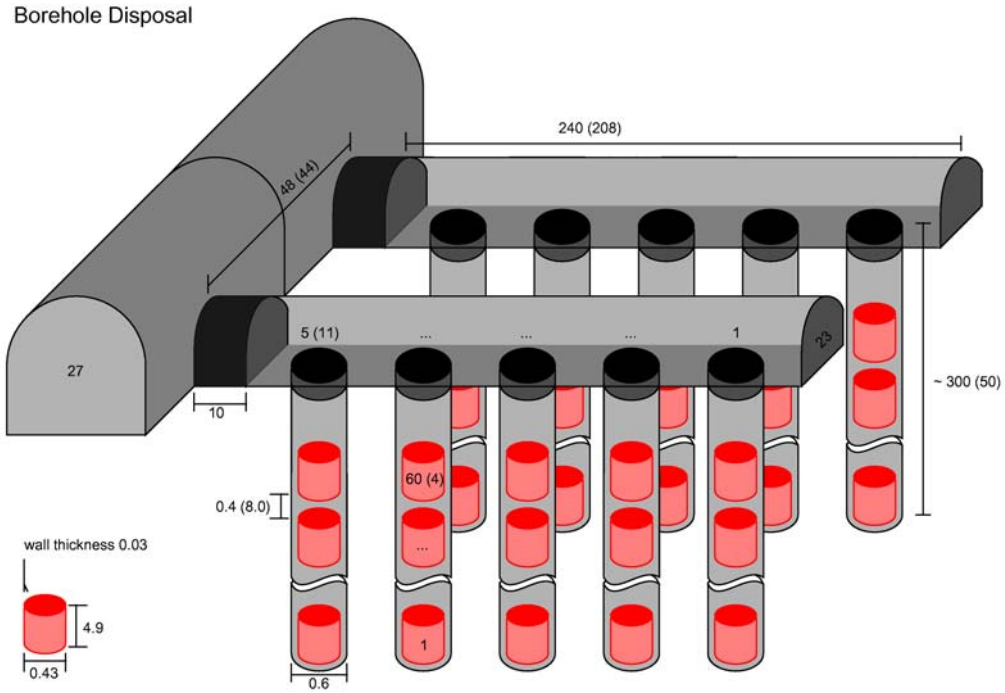

Fig. 1.1 Simplified borehole disposal concept

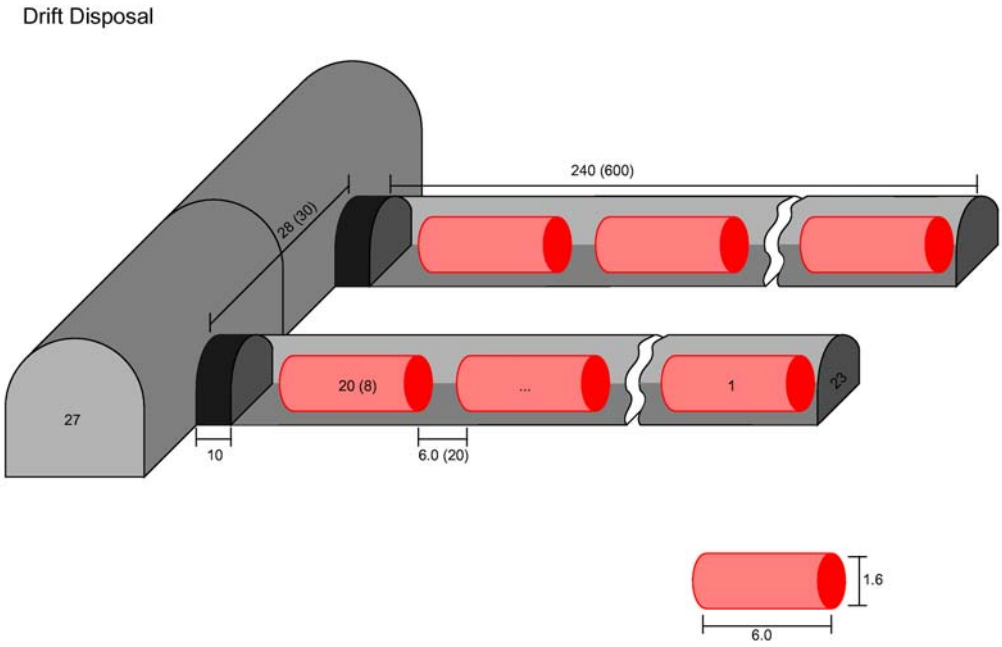

Fig. 1.2 Simplified drift disposal concept

1.2 Calculation of geometry and voids

In the following the void volumes that are available for storing liquid and gas are calculated for each of the concepts under consideration. The disposal field is considered to consist of an arbitrary number of identical cells and the volume is calculated for one of these. In the borehole concept one cell consists of five identical boreholes, one loading drift and a section of an access drift as shown in Fig. 1.1. In the drift disposal concept one cell is composed of one disposal drift and a section of the access drift, see Fig. 1.2.

The data used here are close to those which are presently projected for a German repository in salt or clay, but since there are not yet final concepts they should be seen as no more than typical example data.

Voids exist in the pore spaces of the backfill and the seals as well as in the containers. For the porosity the values according to Tab. 1.2 are assumed. These values were chosen as generic examples, assuming that the backfill consists of loose crushed salt or clay-sand mixture and the seals are made of pre-compacted blocks.

Tab. 1.2 Porosities of backfill and seals

	Salt	Clay
Backfill	0.3	0.4
Seals	0.2	0.2

The voids in the containers are assumed to be 0.15 m^3 per BSK-3 and 3.0 m^3 per Pollux, as indicated in Tab. 1.1. Tab. 1.3 contains the calculation of the voids available for storage of liquid or gas in the different concepts under consideration.

1.3 Substances in the repository

Different chemical substances occur in the repository near field and play their roles in the corrosion process. The considered cases are based on the assumption that water or brine and iron, as well as some amount of air, are there at the beginning. During the anaerobic

Tab. 1.3 Calculation of geometrical dimensions and void volumes in the disposal field. Values in blue have been calculated, black values are input data

	Salt		Clay	
	Borehole	Drift	Borehole	Drift
Diameter of borehole/drift [m]	0.600	5.412	0.600	5.412
Cross-section of borehole/drift [m^2]	0.283	23.000	0.283	23.000
Diameter of container [m]	0.430	1.600	0.430	1.600
Length of container [m]	4.900	6.000	4.900	6.000
Container volume [m^3]	0.712	12.064	0.712	12.064
Container distance [m]	0.400	6.000	8.000	20.000
Length of seal [m]	10	10	10	10
Number of containers per borehole/drift	60	20	4	8
Length of borehole/drift without seal [m]	318.0	240.0	51.6	208.0
Void per container [m^3]	0.150	3.000	0.150	3.000
Length of loading drift [m]	250	-	600	-
Length of loading drift seal [m]	10	-	10	-
Cross-section of loading drift [m^2]	23	-	23	-
Loading drift distance [m]	48	28	48	40
Cross-section of access drift [m^2]	27	27	27	27
Number of boreholes/drifts per cell	5	1	11	1
Total volume of borehole/drift without seal [m^3]	89.91	5520.00	14.59	4784.00
Total volume of cell [m^3]	7739.7	6506.0	15517.6	6094.0
Backfilled volume per borehole/drift [m^3]	47.22	5278.73	11.74	4687.49
Backfilled volume per cell [m^3]	7282.1	6034.7	15225.2	5767.5
Void volume per borehole/drift without seal [m^3]	23.17	1643.6	5.3	1899.0
Void volume per cell without seals [m^3]	2229.6	1870.4	6096. 7	2331.0

corrosion process water is consumed and hydrogen gas and magnetite are generated. In the salt case some solid salt is precipitated from the saturated brine since some water is consumed.

In clay, there are only minor amounts of minerals that can be dissolved in the water. For simplicity reasons, it is assumed that the liquid in the repository is fresh water. In salt, however, the liquid intruding to repository voids will in most cases have made its way

through layers of halite, and therefore be more or less saturated with NaCl. Other minerals can also be dissolved, but since, e.g., magnesium-containing brine can have detrimental effects on seal materials, and minerals like carnallitite can induce undesirable chemical effects, one will, as far as possible, position the repository within a pure halite environment. Therefore, it is assumed that the liquid in the salt case is always saturated NaCl solution.

All gases in the repository are assumed to obey the ideal gas equation $pv = \mathrm{R}T$ with v denoting the molar volume. Since temperature effects are not considered in this report, the temperature is always taken to be the norm temperature of 273.15 K, though this is not realistic for a deep underground repository with heat-producing waste.

In Tab. 1.4 some general data are compiled that are needed for calculation of the corrosion process. Some of these data are formation-specific. The content of dissolved oxygen gas in brine is taken to be 0.2 mg/l which is a typical value for deep waters. In clay, however, the chemical conditions are always reducing; therefore, it is assumed that deep water does not contain dissolved oxygen. Another formation-specific value is the maximum gas pressure which is calculated from the hydrostatic pressure at the seal and the gas entry pressure. While the latter is taken to be 0.2 MPa in all cases, the former is higher in salt because of the heavier fluid, as explained above.

Tab. 1.4 General data

Atomic mass of Fe [g/mol]	55.84
Atomic mass of O [g/mol]	16.00
Atomic mass of H [g/mol]	1.007
Atomic mass of Na [g/mol]	22.98
Atomic mass of Cl [g/mol]	35.45
Molecular mass of H_2O [g/mol]	18.014
Density of iron [kg/m^3]	7900
Density of magnetite [kg/m^3]	5200
Molar norm-volume of gas [N-m^3/mol]	0.0224
Atmospheric pressure [MPa]	0.1013
Oxygen content of air	0.21
Density of rock salt [kg/m^3]	2168

Tab. 1.4 General data

Solubility of NaCl [g NaCl / mol H_2O]		6.54065
Solubility of NaCl [kg NaCl / kg H_2O]		0.36309
	Salt	Clay
Oxygen content of water/brine [mg/l]	0.2	0
Oxygen content of water/brine [mol/m^3]	0.00625	0
Density of liquid [kg/m^3]	1193	1000
Salt content in liquid [kg/m^3]	317.78	0
Water content in liquid [mol/m^3]	48586	55512
Volume of precipitate per volume of liquid	0.1466	0
Maximum gas pressure [MPa]	5.67	5.11

Based on the data given in Tab. 1.3 and Tab. 1.4 masses and amounts of iron in the boreholes or drifts as well as in the total cells can be calculated, see Tab. 1.5.

Tab. 1.5 Iron in the repository

	Salt		Clay	
	Borehole	Drift	Borehole	Drift
Mass of iron per container [kg]	1544	60000	1544	60000
Mass of iron per borehole/drift [kg]	92640	1200000	6176	480000
Mass of iron per cell [kg]	463200	1200000	67936	480000
Volume of iron per container [m^3]	0.195	7.595	0.195	7.595
Volume of iron per borehole/drift [m^3]	11.727	151.899	0.782	60.759
Volume of iron per cell [m^3]	58.633	151.899	8.599	60.759
Amount of iron per container [mol]	27650	1074499	27650	1074499
Amount of iron per borehole/drift [mol]	1659026	21489971	110602	8595989
Amount of iron per cell [mol]	8295129	21489971	1216619	8595989

1.4 Aerobic corrosion and oxygen balance

Provided that there is no convergence or fluid intrusion in the operating phase, at the time of repository closure the available void volumes are filled with air under atmospheric pressure. After tight closure the oxygen remains in the near field and will cause aerobic corrosion of the steel containers. The aerobic corrosion process requires the presence of water without consuming it. It follows the equation

$$2\ Fe + 3/2\ O_2 + H_2O \rightarrow 2\ FeOOH \rightarrow Fe_2O_3 + H_2O,$$

that is, one mole of iron is corroded by 3/4of a mole of oxygen gas. Since there is always certain humidity in the air, the process does not require intrusion of liquid water, although that would accelerate it considerably.

In order to investigate the role of the remaining oxygen, the aerobic corrosion process and the fraction of metal affected by it are presented in Tab. 1.6. It is assumed that the total gaseous oxygen, including that in the loading drifts and access galleries, is available for aerobic corrosion of the containers in the emplacement boreholes or drifts.

Another possible source of oxygen is the water that intrudes to the near field. Depending on its origin, it can contain more or less dissolved oxygen. The concentration given in Tab. 4 is a value that is not expected to be exceeded. The aerobic corrosion due to this concentration of dissolved oxygen is also estimated in Tab. 1.6, assuming that the repository voids can only once be filled with brine. This is realistic because there is no flow through the near field in the salt case, and in the clay case, as mentioned above, there is no dissolved oxygen.

It becomes clear that the aerobic corrosion process does not play an essential role and can be neglected in nearly all cases. The corrosion due to air oxygen remains well below 1% of the total iron mass, except in the clay borehole case where it reaches about 6%, due to the relatively high oxygen/iron-ratio. The oxygen dissolved in intruding water can only corrode a fraction of some millionths of the total mass of iron. Therefore, except for specific cases with a high residual air/iron-ratio when a high degree of numerical accuracy is required, the complete negligence of aerobic corrosion is justifiable.

Tab. 1.6 Calculation of aerobic corrosion due to oxygen from operating phase

	Salt		Clay	
	Borehole	Drift	Borehole	Drift
Gaseous oxygen per borehole/drift [N-m^3]	4.86	345.16	1.11	398.79
Gaseous oxygen per cell [N-m^3]	468.22	392.79	1280.30	489.51
Amount of gaseous oxygen (O_2) per borehole/drift [mol]	217	15409	50	17803
Amount of gaseous oxygen per cell [mol]	20902.75	17535.17	57156.28	21853.09
Mass of iron that can be corroded by gaseous oxygen per cell [kg]	1556.28	1305.55	4255.48	1627.04
Amount of iron that can be corroded by gaseous oxygen per cell [mol]	27870.33	23380.22	76208.38	29137.45
Fraction of iron that can be corroded by gaseous oxygen	0.0034	0.0011	0.0626	0.0034
Amount of oxygen dissolved in brine per cell [mol]	13.94	11.69	0	0
Amount of iron that can be corroded by dissolved oxygen per cell [mol]	18.58	15.59	0	0
Mass of iron that can be corroded by dissolved oxygen per cell [kg]	1.04	0.87	0	0
Fraction of iron that can be corroded by dissolved oxygen	2.24E-06	7.25E-07	0	0

1.5 Anaerobic corrosion: water, gas and volume balance

The anaerobic corrosion is the most important chemical process in a repository with steel containers. This process transforms iron to magnetite, consuming water and producing hydrogen gas. It follows the equation

$$3\ Fe + 4\ H_2O \rightarrow Fe_3O_4 + 4\ H_2.$$

Three moles of iron are transformed into one mole of magnetite, consuming four moles of water and releasing four moles of hydrogen gas. Since magnetite has a lower density than iron a volume increase of the solid material occurs during the corrosion process.

With the atomic masses and densities given in Tab. 1.4 and again assuming the canister steel were pure iron, the factor by which the volume increases can be determined to be nearly exactly 2.1, see Tab. 1.7.

Tab. 1.7 Calculation of the volume increase factor on anaerobic corrosion of iron

Volume of 3 moles of Fe [m^3]	0.2121
Volume of 1 mole of Fe_3O_4 [m^3]	0.4452
Volume increase factor	2.0996

When considering salt it must be taken into account that the fluid in the pore spaces is not fresh water but assumed to be saturated NaCl solution with a density of 1193 kg/m^3 and a salt content of 6.54 g NaCl per mole of H_2O, see Tab. 1.4. These values are valid for a temperature of 310 K, the effects of thermal expansion are neglected.

In salt, an additional generation of solid material during the anaerobic corrosion results from the consumption of water. Since all the liquid is NaCl solution, solid salt precipitates when water is consumed. The volume ratio of solid salt precipitate and consumed brine is 0.1466.

Corrosion often proceeds inhomogeneously in the form of pitting corrosion. Therefore, the corrosion process is assumed to destroy the integrity of the containers and to allow gas and liquid to intrude. If this were not the case, there would be no release of contaminants.

For the estimations it is assumed that no convergence takes place. In the following, the water, gas and volume balances are considered under different assumptions, resulting in four cases to be considered:

1. *Totally flooded pore space, water-impermeable host rock and seal:* The total pore space, but not the container void, is filled with fluid (NaCl solution or fresh water) from the beginning. For the corrosion process only the water inside the borehole or drift is available, that is, no water or brine can pass the seals. Gas can be stored in the volumes that are no longer occupied by solid or liquid phases after corrosion, as well as in the container voids. When the gas pressure exceeds the hydrostatic pressure at

the seal by more than the so-called gas entry pressure, gas is released through the seal. This scenario describes the more or less unrealistic situation of a borehole or drift in a watertight environment that is tightly sealed after fluid intrusion.

2. *Residual saturation of pore space, water-impermeable seal:* The pore space is mainly filled with air but contains a residual saturation of brine which is assumed to be 1% of the pore space. Concerning the other assumptions this case is equivalent to the preceding one. It is only considered for salt in which case it can be regarded as the normal evolution scenario. In clay, however, total flooding of the pore space is the normal scenario.

3. *Full corrosion of containers, water-permeable seal, no gas storage:* The seal is permeable for liquid and gas. The containers are assumed to be defect, so the container voids are filled with liquid. Brine or water is provided as much as needed for total corrosion of the iron. The gas escapes from the near field and does not cause pressure build-up.

4. *Full corrosion of containers, water-permeable seal, gas storage:* The seal is permeable for liquid and gas, but a certain gas storage volume is available in the boreholes or drifts. It is assumed that the total container voids as well as 10% of the pore space act as gas storage volumes. These volumes are reduced during the corrosion process due to the volume increase of the solid materials. Gas is assumed to be stored under hydrostatic pressure. Gas that cannot be stored is released.

1.5.1 Totally flooded pore space, water-impermeable host rock and seal

The case considered here is not too realistic because it is assumed that no fluid can intrude the disposal borehole or drift through the seal or any other pathway, but nevertheless the pore space is completely filled with water or brine from the beginning. This would only be possible if the pore spaces were filled before sealing the disposal section. Consequently, the containers are considered to be undamaged when the fluid intrudes, and so the container voids are assumed to contain no fluid. This estimation shows, however, how much of the iron present in the borehole or drift can be corroded by the amount of water or brine the pore volume is able to store. It gives an impression of the relation of metal, fluid, gas, and corrosion products within a closed system.

The generation of hydrogen gas leads to a considerable hypothetical pressure increase. It is, however, unrealistic to assume that the seal is totally tight even for gas under extreme pressure. Therefore, it is supposed in the calculation that the gas pressure can not exceed the sum of the hydrostatic pressure in the depth of the seal and the gas entry pressure. The seal is assumed to be located 500 m below surface. As explained in 1.1.1, the hydrostatic pressure is 5.47 MPa in the salt case and 4.91 MPa in the clay case. The gas entry pressure is assumed to be 0.2 MPa in each case. The norm pressure is 0.1013 MPa.

Tab. 1.8 contains the results for this case. While in the salt-borehole case the available brine completely vanishes during the corrosion process, corroding not quite a third of the container iron, in the salt-drift case as well as in both clay cases there is nearly twice as much brine or water as needed for corroding the total iron. This is because in disposal drifts, and generally in clay, there is more backfill between the containers than in salt boreholes, and in the scenario under consideration, the porous backfill keeps the liquid.

Tab. 1.8 Water, gas and volume balance in case of totally flooded pore space and water-impermeable seal. All values refer to one borehole or drift

	Salt		Clay	
	Borehole	Drift	Borehole	Drift
Start volume of liquid [m^3]	14.17	1583.62	4.70	1875.00
Start void volume [m^3]	9.00	60.00	0.60	24.00
Start amount of water [mol]	688228	76940862	260758	104085496
Start volume of iron [m^3]	11.73	151.90	0.78	60.76
Corroded amount of iron [mol]	516171	21489971	110602	8595989
Corroded volume of iron [m^3]	3.65	151.90	0.78	60.76
Consumed amount of water [mol]	688228	28653295	147469	11461318
Consumed volume of liquid [m^3]	14.17	589.75	2.66	206.46
Volume of precipitate [m^3]	2.08	86.44	0.00	0.00
End volume of magnetite [m^3]	7.66	318.93	1.64	127.57

Tab. 1.8 Water, gas and volume balance in case of totally flooded pore space and water-impermeable seal. All values refer to one borehole or drift

	Salt		Clay	
	Borehole	Drift	Borehole	Drift
End void volume [m^3]	17.08	396.27	2.40	163.65
End volume of liquid [m^3]	0.00	993.87	2.04	1668.53
End amount of water [mol]	0.00	48287567	113289	92624178
Fraction of iron corroded	0.31	1.00	1.00	1.00
Norm-volume of air [N-m^3]	9.00	60.00	0.60	24.00
Amount of hydrogen generated [mol]	688228	28653295	147469	11461318
Norm-volume of hydrogen gas[N-m^3]	15416	641834	3303	256734
Actual gas pressure [MPa]	5.67	5.67	5.11	5.11
Norm-volume of storable gas [N-m^3]	956	22180	121	8255
Norm-volume of gas released from borehole/drift [N-m^3]	14469	619714	3183	248502

Only a small fraction of the produced gas can be stored inside the borehole or drift, in all cases more than 94% of the gas is released to the loading drift or access gallery. In all cases the increase of solid volume is less than the volume vacated by water that is consumed in the corrosion process. In reality, however, there will be a compaction process, at least in the salt case, which reduces the volumes available for absorbing the iron volume increase.

Figures 1.3 and 1.4 are graphical presentations of the volume balances in this scenario for the salt borehole and the salt drift case.

1.5.2 Residual saturation of pore space, water-impermeable seal

The situation considered here is more realistic than that of the previous chapter. It is assumed that the seal is impermeable for liquids, and therefore, the pore space in the backfill remains dry. Nevertheless, there is a certain residual saturation, due to some moisture that was already in the backfill at the time of seal emplacement. This moisture content is supposed to be 1% of the pore volume. Apart from the amount of water available for corrosion, this case is equivalent to the preceding one. It does not make sense, however, to

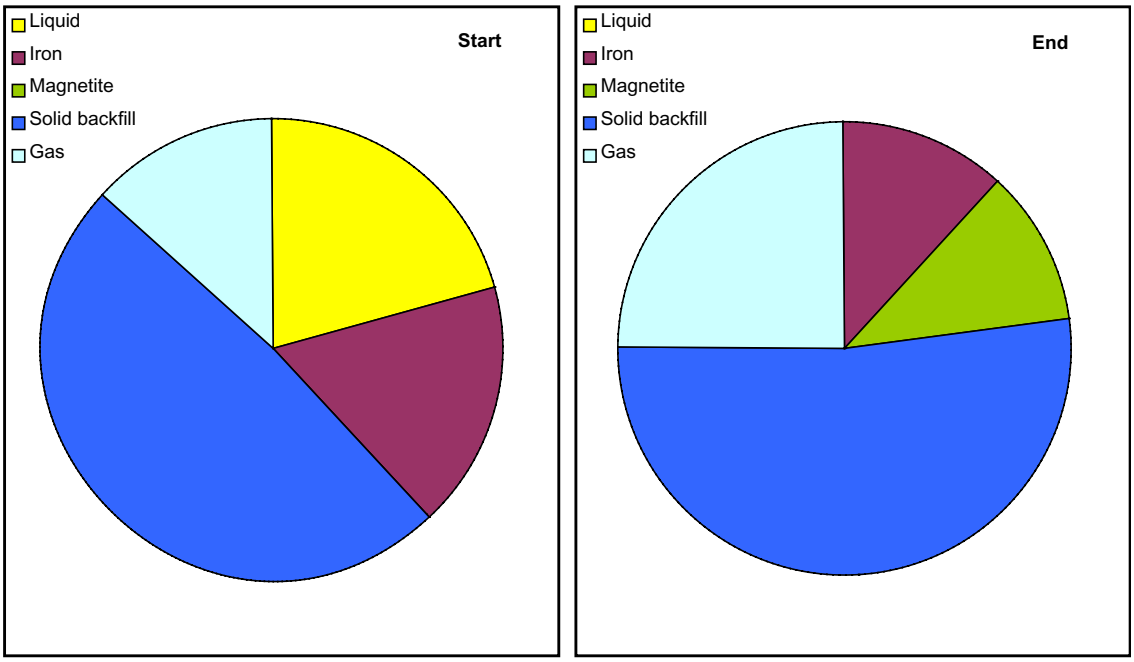

Fig. 1.3 Graphical presentation of the volume balance in case of totally flooded pore space and impermeable seal (salt borehole)

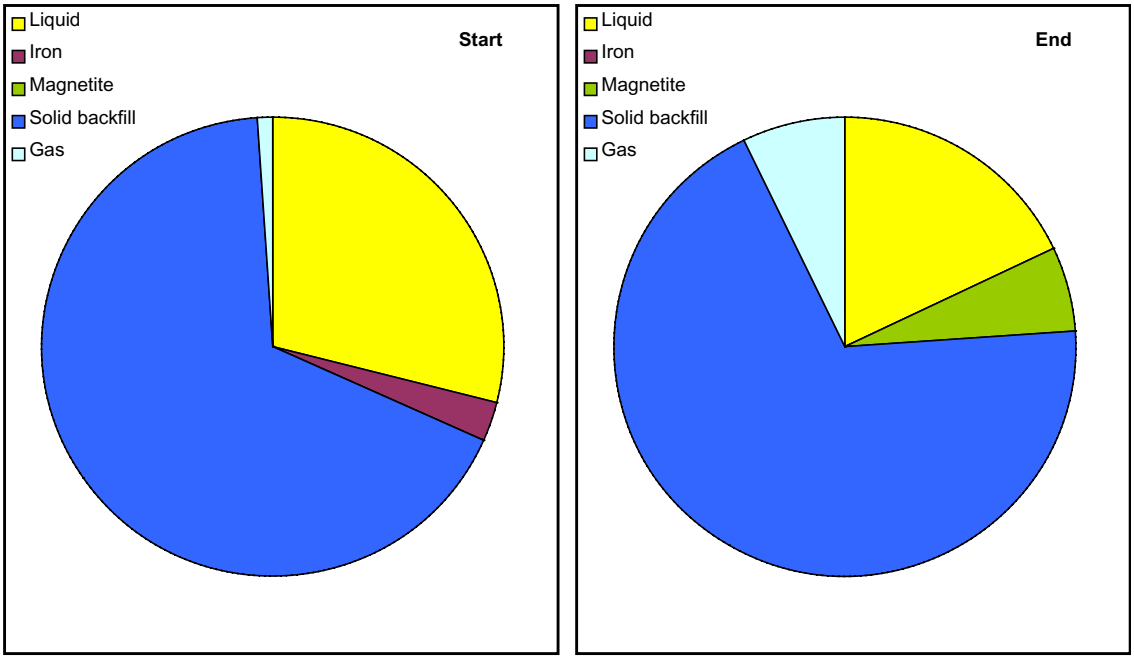

Fig. 1.4 Graphical presentation of the volume balance in case of totally flooded pore space and impermeable seal (salt drift)

consider this situation for clay because, unlike salt, clay is never completely watertight and will in any case be completely flooded after some time. Tab. 1.9 contains the calculation for this case, referring to one borehole or drift.

Tab. 1.9 Water, gas and volume balance in case of residual saturation in pore space and impermeable seal. All values refer to one borehole or drift

	Salt	
	Borehole	Drift
Saturation of pore space	0.01	0.01
Start volume of liquid [m^3]	0.14	15.84
Start void volume [m^3]	23.02	1627.78
Start amount of water [mol]	6882	769409
Start volume of iron [m^3]	11.73	151.90
Corroded amount of iron [mol]	5162	577056
Corroded volume of iron [m^3]	0.0365	4.0788
Consumed amount of water [mol]	6882	769409
Consumed volume of liquid [m^3]	0.1417	15.8362
Volume of precipitate [m^3]	0.0208	2.3212
End volume of magnetite [m^3]	0.0766	8.5641
End void volume [m^3]	23.10	1636.81
End volume of liquid [m^3]	0.00	0.00
End amount of water [mol]	0.00	0.00
Fraction of iron corroded	0.0031	0.0269
Norm-volume of air [N-m^3]	23.02	1627.78
Amount of hydrogen generated [mol]	6882	769409
Norm-volume of hydrogen gas[N-m^3]	154	17235
Actual gas pressure [MPa]	0.78	1.17
Norm-volume of storable gas [N-m^3]	1293	91616
Norm-volume of gas released from borehole/drift [N-m^3]	0	0

The available brine can corrode no more than about 0.3% of the container iron in the borehole case and 1.7% in the drift case. Nevertheless, there is a pressure increase due to gas production. The gas pressure does not become high enough to cause release of gas from the borehole or drift but could possibly hinder convergence and brine intrusion. These effects have not been considered here.

1.5.3 Full corrosion of containers, water-permeable seal, no gas storage

In the following it is assumed that the seal is permeable for brine or water, allowing as much liquid as needed for full corrosion to intrude to the borehole or drift. This is a more or less realistic assumption for seals that are not totally tight, as well as for the clay case where always a certain water flow is possible. A time dependency is not considered but it is supposed that water or brine is supplied through the surrounding host rock fast enough and in a sufficient quantity to support an undisturbed corrosion process. The gas is assumed to escape from the near field without any resistance. The containers are supposed to be defect from the beginning and the voids are flooded. This calculation gives an impression of the maximum possible solid volume increase due to corrosion.

The calculation results are shown in Tab. 1.10. Again, one single borehole or emplacement drift is considered here. The volume increase of solid materials reduces the pore space in the backfill as well as the container voids.

It can be seen that some liquid is present in the borehole or drift even at the end of the process. The salt borehole case is the only one in which the liquid volume is essentially lower at the end than in the beginning. This shows that the volume increase is in any case absorbed by the available pore and void volumes. If the pore space vanished completely, however, there would be no room for liquid and therefore, the corrosion process would come to an end.

The amount of hydrogen gas that is generated by corrosion is considerable. In the calculations for this case the gas is assumed to leave the near field without any effects, but this is not realistic. In reality there will be a gas pressure build-up to a value slightly above the hydrostatic pressure in the repository. The hypothetical pressure value given in Tab. 1.10 is calculated from the hydrogen volume and the initial void volume. This is the value the pressure would reach if the gas homogeneously spread over the total near field and dis-

Tab. 1.10 Water, gas and volume balance in case of water-permeable seals and no gas storage

	Salt		Clay	
	Borehole	Drift	Borehole	Drift
Start volume of liquid [m^3]	23.17	1643.62	5.30	1899.00
Start amount of water [mol]	1125498	79855992	294065	105417793
Start volume of iron [m^3]	11.73	151.90	0.78	60.76
Start amount of iron [mol]	1659026	21489971	110602	8595989
Consumed amount of water [mol]	2212034	28653295	147469	11461318
Consumed volume of liquid [m^3]	45.53	589.75	2.66	206.46
Volume of precipitate [m^3]	6.67	86.44	0.00	0.00
End volume of magnetite [m^3]	24.62	318.93	1.64	127.57
End volume of liquid [m^3]	3.60	1390.14	4.44	1832.18
End amount of water [mol]	174749	67540600	246343	101708800
Volume of liquid replenished from outside [m^3]	25.96	336.27	1.80	139.65
Amount of hydrogen generated [mol]	2212034	28653295	147469	11461318
Norm-volume of hydrogen gas [N-m^3]	49550	641834	3303	256734
Norm-volume of hydrogen gas per cell [N-m^3]	14864871	12836676	145345	2053868
Hypothetic pressure in repository [MPa]	675	695	2	89

placed all liquid, without being able to escape itself. That is, of course, an unrealistic assumption. The high values show, however, that it is impossible to store all produced gas inside the near field, except in the clay borehole case due to the relatively high pore volumes. In all other cases there will be a considerable release of hydrogen gas from the repository via suitable pathways in the host rock, which might be created by the gas pressure itself.

1.5.4 Full corrosion of containers, permeable seals, gas storage

Concerning the gas, the following investigation is slightly more realistic than the preceding one. In the near field there are always volumes the gas cannot escape from, e.g. in the roof regions of drifts. Such volumes are called gas storage volumes. It is assumed in the following that the total container voids as well as a fraction of 10 % of the pore space in backfill act as gas storage volumes. During corrosion the solid volumes increase, and

as a result the gas storage volume decreases. It is assumed that the relative gas storage capacity, that is the ratio of the gas storage volume and the total void and pore volume, remains constant. Tab. 1.11 shows the results of this estimation.

Tab. 1.11 Water, gas and volume balance in case of water-permeable seals with gas storage

	Salt		Clay	
	Borehole	Drift	Borehole	Drift
Relative gas storage capacity of backfill pore volume	0.10	0.10	0.10	0.10
Start gas storage capacity of bore-hole/drift [m^3]	10.42	218.36	1.07	211.50
Total relative gas storage capacity	0.4497	0.1329	0.2019	0.1114
Norm-volume of air [m^3]	23.17	1643.62	5.30	1899.00
Air volume under pressure [m^3]	0.41	29.36	0.11	37.65
Start volume of liquid [m^3]	22.75	1614.25	5.19	1861.35
Start amount of water [mol]	1105389	78429288	288236	103328004
Start volume of iron [m^3]	11.73	151.90	0.78	60.76
Start amount of iron [mol]	1659026	21489971	110602	8595989
Consumed amount of water [mol]	2212034	28653295	147469	11461318
Consumed volume of liquid [m^3]	45.53	589.75	2.66	206.46
Volume of precipitate [m^3]	6.67	86.44	0.00	0.00
End volume of magnetite [m^3]	24.62	318.93	1.64	127.57
End pore volume [m^3]	3.60	1390.14	4.44	1832.18
End gas storage volume [m^3]	1.62	184.69	0.90	204.06
End norm volume of stored gas [m^3]	90.52	10337.31	45.20	10293.56

Tab. 1.11 Water, gas and volume balance in case of water-permeable seals with gas storage

	Salt		Clay	
	Borehole	Drift	Borehole	Drift
End volume of liquid [m^3]	1.98	1205.45	3.54	1628.12
End amount of water [mol]	96171	58567537	196597	90381040
Volume of liquid replenished from outside [m^3]	24.76	180.95	1.01	-26.76
Amount of hydrogen generated [mol]	2212034	28653295	147469	11461318
Norm-volume of hydrogen gas[N-m^3]	49550	641834	3303	256734
Actual gas pressure [MPa]	5.67	5.67	5.11	5.11
Norm-volume of storable gas [N-m^3]	91	10337	45	10294
Norm-vol. of gas released from boreh./drift [N-m^3]	49482	633140	3263	248339
Norm-volume of hydrogen gas per cell [N-m^3]	14844663	12662802	143589	1986712
Hypothetic pressure in cell [MPa]	674	686	2	86

The results are rather similar to those of the preceding calculation, but they will be better comparable to those obtained from a time-dependent modelling which takes account of the gas storage effect and liquid displacement resulting from it.

In the clay-drift case, a negative value has been calculated for the volume of liquid replenished from above. This shows that in total, the gas stored in the storage volume displaces more water than is consumed by the corrosion process, and there is a total flow out of the near field.

Figures 1.5 and 1.6 are graphical presentations of the volume balances in this scenario. Only the salt cases are presented.

1.6 Conclusions

The estimations presented in this chapter are only a rough approach to the processes that occur in the near field during corrosion of the containers. Time dependency has not been taken into account and neither have temperature effects or convergence, though the latter is very important in rock salt. Nevertheless, some conclusions can be drawn already from these simple estimations:

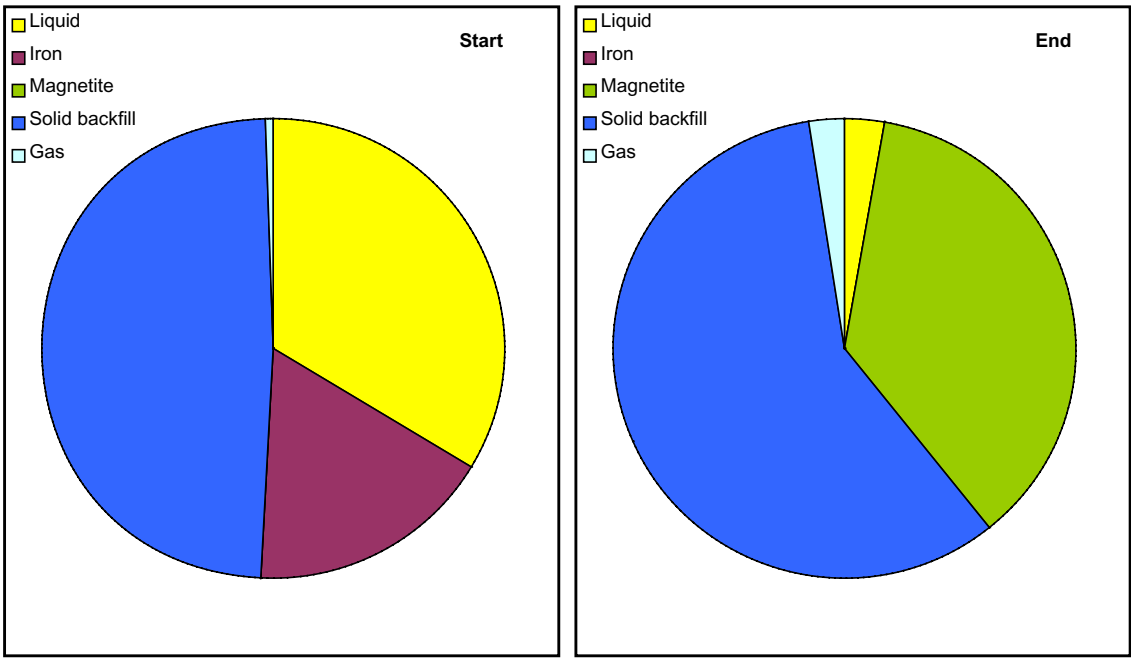

Fig. 1.5 Graphical presentation of the volume balance in case of full corrosion, permeable seals and gas storage (salt borehole)

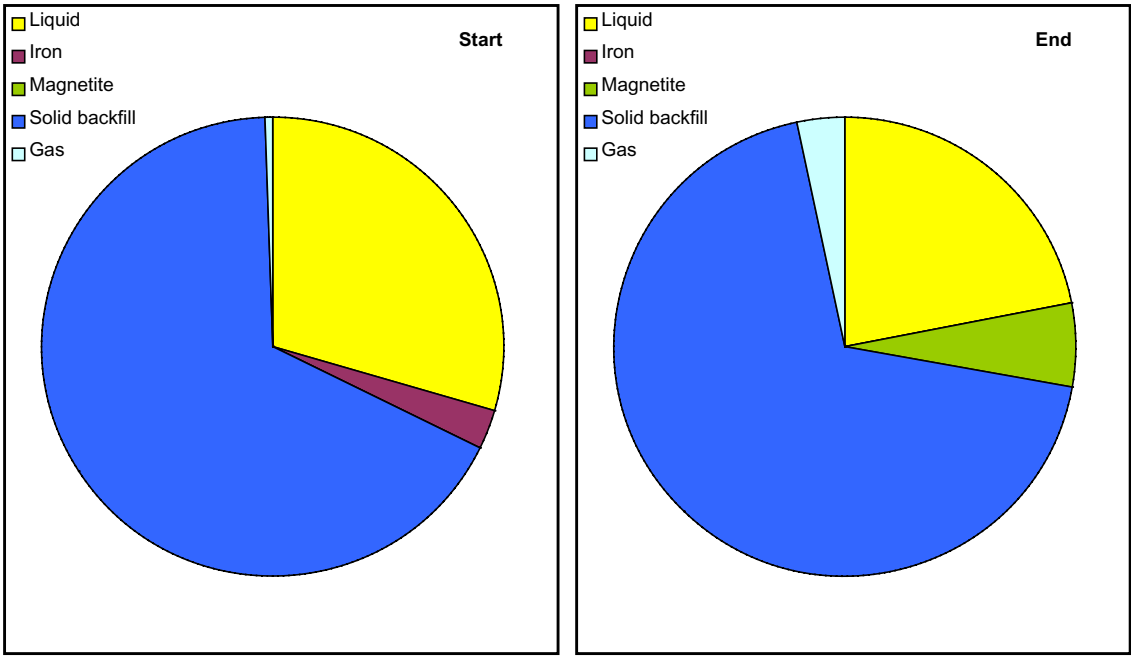

Fig. 1.6 Graphical presentation of the volume balance in case of full corrosion, permeable seals and gas storage (salt drift)

- The aerobic corrosion process does not play an important role. In all cases except the clay borehole case less than 1 % of the iron is corroded by the oxygen from the operating phase. In the clay borehole case this fraction is about 5 %. The fraction of iron corroded by dissolved oxygen is about 1 millionth maximum.

- In most cases, the water present in the borehole or drift after a total flooding of the pore spaces and voids suffices to corrode all the iron anaerobically. Only in the salt borehole case there is not enough water in the borehole for corroding all iron.

- If the borehole or drift is not flooded but contains some residual water in the backfill, this will only corrode a small fraction of about 1 % of the iron. Nevertheless, a considerable gas pressure can result from this effect.

- If the seals are not totally tight and total iron corrosion is possible, the volume increase of the iron when being transformed to magnetite is considerable. This effect should by no means be neglected in time-dependent calculations.

- Hydrogen production is a very important effect. The hypothetic gas pressure, that is the pressure that would occur if the gas could not escape from the near field, reaches up to about 700 MPa. This shows that the gas will in any case find its way to escape from the repository, possibly acting as a propellant and displacing liquids from parts of the repository. The gas effects must in any case be taken into account in detailed calculations.

2 Time-dependent modelling of corrosion-induced processes

Apart from gas production, corrosion-induced processes have not been considered in German performance assessment calculations so far. The estimations of the previous chapter have shown, however, that such effects can have a considerable influence on the results and should generally not be neglected. These estimations aim at the end-state of the repository system after all iron is corroded, regarding balances of mass and volumes, but are not suitable for yielding information about the temporal evolution

To describe correctly the time evolution of the near field under consideration of all corrosion-induced processes, it is necessary to use a model that calculates these effects time-stepwise and takes account of their mutual influences. Such a model has been developed and implemented in the near field code LOPOS, which is a part of the EMOS package for long-term safety and performance assessment, for disposal boreholes and drifts. Since LOPOS was developed and is primarily suitable for repositories in rock salt, the test calculations have been performed for salt formations. Nevertheless it is possible to use the model also for clay formations; in this case the rock convergence is set to zero.

This chapter describes the model and the underlying assumptions as well as the results of the test calculations.

2.1 Segment models for disposal boreholes and drifts

In the following, extended models of a disposal borehole and a disposal drift are introduced. The borehole and drift can take properly conditioned radioactive waste, metal containers and backfill material like crushed salt in the annular gaps, around the containers in the drifts and in the plugs. In the following subchapters modelling of the processes occurring under the different conditions in the borehole and the drift and their implementation in the LOPOS module of the EMOS code are described. New features of the models are the increase of the volume of solid material, the consumption of water and precipitation of salt during corrosion. The implementation of the models in the computer code LOPOS is verified by means of some test cases. Finally, the radionuclide release from a generic repository is calculated. The results are compared with those obtained from the same repository where, however, the new features of the borehole and drift segments are switched off.

2.1.1 Model assumptions and effects

The long term safety of a waste repository is determined by the potential release of the stored radionuclides to the biosphere. To release the nuclides a transport medium and a driving force are necessary. Here, only brine is considered as the transport medium.

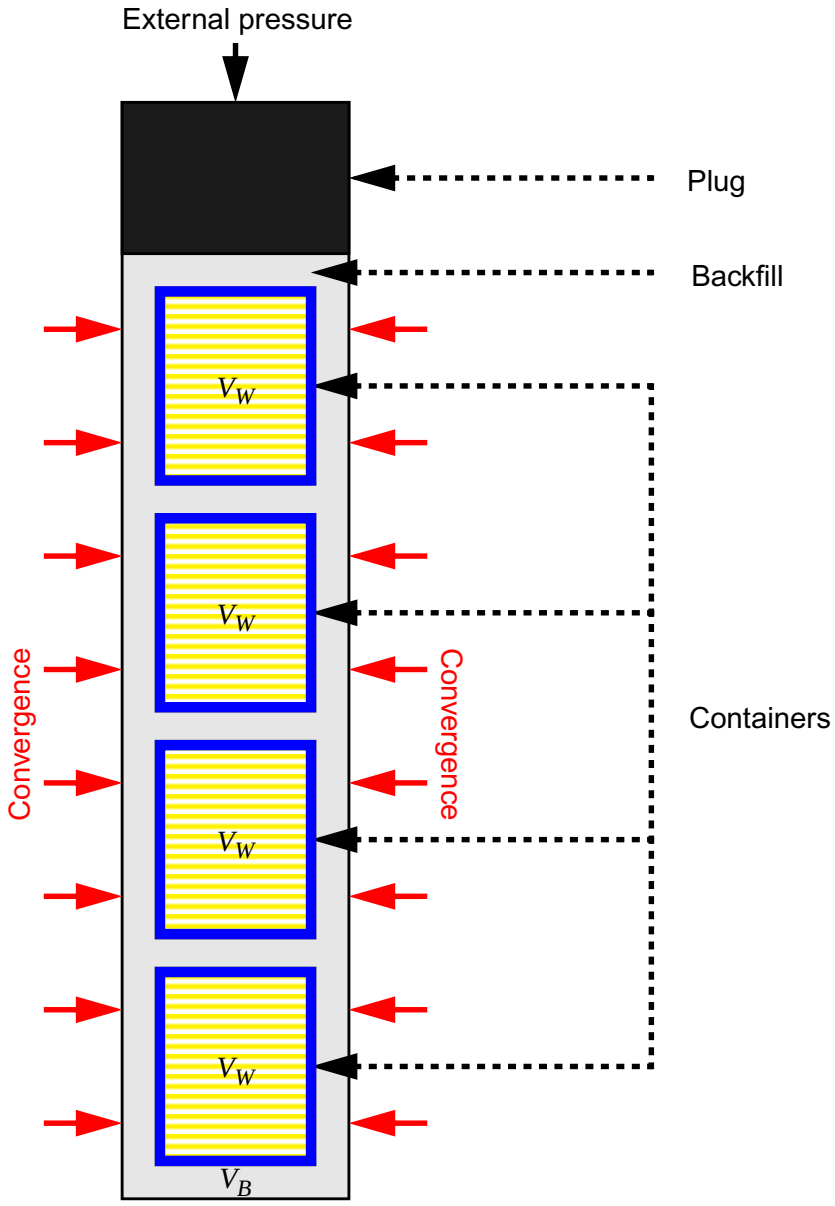

Fig. 2.1 Scheme of a borehole with waste containers

The primary driving forces for the transport medium are

- convergence of the salt rock resulting in a reduction of void volumes in the waste and pore volumes in the backfill material which causes extrusion of contaminated brine,

- displacement of contaminated brine by gas which is produced by corrosion of the steel container.

Additionally, during corrosion of the steel, iron reacts to magnetite. During this reaction, water is extracted from the brine and salt precipitates. The produced magnetite requires a greater volume at the same location than the steel container did. This may lead to a further extrusion of the brine from the disposal borehole. On the other hand, due to the extraction of water, the brine volume is reduced and intrusion of the brine from neighbouring drifts may occur. These competitive effects are investigated below.

Fig. 2.1 shows the individual components of a disposal borehole. A similar figure holds for a disposal drift. The equations specifying the driving forces for contaminated brine, expelled from the borehole or drift, are derived from a volume balance, described in the following.

2.1.2 Balance of the volumes

As an example the volume balance is shown for the disposal borehole, only. The volume balance for the disposal drift can be derived in the same way. The total volume of the disposal borehole V is a composition of that of the backfill material, of the waste and of the iron containers, i.e.,

$$V = V_B + V_W + V_{SM}. \qquad (2.1)$$

where V_B refers to the volume of the backfill material in the annular gap and the plugs above and possibly between the container, V_W is the volume of the waste in the containers and V_{SM} is the solid material volume of the containers, i.e. iron and/or magnetite, and of the salt which precipitates during water consumption by corrosion. Fig. 2.2 sketches the change in volumes of solid material and of backfill material during corrosion of the containers. It also outlines the resulting compaction of the waste in the container.

The total pore volume V_P in the borehole initially (t = 0) consists of the pores in the backfill material V_{PS} and the voids in the waste V_{PW}, i.e.,

$$V_P(0) = V_{PS}(0) + V_{PW}(0) = \varphi_B(0) \cdot V_B(0) + \varphi_W(0) \cdot V_W(0), \qquad (2.2)$$

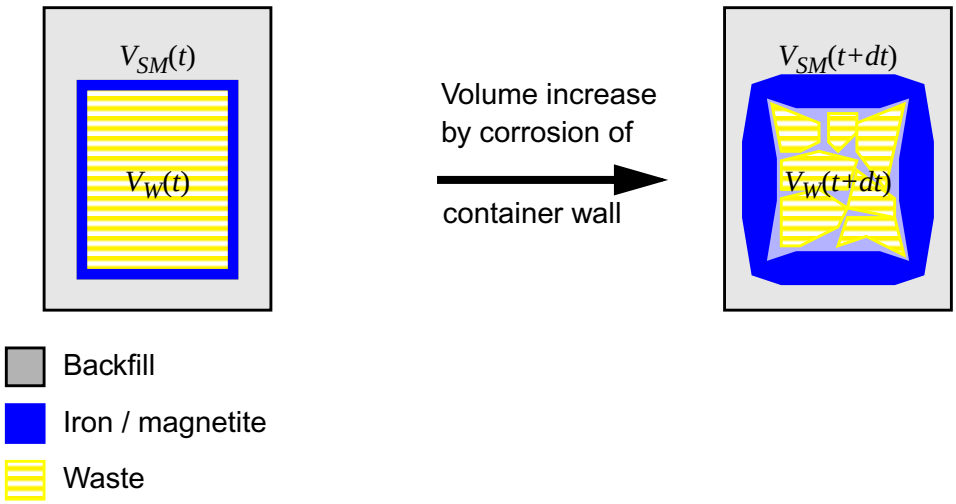

Fig. 2.2 Volume change during corrosion of a thick walled container

where $\varphi_B(0)$ and $\varphi_W(0)$ are the initial values of the backfill porosity and the average porosity of the waste, respectively. The later follows from the input data initial void volume $V_{PW}(0)$ in the waste and initial total volume $V_W(0)$ of the waste itself, i.e.

$$\varphi_W(0) = \frac{V_{PW}(0)}{V_W(0)} . \qquad (2.3)$$

The time evolution of the total pore volume is determined by the volume reduction of the pores in backfill and voids in waste by convergence of the surrounding salt rock. Additionally, the total pore volume is reduced by the volume increase of the steel containers during corrosion, where iron converts to magnetite and salt precipitates.

2.1.3 Time evolution of the volumes

The volume decrease of the disposal borehole as a whole results only from convergence of the salt rock. It is assumed that the volume increase of the solid material only causes reduction of the pore total volume in the borehole, provided that there is any left. A volume increase of the borehole by the expansion of the solid phase is not considered due to the assumption that there is sufficient pore space available for the volume enlargement.

Thus, the volume change of the borehole with time is described as

$$V(t) \;=\; V_B(t) \;+\; V_W(t) \;+\; V_{SM}(0)\,, \qquad (2.4)$$

where the change of the total volume of the borehole results in a change of the volumes of the backfill material and of the waste. Both the backfill material and the waste can be compacted. The volume $V_{SM}(0)$ is the initial volume of solid material which is the initial iron volume of the containers $V_{Fe}(0)$.

The development of the pore volume V_P by convergence and corrosion at any time can be expressed as

$$V_P(t) \;=\; \varphi_B(t) \cdot V_B(t) \;+\; \varphi_W(t) \cdot V_W(t) \;+\; V_{SM}(0) \;-\; V_{SM}(t)\,. \qquad (2.5)$$

For the time evolution of the pore volume, hence, follows

$$\frac{\mathrm{d}V_P}{\mathrm{d}t} \;=\; \frac{\mathrm{d}V_{PB}}{\mathrm{d}t} + \frac{\mathrm{d}V_{PW}}{\mathrm{d}t} - \frac{\mathrm{d}V_{SM}}{\mathrm{d}t}\,. \qquad (2.6)$$

For simplicity, it is assumed that the backfill material and the waste are compacted with the same convergence rate, i.e.

$$\frac{\mathrm{d}V_{PB}}{\mathrm{d}t} \;=\; -K \cdot V_B, \qquad (2.7)$$

$$\frac{\mathrm{d}V_{PW}}{\mathrm{d}t} \;=\; -K \cdot V_W\,, \qquad (2.8)$$

where K refers to the average convergence of the borehole. For both cases, the convergence rate is then determined by an average porosity of the waste and backfill material, i.e.

$$K \;=\; K(\varphi_m)\,. \qquad (2.9)$$

This average porosity φ_m is defined as the ratio of the total pore volume and the total volume of the borehole,

$$\varphi_m(t) \quad = \quad V_P(t) \,/\, V(t)\,. \qquad (2.10)$$

The time evolution of the container volume during corrosion is calculated as follows. The development of metal mass $m(t)$ with time is given by

$$m(t) \quad = \quad m_0 \cdot \mathrm{e}^{-u_m \cdot (t - t_i)} \qquad \text{for } t > t_i, \qquad (2.11)$$

where m_0 is the initial mass of metal and u_m is the corrosion rate. The time t_i denotes beginning of metal corrosion. This relation only holds, if there is enough water present. If all the water is consumed, some numerical tricks have to be used in the computation.

Conversion of iron into magnetite results in gas production and water consumption. Iron (Fe) corrosion is described by the following reaction:

$$3\mathrm{Fe} + 4\mathrm{H_2O} \rightarrow \mathrm{Fe_3O_4} + 4\mathrm{H_2}, \qquad (2.12)$$

i.e. 3 mol Fe consume 4 mol H_2O and produce 4 mol H_2.

From this relation, the masses of magnetite, consumed water and generated hydrogen gas can be calculated. Using mass and density of iron, precipitated salt and magnetite the volume of the solid material at time t is given by

$$V_{SM}(t) \quad = \quad V_{SM}(0) \cdot \left(g_c \cdot \left(1 - \mathrm{e}^{-u_m t} \right) + \mathrm{e}^{-u_m t} \right). \qquad (2.13)$$

The factor $g_c = 2.668$ results from the volume increase factor (Tab. 1.7) plus the volume of salt precipitate per volume of iron (Tab. 1.11). In eq. 2.13 the volume $V_{SM}(t)$ includes that of salt which precipitates during water consumption.

The conversion of iron to magnetite is related to the gas production via eq. 2.12. The gas production rate directly results from the mass reduction rate of the iron where Γ_m mol of gas per kg of iron are generated. The gas production rate $\dot{n}_G$ [mol/a] is, thus, given by

$$\dot{n}_G \quad = \quad m_0 \cdot \Gamma_m \cdot u_m \cdot \exp(-u_m t). \qquad (2.14)$$

2.1.4 Pressure calculation during the intrusion phase

The time period where liquid, water or brine, intrudes into a segment of the repository, i.e a chamber, a drift or a borehole, is called the intrusion phase of that segment. It is assumed, that during the intrusion phase the liquid entering the borehole has no power contact with the liquid in the charging drift above the disposal borehole. In that case, the fluid pressure in the borehole is computed from the hydrostatic pressure of the intruded liquid and from the gas pressure.

The volume which can accommodate liquid is determined at any time by the current pore volume and the current volume of the gas. Inflow of liquid in the borehole takes place as long as the fluid pressure is lower than the one in the neighbouring segments, referred to the same depth. If the liquid inflow occurs from a brine inclusion in the neighbourhood of the borehole, the drift can possibly be filled from the borehole, below. This case would imply that the gas can escape through the borehole plug with a low overpressure.

2.1.5 Liquid and gas volume balances

The pore volume in the borehole is filled with gas or air and/or liquid at any time. Thus,

$$V_P(t) = V_L(t) + V_G(t) \qquad (2.15)$$

yields the following expression for volume change with time

$$\frac{\mathrm{d}V_P}{\mathrm{d}t} = \frac{\mathrm{d}V_L}{\mathrm{d}t} + \frac{\mathrm{d}V_G}{\mathrm{d}t}. \qquad (2.16)$$

The equation for ideal gases is applied for the generated hydrogen gas which states that the gas volume depends on temperature T and gas pressure p_G, i.e.

$$V_G = \frac{n_G \cdot R \cdot T}{p_G}. \qquad (2.17)$$

The time evolution of the gas volume due to gas production and compression or expansion is, thus, given by

$$\frac{\mathrm{d}V_G}{\mathrm{d}t} = \frac{\dot{n}_G}{n_G} \cdot V_G - \frac{\dot{p}_G}{p_G} \cdot V_G - S_{N,G}. \quad (2.18)$$

Here, $S_{N,G}$ is the net gas flow, which in the present modelling is not calculated explicitly, but considered rather by limiting the gas volume which a segment can store, the so called gas-storage volume.

The time evolution of the liquid volume due to in- and outflow of brine and water consumption is given by

$$\frac{\mathrm{d}V_L}{\mathrm{d}t} = -S_N - \frac{\mathrm{d}V_{L\rightarrow G}}{\mathrm{d}t}, \quad (2.19)$$

where S_N describes the net liquid flow. The water consumption rate is proportional to gas production rate

$$\frac{\mathrm{d}V_{L\rightarrow G}}{\mathrm{d}t} = \Omega_L \cdot \dot{n}_G, \quad (2.20)$$

where Ω_L is the volume of water [m^3] consumed generating 1 mol of H_2 gas.

Using eqs. 2.13 and 2.14, the volume of solid material developes as follows:

$$\frac{\mathrm{d}V_{SM}}{\mathrm{d}t} = (g_c - 1) \cdot V_{SM}^0 \cdot u_m \mathrm{e}^{-u_m t} = \frac{\dot{n}_G \cdot (g_c - 1) \cdot V_{SM}^0}{\Gamma_m \cdot m_0}, \quad (2.21)$$

where V_{SM}^0 is the initial volume of the solid material and, thus, equals the initial volume of iron $V_{Fe}(0)$. With

$$\rho_{Fe} = \frac{m_0}{V_{Fe}^0} \qquad (2.22)$$

and the definition

$$\Omega_{SM} = \frac{g_c - 1}{\Gamma_m \cdot \rho_{Fe}}\ , \qquad (2.23)$$

finally, the following expression for the volume of solid material is obtained:

$$\frac{\mathrm{d}V_{SM}}{\mathrm{d}t} = \Omega_{SM} \cdot \dot{n}_G . \qquad (2.24)$$

The time evolution of the total pore volume follows from eq. 2.6, where the time evolution of the volumes of backfill material and of waste ($\mathrm{d}V_B/\mathrm{d}t$ and $\mathrm{d}V_W/\mathrm{d}t$, respectively) results from convergence (compare eqs. 2.7 and 2.8).

Using eqs. 2.6 to 2.8, eqs. 2.18 to 2.20 and eq. 2.24 equation 2.16 yields

$$K \cdot (V_B + V_W) - S_N - \dot{n}_G \cdot (\Omega_L - \Omega_{SM}) + \left(\frac{\dot{n}_G}{n_G} - \frac{\dot{p}_G}{p_G}\right) \cdot V_G = 0\,. \qquad (2.25)$$

2.1.6 Adaptation of the segment model into the segment structure

In the following, the current segment and its neighbour segments are denoted by the indices i and j, respectively.

The convergence rate for the backfilled volume in segment i is given by [1], [2]

$$K_i \cdot V_{B,\,i} = \beta_{B,\,i} \cdot f_p(p_i) \qquad (2.26)$$

and the convergence rate for the pore volume in waste is given by

$$K_i \cdot V_{W,\,i} = \beta_{W,\,i} \cdot f_p(p_i). \qquad (2.27)$$

Using

$$\beta_i = \beta_{B,\,i} + \beta_{W,\,i} \qquad (2.28)$$

gives

$$K_i \cdot (V_{B,\,i} + V_{W,\,i}) = \beta_i \cdot f_p(p_i). \qquad (2.29)$$

The liquid flow from and into the borehole is described by Darcy law. The net flow of segment i is defined as the sum of all flows $S_{i,j}$ into and from the segment i, i.e.,

$$S_{N,i} = \sum_j S_{i,j} = \sum_j R^{-1}_{i,j} \cdot (p_i - p_j), \qquad (2.30)$$

where j runs over all neighbour segments of i and $R_{i,j}$ denotes the flow resistance as defined in [2]. A net flow $S_{N,i} > 0$ implies that the liquid volume is decreasing by the net outflow. The intrusion phase of incompletely filled segments is modelled as given in [2].

In the following, it is assumed that segment i is filled with brine, except the gas-storage volume. Additionally, the gas stored in the segment is assumed to be distributed uniformly in the pore volume of backfill and waste, so that the brine reaches the top of the segment.

For segments in which a considerable vertical extension has to be taken into account, p_i represents the fluid pressure in the middle of the segment i. If the segments i and j are at different depth, the following relation applies to $S_{N,i}$

$$S_{N,i} = \sum_j R^{-1}_{i,j} \cdot (p_i - p_j + \Delta_{i,j} \cdot \rho_L \cdot g), \qquad (2.31)$$

where $\Delta_{i,j}$ is the vertical distance between the centres of the segments i and j and

$$\Delta_{i,j} > 0 \qquad (2.32)$$

applies to segment i above segment j.

Under the simplifying assumption that the gas will be distributed uniformly in the pores in the borehole, the gas pressure equals to the respective fluid pressure. Therefore, the volume change of the gas in segment i is given by

$$\frac{\dot{n}_{G,i}}{n_{G,i}} \cdot V_{G,i} = \frac{\dot{n}_{G,i} \cdot R \cdot T_i}{p_i} = \frac{\gamma_i}{p_i / p_{P,r}} \qquad (2.33)$$

where T_i is the temperature of segment i, the parameter γ_i is defined by

$$\gamma_i = \frac{\dot{n}_{G,i} \cdot R \cdot T_i}{p_{P,r}} \qquad (2.34)$$

and $p_{P,r}$ represents the rock pressure at reference level [1], which serves as a scaling constant.

Volume change of the gas by compression or expansion is described by

$$\frac{\dot{p}_i}{p_i} \cdot V_{G,i} = \frac{\dot{p}_i \cdot R \cdot T_i \cdot n_{G,i}}{p_i^2} = \frac{\delta_i \cdot \dot{p}_i / p_{P,r}}{(p_i / p_{P,r})^2}, \qquad (2.35)$$

where the parameter δ_i is defined as

$$\delta_i = \frac{n_{G,i} \cdot R \cdot T_i}{p_{P,r}}. \qquad (2.36)$$

Using eqs. 2.29, 2.31, 2.33 and 2.35 expression 2.25 for every segment i yields a system of nonlinear equations from which the time-dependent fluid pressure p_i is calculated, i.e.

$$\beta_i \cdot f_p(p_i) - \sum_j R^{-1}_{i,j} \cdot (p_i - p_j + \Delta_{i,j} \cdot \rho_L \cdot g) \qquad (2.37)$$

$$- \dot{n}_{G,i} \cdot (\Omega_{L,i} - \Omega_{SM,i}) + \frac{\gamma_i}{p_i / p_{P,r}} - \frac{\delta_i \cdot \dot{p}_i / p_{P,r}}{(p_i / p_{P,r})^2} = 0 .$$

This system of equations is solved by the Newton method.

2.1.7 Effects of gas storage

In general, only some of the gas generated by corrosion escapes from the disposal borehole. It can partly be stored in the pore volume of the backfill as well as in the waste. The available space for gas storage is called gas-storage volume. In LOPOS, the gas-storage volume is calculated as a fraction f_{Gas} of the total pore volume which is time dependent. The fraction f_{Gas}, however, is assumed to be a constant input parameter. Hence, the volume of gas which is stored in the disposal borehole reduces with time proportional to the total pore volume.

At the beginning the gas storage volume is filled with air present in the mine. Gas that is not contained in the gas storage will be released through the plug when liquid enters the disposal borehole. In most cases, gas can only escape, if the pressure in the borehole exceeds the external pressure by more than the gas entry pressure of the plug. For simplicity, the gas entry pressure is neglected in the following.

As the pressure increases with the inflowing liquid, the gas in the gas-storage volume is compressed. Therefore, the gas-storage volume, in general, will be no more completely filled. The continuous gas production will then replenishment the gas-storage volume, while liquid is displaced. The fluid pressure is calculated with eq. 2.37, the liquid flow follows from

$$S_{i,j} = R^{-1}_{i,j} \cdot (p_i - p_j + \Delta_{i,j} \cdot \rho_L \cdot g) . \qquad (2.38)$$

The time evolution of the volumes of liquid, gas and solid material are determined by numerical integration of the eqs. 2.18 to 2.20 and 2.24. When the gas-storage volume is filled, liquid and gas are released from the borehole. In this case, the parameter β in the convergence term in eq. 2.37 has to be replaced by $\beta' = \beta \cdot (1 - f_{\mathrm{Gas}})$, i.e. only a fraction (1-f_{Gas}) of liquid is released from the borehole. The volume increase of solid material also induces displacement of liquid and gas, which requires replacement of Ω_{SM} by $\Omega'_{SM} = \Omega_{SM} \cdot (1 - f_{\mathrm{Gas}})$ in eq. 2.37. The term describing the consumption of water during metal corrosion remains unchanged, also with filled gas-storage volume.

2.2 Verification

The implementation of the disposal borehole and disposal drift models in the near field module LOPOS of the EMOS computer code is verified by means of some test cases. A simple segment structure as shown in Fig. 2.3 is used in these test cases. The input data for the LOPOS calculations are given in Tables 2.1 to 2.5.

According to the derivations in Tab. 1.8, 1 m^3 of saturated NaCl-solution corrodes 0.2576 m^3 metal and generates 0.5405 m^3 of magnetite, while 0.1466 m^3 of salt precipitates. Thus, the volume increase of solid material per cubic meter brine is 0.4295 m^3.

The hydrostatic pressure in the disposal drift is calculated as follows: The floor of the drift is at a depth of 500 m. For simplicity it is assumed that up to the top of the salt formation at about 200 m depth the mine is filled with NaCl solution with a density of 1193 kg/m^3. Above that level up to the surface there is water with a density of 1000 kg/m^3. This yields a hydrostatic pressure of 5.47 MPa at the reference level, which is the floor of the drift.

The potential gas-storage volume is estimated from the pore space in the waste and from the residual gas saturation of the backfill material. Different constant fractions f_{Gas} of the pore volume are derived as gas-storage volume. For test cases 2a, 4a, 5a and 6a gas storage is neglected. For test case 1 and 3 the residual gas saturation in the pore volume of backfill has been considered for gas storage, only, while for test cases 2b, 4b, 5b and 6b additional gas storage in the waste containers is assumed. These data for f_{Gas} are listed in Table 2.4.

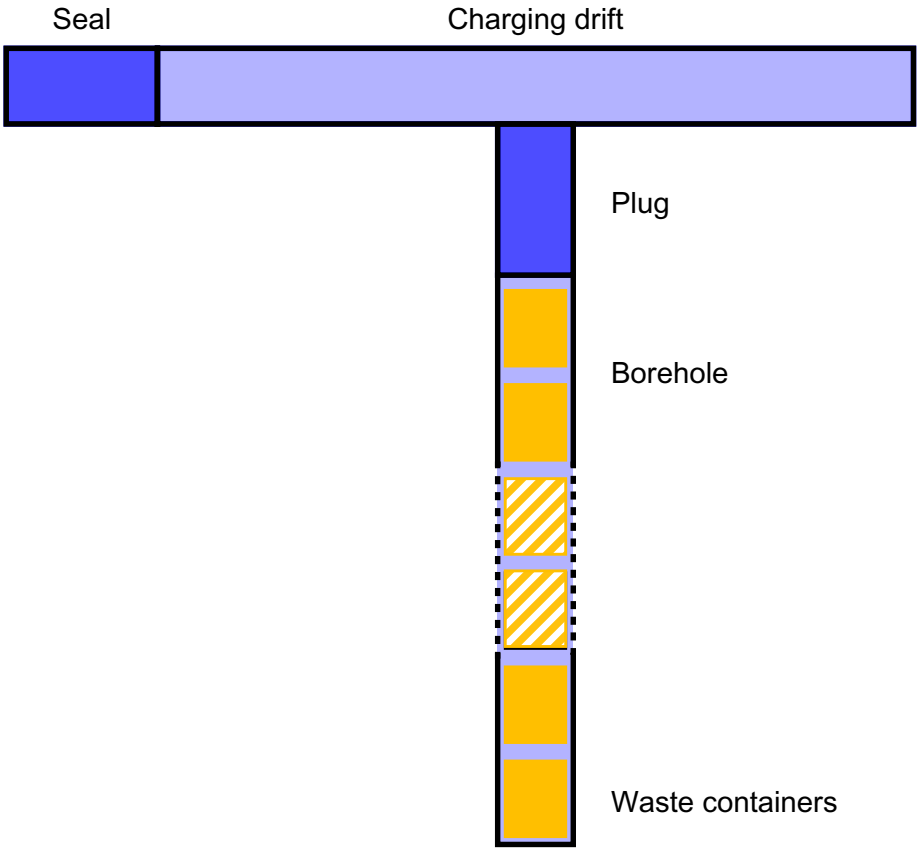

Fig. 2.3 Schematic representation of the simplified repository model

Tab. 2.1 General data for the test cases

Parameter	Dimension	Value
Viscosity of brine μ	Pa·s	$1{,}9 \cdot 10^{-3}$
Density of brine ρ_L	kg/m^3	1193
Density of rock ρ_S	kg/m^3	2168
Density of metal ρ_{Fe}	kg/m^3	7900
Reference level z_{ref}	m to surface	500
Atmospheric pressure p_{atm}	MPa	0,1013
Rock pressure at reference level $p_{P,r}$	MPa	10,65
Hydrostatic pressure at reference level p_{hyd}	MPa	5,47

Tab. 2.2 Data for metal corrosion and gas production

Parameter	Dimension	Value
Initial value of iron mass m_0	kg	92 640
Corrosion rate u	1/a	$4.0 \cdot 10^{-3}$
Number of moles H_2-gas per kg corroded metal Γ_M	mol/kg	23.875
Number of moles H_2O per m^3 of brine	mol/m^3	48 586
Volume increase factor of solid material g_c	-	2.668

Tab. 2.3 Geometrical data

Parameter	Dimension	Value
Radius of the disposal borehole	m	0.30
Length of the disposal borehole	m	318.0
Initial porosity of borehole backfill	-	0.30
Radius of the borehole plug	m	0.30
Length of the borehole plug	m	10.0
Initial porosity of plug material	-	0.20
Initial brine volume test case 1, 3	m^3	14.17
Cross section of the charging drift	m^2	23.0
Length of the charging drift	m	50.0
Initial porosity of drift backfill	-	0.40
Cross section of the drift sealing	m^2	23.0
Length of the drift sealing	m	10.0
Porosity of the drift sealing	-	0.20
Permeability of the drift sealing	m^2	$1.0 \cdot 10^{-12}$
Initial waste volume	m^3	30.966
Initial pore volume in the waste	m^3	9.000

2.2.1 Test case 1

In test case 1, a disposal borehole is considered in which the gas-storage volume in backfill and waste is completely filled with air at a gas pressure of 0,1 MPa. The rest of the pore volume in the backfill and in the waste containers is filled with brine at t = 0. The

Tab. 2.4 Gas storage fractions

Test case (borehole)	f_{Gas}		Test case (drift)	f_{Gas}
Test case 1	0.388		Test case 5a	0.000
Test case 2a	0.000		Test case 5b	0.133
Test case 2b	0.450		Test case 6a	0.000
Test case 3	0.388		Test case 6b	0.133
Test case 4a	0.000			
Test case 4b	0.450			

Tab. 2.5 Data used in convergence formula and permeability-porosity relation [2]

Parameter	Dimension	Value
Reference value of convergence rate K_{ref}	1/a	$1.0 \cdot 10^{-6}$
Stress exponent m	-	5
Initial convergence rate at reference level K_0	1/a	$1.0 \cdot 10^{-3}$
Parameter of the convergence formula h_1	-	-2.00
Parameter of the convergence formula g_1	-	-1.00
Parameter in convergence formula g_2 dry backfill	-	10.0
Parameter in convergence formula g_2 wet backfill	-	1000.0
Reference porosity φ_r	-	0.30
Parameter k_0 of the permeability-porosity relation	m^2	$4.86 \cdot 10^{-10}$
Exponent n of the permeability-porosity relation	-	4.714

neighbouring drift does not contain any liquid which implies that the consumed water during corrosion will not be replaced. The generated gas is assumed to escape through the borehole plug without resistance. At first, no convergence of the salt is assumed.

Fig. 2.4 shows the time evolution of the volumes of the borehole, the pores, the brine, the solid material in m^3 and the average porosity. Since no convergence is assumed, the total volume of the disposal borehole remains constant. As long as there is liquid for the corrosion process, the volumes of the pores and of the liquid are reduced while the volume of the solid material is increased. After approximately 93.3 years, the liquid is consumed.

At that time, no corrosion occurs any more and the pore volume and the solid material volume remain constant. Table 2.6 summarises the results of the calculation in terms of volume balances.

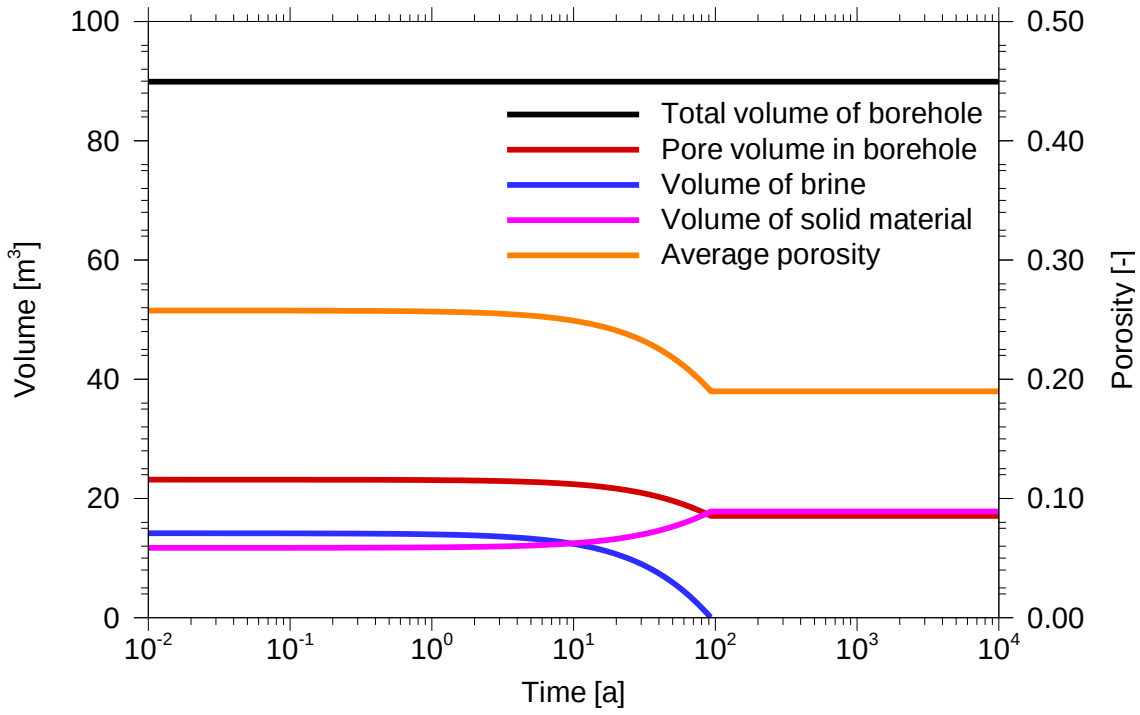

Fig. 2.4 Test case 1: time evolution of volumes and porosity

Tab. 2.6 Results of test case 1

Time [a]	0.0	93.3	10 000
	Volume [m^3]		
Total volume of the disposal borehole	89.91	89.91	89.91
Pore volume	23.17	17.08	17.08
Volume of brine	14.17	0.00	0.00
Volume of brine squeezed out into the drift	0.00	0.00	0.00
Volume of brine replenished from the drift	0.00	0.00	0.00
Volume of brine used for corrosion	-	14.17	-
Increase of the volume of solid material	-	6.09	-
Volume of solid material	11.73	17.82	17.82

Fig. 2.5 shows the fluid pressure in the disposal borehole in MPa and the gas production rate in mol/a. With decreasing fluid level in the disposal borehole, the fluid pressure reduces since the generated gas can escape without resistance. After consumption of the brine the gas generation stops, i.e. the gas production rate is zero.

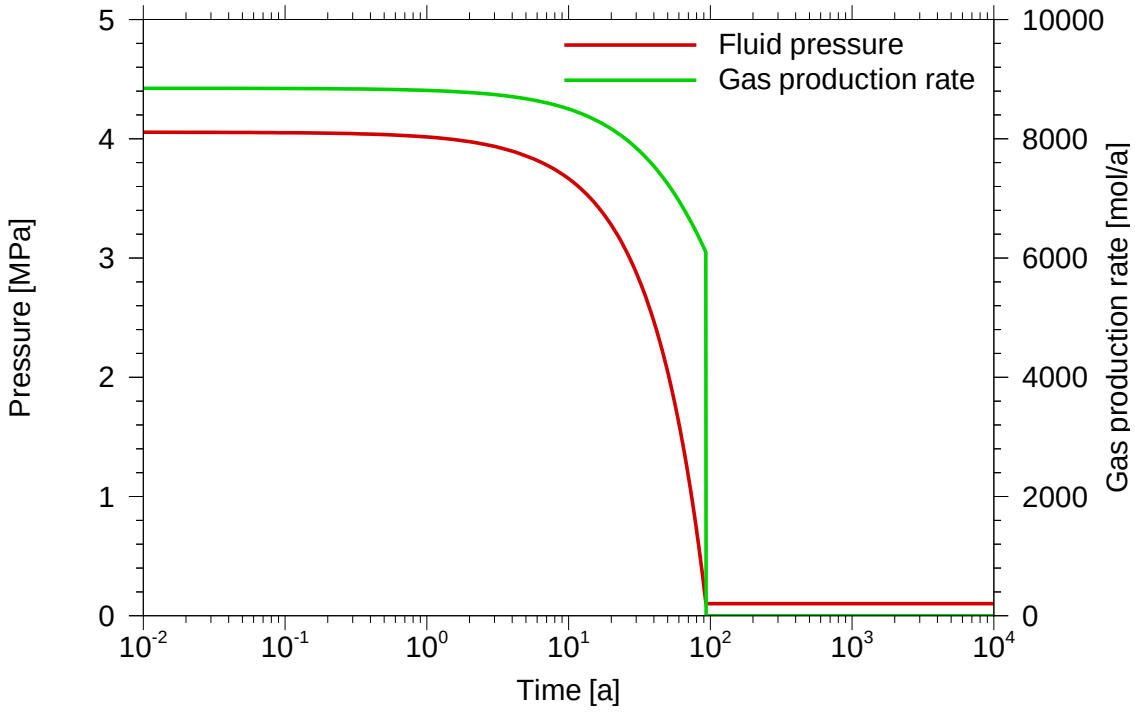

Fig. 2.5 Test case 1: time evolution of fluid pressure and gas production rate

2.2.2 Test case 2a

In test case 2a, a disposal borehole is considered in which no gas storage is initially assumed. Therefore, the total pore volume is filled with brine at $t = 0$. The neighbouring drift is also filled with brine and has a hydrostatic pressure. During corrosion of the metal water is consumed which is replenished by brine from the charging drift. At the same time, the volume of the solid material increases which leads to a reduction of the pore volume and the brine in the disposal borehole. Fig. 2.6 shows the time evolution of volumes of the borehole, the pores, the brine and the solid material in m^3 and the average porosity. Table 2.7 summarises the results of the calculation in terms of volume balances.

Fig. 2.7 shows the flow of brine between disposal borehole and charging drift in m^3/a. This brine replaces the water consumed by corrosion.

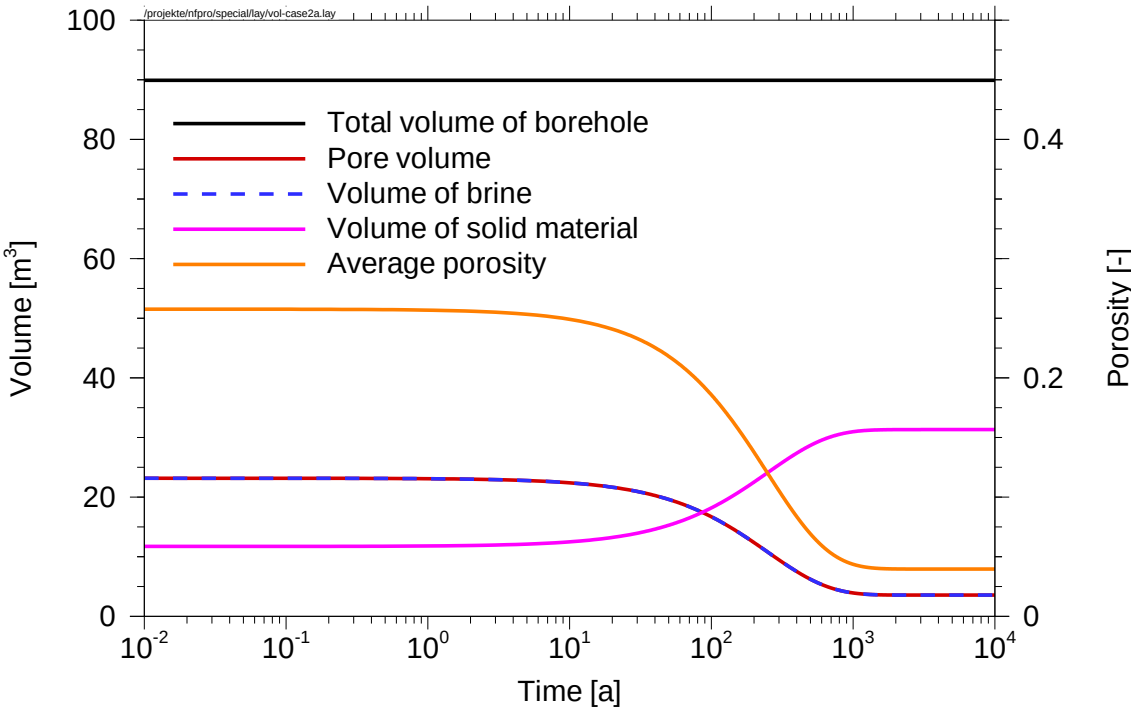

Fig. 2.6 Test case 2a: time evolution of volumes and porosity

Tab. 2.7 Results of test case 2a without gas storage

Time [a]	0,0		10 000
	Volume [m^3]		
Total volume of the disposal borehole	89.91		89.91
Pore volume	23.17		3.57
Volume of gas	0.00		0.00
Volume of brine	23.17		3.57
Volume of brine squeezed out into the drift	0.00		0.00
Volume of brine replenished from the drift	0.00		26.01
Volume of brine used for corrosion			45.61
Increase of the volume of solid material			19.60
Volume of solid material	11.73		31.33

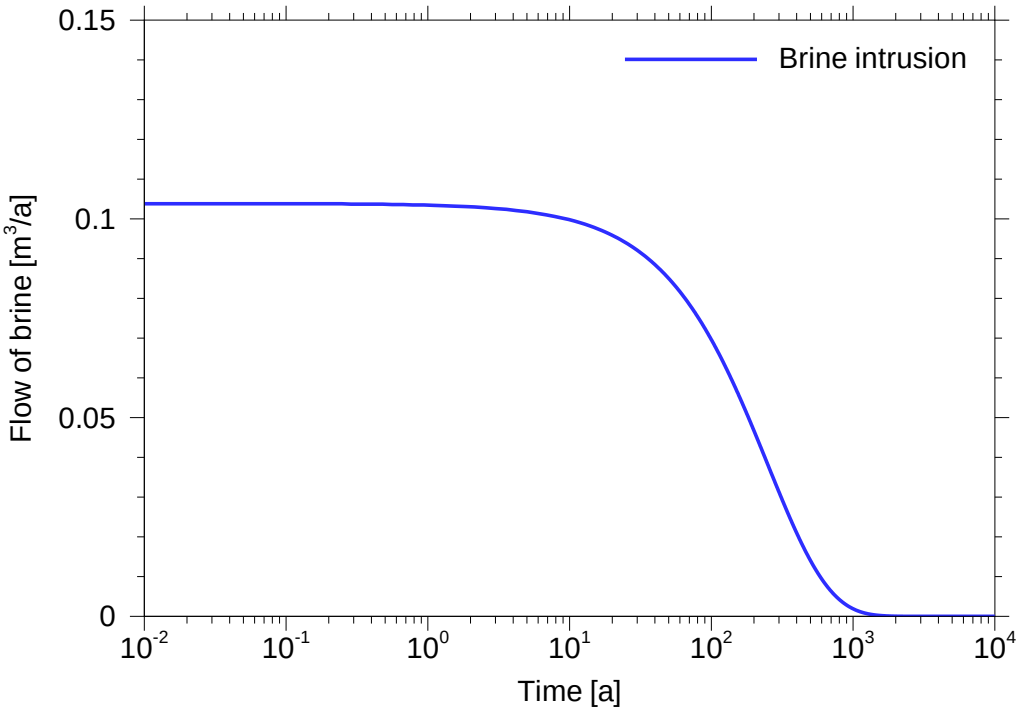

Fig. 2.7 Test case 2a: Flow of brine between disposal borehole and charging drift

2.2.3 Test case 2b

In test case 2b, a gas-storage volume in the disposal borehole is considered. The gas-storage volume is initially filled with air at atmospheric pressure. During the instantaneous flooding of the disposal borehole and of the charging drift with brine, the air trapped in the storage volume is compressed. Since the gas is assumed to be uniformly distributed along the disposal borehole, the gas pressure corresponds to the respective hydrostatic pressure. As a result, after flooding of the disposal borehole with brine the gas storage is no more completely filled with gas. The progressing gas generation tends to replenish the gas-storage volume, whereby brine is squeezed out of the disposal borehole.

After replenishment of the gas storage volume, the further generated gas can escape from the disposal borehole. The consumed water during corrosion of the iron is then replaced by brine from the neighbouring drift. The inflow is limited by the generated gas and increased volume of solid material.

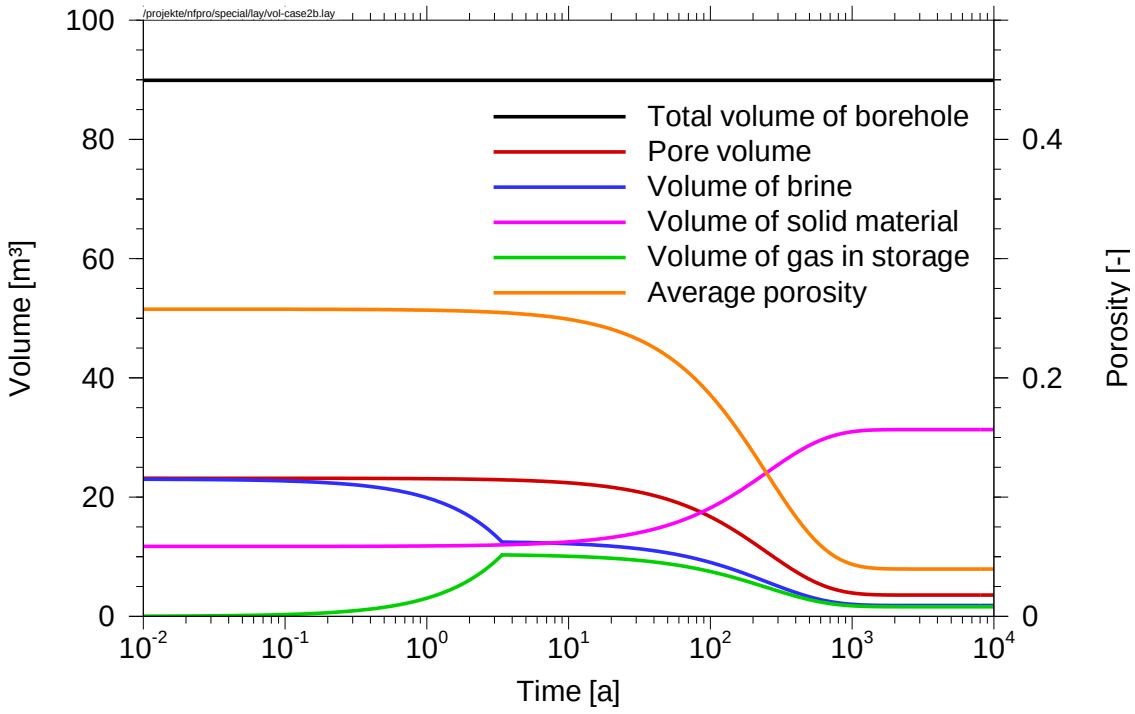

Fig. 2.8 Test case 2b: time evolution of volumes and porosity

Tab. 2.8 Results of test case 2b with gas storage

Time [a]	0.0	3.4	10 000
	Volume [m^3]		
Total volume of the disposal borehole	89.91	89.91	89.91
Pore volume	23.17	22.91	3.58
Volume of gas	0.17	10.31	1.61
Volume of brine	23.00	12.60	1.97
Volume of brine squeezed out into the drift	0.00	9.82	9.82
Volume of brine replenished from the drift	0.00	0.00	34.37
Volume of brine used for corrosion		0.58	45.58
Increase of the volume of solid material		0.26	19.59
Volume of solid material	11.73	11.99	31.32

Fig. 2.8 shows the time evolution of the volumes of the borehole, the pores, the brine, the gas in storage, the solid material in m^3 and of the average porosity. Table 2.8 summarises the results of the calculation in terms of volume balances.

Fig. 2.9 shows the fluid pressure in the disposal borehole in MPa, the gas production rate and the flow of gas from the disposal borehole in mol/a. After approximately 3.4 a, the gas release from the disposal borehole starts since the storage volume is filled with gas. The flow of gas is somewhat greater than the gas production rate due to the volume increase of the solid material which causes gas extrusion.

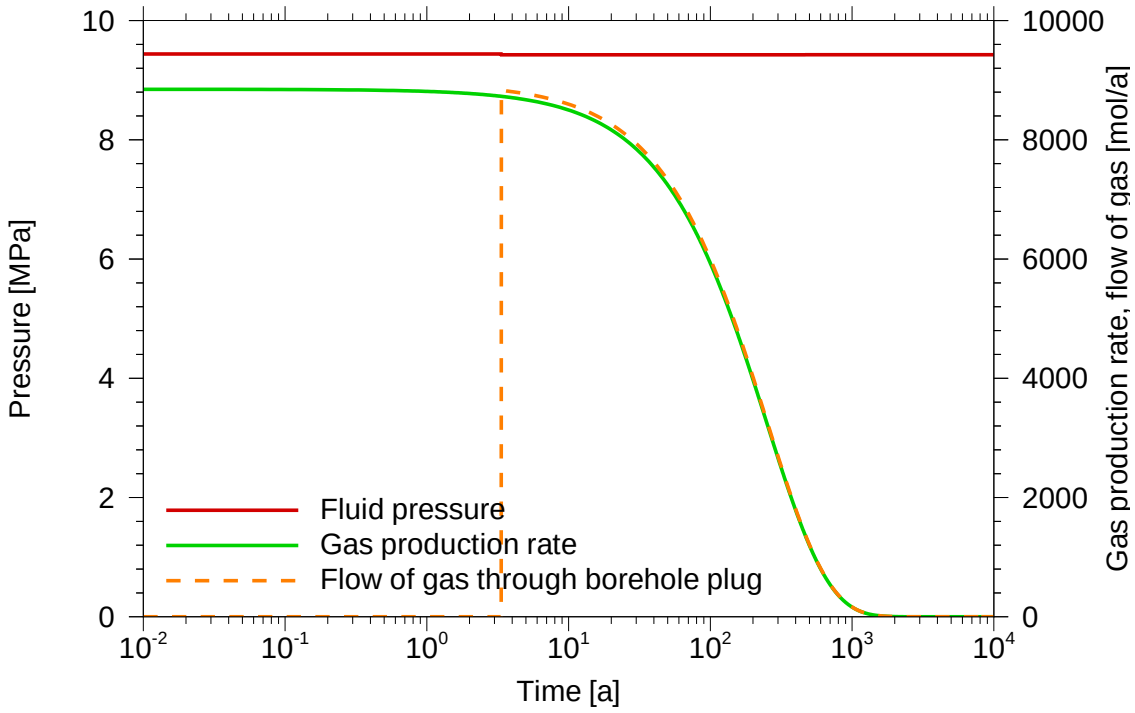

Fig. 2.9 Test case 2b: time evolution of fluid pressure and gas release

In Fig. 2.10 the flow of brine between disposal borehole and charging drift is given in m^3/a. As long as the gas-storage volume is not completely filled, the displacement of brine by gas outbalances the water consumption. A flow of brine of approximately 3 m^3/a from the disposal borehole is observed. After replenishment of the gas-storage volume, the further generated gas can escape from the disposal borehole. The consumed water is replaced by inflowing brine of about 0.14 m^3/a from the charging drift.

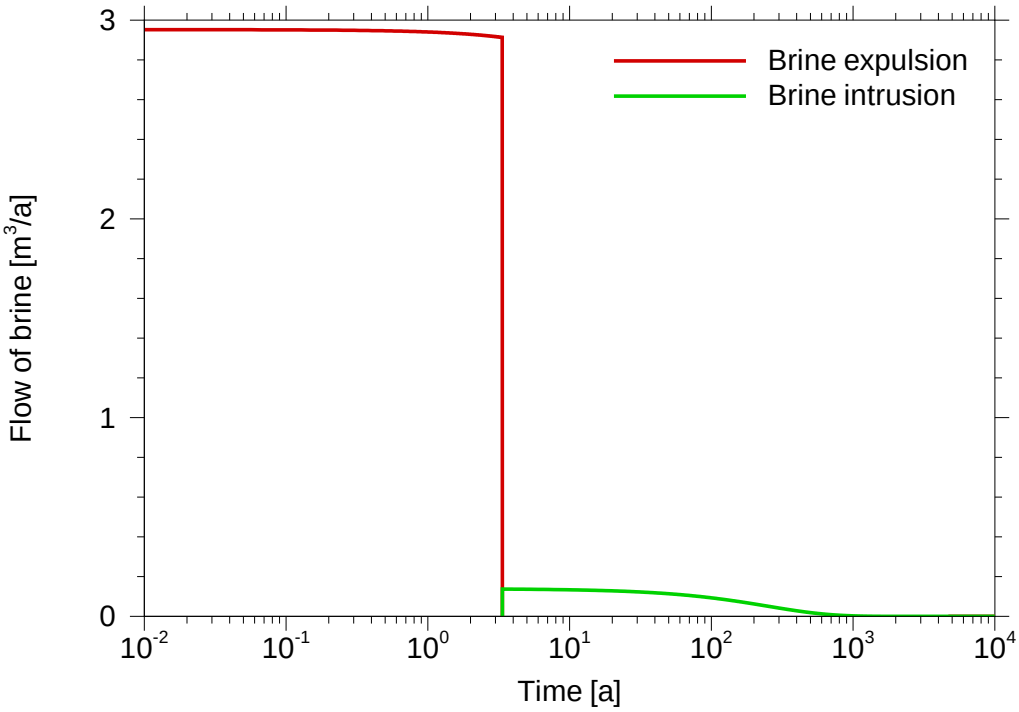

Fig. 2.10 Test case 2b: Flow of brine between disposal borehole and charging drift

2.2.4 Test case 3

The test case 3 corresponds to the first one with the difference that the convergence of the salt formation is considered using the approach described in [1], [2] and the parameters listed in Table 2.5. Fig. 2.11 shows the time evolution of the volumes of the borehole, the pores, the brine, the solid material in m^3 and of the average porosity.

Table 2.9 summarises the results of the calculation in terms of volume balances. In contrast to test case 1, the total volume of the disposal borehole is changed by convergence. However, since sufficient pore volume without liquid is available, the balances of the solid material and liquid are the same as in test case 1. The total volume and the pore volume reduce by 9.34 m^3 within 10 000 a due to the convergence.

Fig. 2.12 shows the fluid pressure in the disposal borehole in MPa and the gas production rate in mol/a. With decreasing fluid level in the disposal borehole, the fluid pressure reduces since the generated gas can escape without resistance. After consumption of the brine gas is not generated any more.

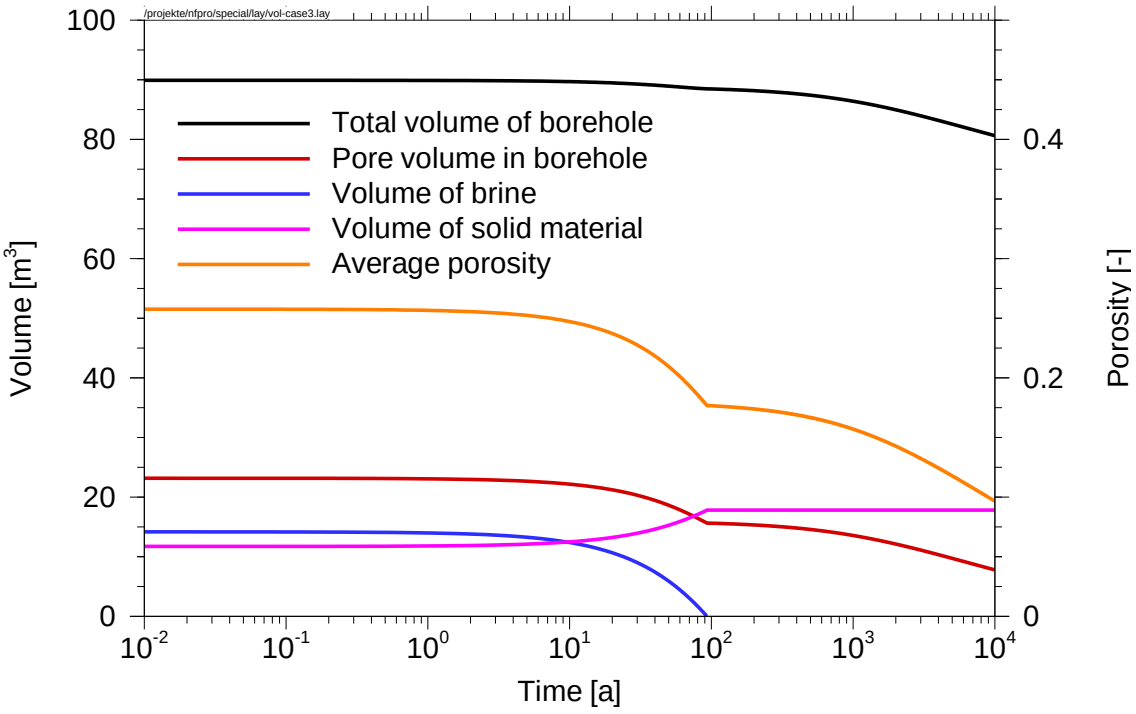

Fig. 2.11 Test case 3: time evolution of volumes and porosity

Tab. 2.9 Results of test case 3

Time [a]	0.0	93.3	10 000
	Volume [m^3]		
Total volume of the disposal borehole	89.91	87.89	80.57
Pore volume	23.17	15.06	7.73
Volume of brine	14.17	0.00	0.00
Volume of brine squeezed out into the drift	0.00	0.00	0.00
Volume of brine replenished from the drift	0.00	0.00	0.00
Volume of brine used for corrosion		14.17	
Increase of the volume of solid material		6.09	
Volume of solid material	11.73	17.82	17.82

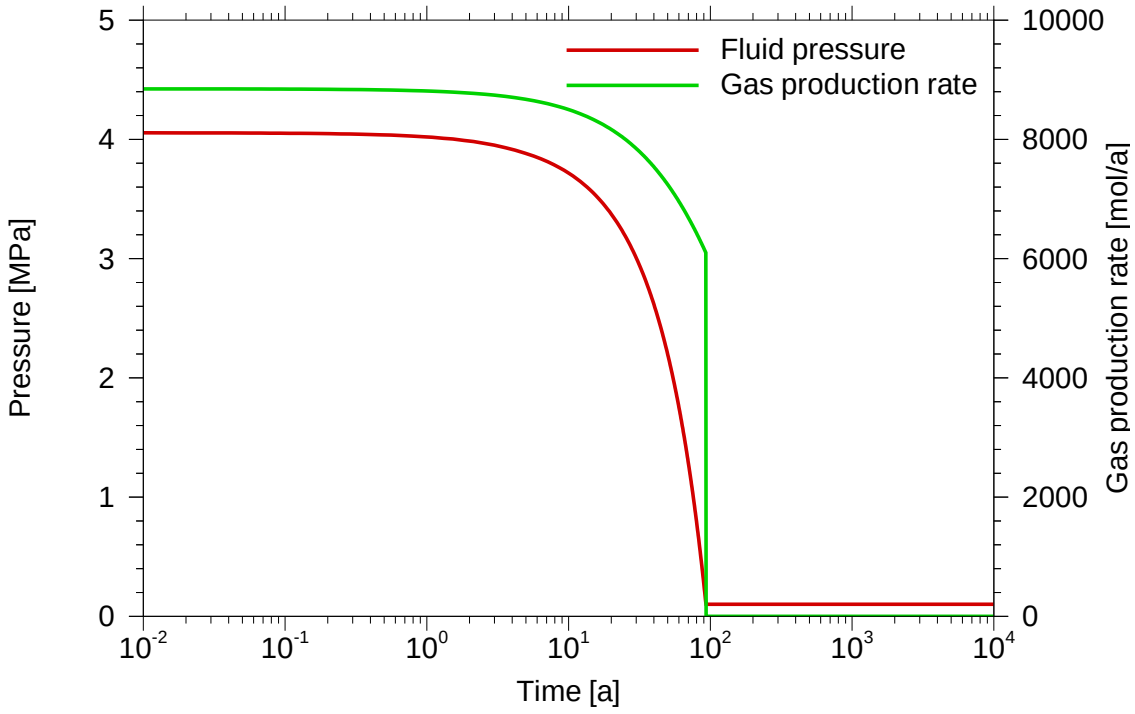

Fig. 2.12 Test case 3: time evolution of fluid pressure and gas production rate

2.2.5 Test case 4a

Test case 4a corresponds to test case 2a, but convergence of the salt formation is considered. Fig. 2.13 shows the time evolution of the volumes of the borehole, the pores, the brine, the solid material in m^3 and of the average porosity. In contrast to test case 2a, the total volume of the disposal borehole in test case 4a changes by convergence.

Table 2.10 summarises the results of the calculation in terms of volume balances. The total volume is reduced by only approximately 1.05 m^3 within 10 000 a by convergence. This amount is significantly smaller than that of test case 3 due to the greater fluid pressure in the disposal borehole which impedes convergence. In comparison to test case 2a, less brine flows from the charging drift into the disposal borehole. Accordingly, less brine remains in the disposal borehole at the end of the simulation.

Fig. 2.14 shows the brine flow between the disposal borehole and the charging drift in m^3/a. The water consumed by corrosion is replaced by this inflowing brine from the charging drift. After about 1800 years, a small amount of liquid, which was not needed for the corrosion, is squeezed out of the disposal borehole by convergence.

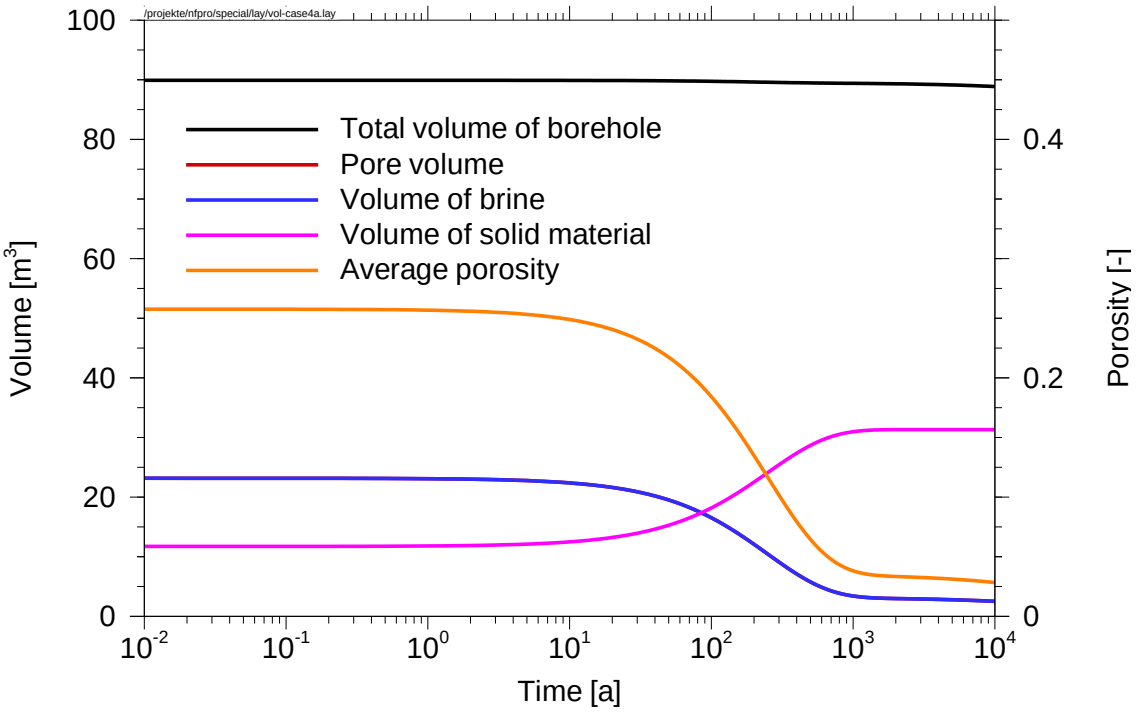

Fig. 2.13 Test case 4a: time evolution of volumes and porosity

Tab. 2.10 Results of test case 4a without gas storage

Time [a]	0.0		10 000
	Volume [m^3]		
Total volume of the disposal borehole	89.91		88.86
Pore volume	23.17		2.52
Volume of gas	0.00		0.00
Volume of brine	23.17		2.52
Volume of brine squeezed out into the drift	0.00		0.46
Volume of brine replenished from the drift	0.00		25.42
Volume of brine used for corrosion			45.61
Increase of the volume of solid material			19.59
Volume of solid material	11.73		31.32

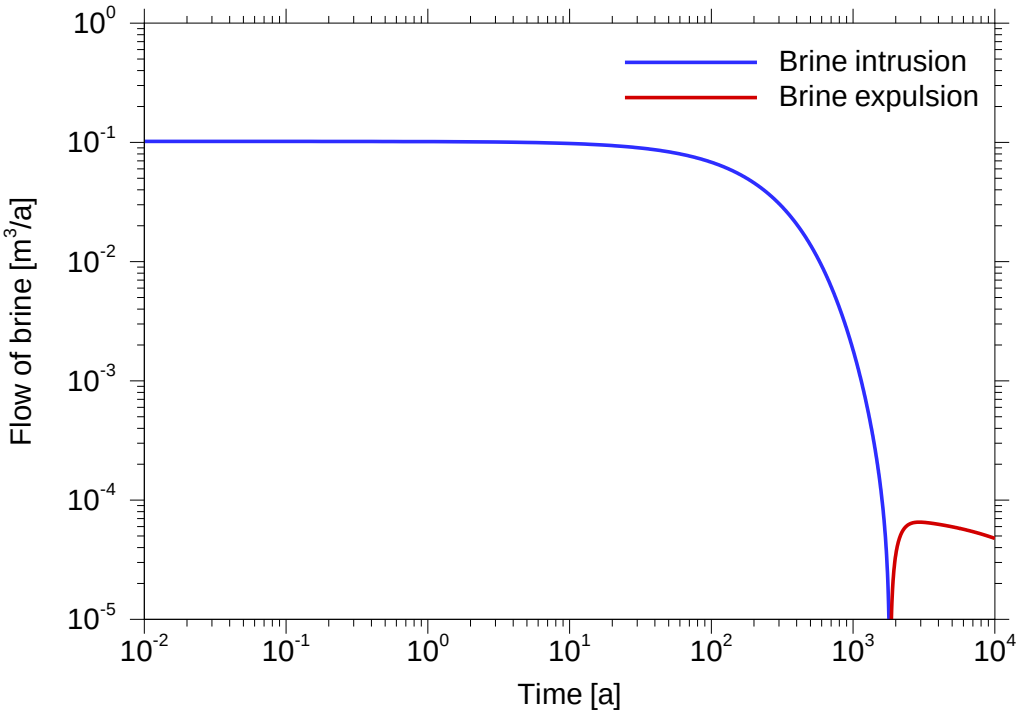

Fig. 2.14 Test case 4a: Flow of brine between disposal borehole and charging drift

2.2.6 Test case 4b

Test case 4b corresponds to test case 2b, but convergence of the salt formation is considered. Fig. 2.15 shows the time evolution of the volumes of the borehole, the pores, the brine, the gas in storage, the solid material in m^3 and of the average porosity. In contrast to test case 2b, the total volume of the disposal borehole changes by convergence.

Table 2.11 summarises the results of the calculation in terms of volume balances. The total volume is reduced by only 1.05 m^3 within 10 000 a by convergence. Correspondingly smaller is the pore volume at the end of the simulation.

Fig. 2.16 shows the fluid pressure in the disposal borehole in MPa, the gas production rate and the flow of gas from the disposal borehole in mol/a. After approximately 3.4 a, gas is released from the disposal borehole because the gas in storage is replenished. The flow of gas is somewhat greater than the gas production rate due to increase of the volume of the solid material and convergence, which cause gas extrusion.

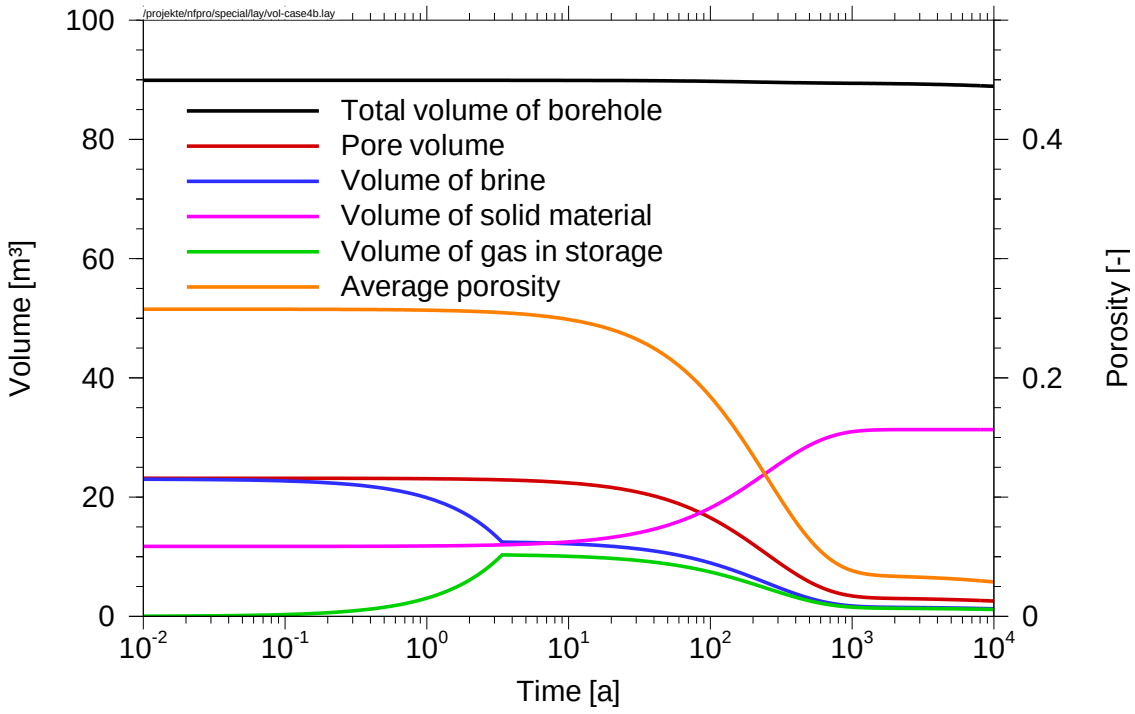

Fig. 2.15 Test case 4b: time evolution of volumes and porosity

Tab. 2.11 Results of test case 4b with gas storage

Time [a]	0.0	3.4	10 000
	Volume [m^3]		
Total volume of the disposal borehole	89.91	89.91	88.86
Pore volume	23.17	22.90	2.52
Volume of gas	0.17	10.30	1.13
Volume of brine	23.00	12.61	1.39
Volume of brine squeezed out into the drift	0.00	9.82	10.06
Volume of brine replenished from the drift	0.00	0.00	34.04
Volume of brine used for corrosion		0.57	45.59
Increase of the volume of solid material		0.26	19.59
Volume of solid material	11.73	11.99	31.32

Fig. 2.17 shows the brine flow between the disposal borehole and the charging drift in m^3/a. As long as the gas-storage volume is not completely filled, the displacement of brine by gas outbalances the water consumption. A brine flow from the disposal borehole of about 3 m^3/a is observed. After replenishment of the gas-storage volume, the gas gen-

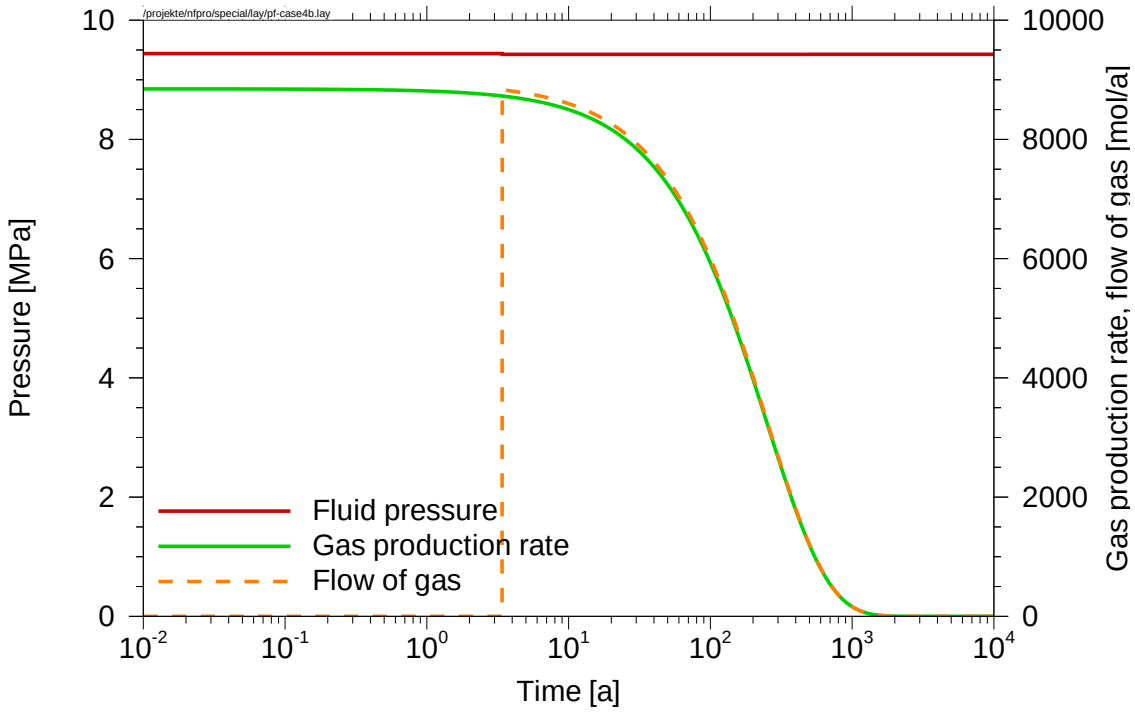

Fig. 2.16 Test case 4b: time evolution of fluid pressure and gas release

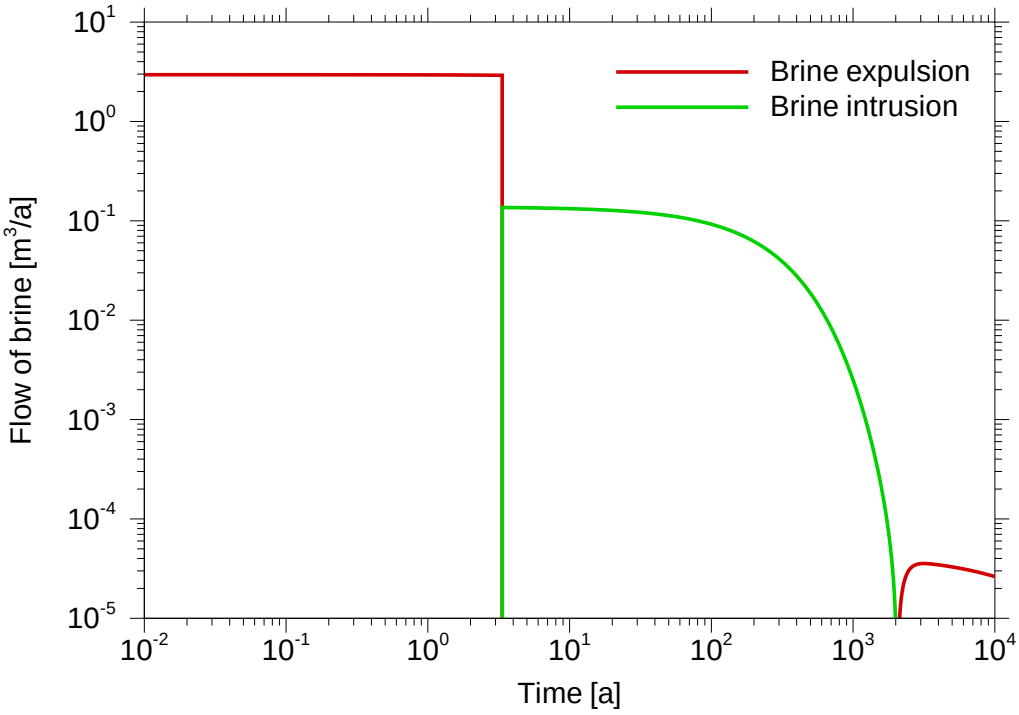

Fig. 2.17 Test case 4b: Flow of brine between disposal borehole and charging drift

erated further can be released. Until replenishment of the gas-storage volume approximately 9.82 m^3 of brine is squeezed out into the charging drift. After that, the water consumed by corrosion is replaced by inflowing brine from the charging drift. After approximately 2050 a, a small amount of liquid which is not used for corrosion is squeezed out from the disposal borehole by convergence.

2.2.7 Test case 5a

In test case 5a, a disposal drift is considered in which initially no gas in the gas storage is assumed. Therefore, the total pore volume is filled with brine at t = 0. The neighbouring charging drift is also filled with brine. Both drifts have a hydrostatic pressure. During metal corrosion water is consumed which is replenished by brine from the charging drift. At the same time, the volume of solid material increases, whereby the pore volume which is available for the brine is reduced. Fig. 2.18 shows the time evolution of the volumes of the disposal drift, the pores, the brine, the solid material in m^3 and of the average porosity. Table 2.12 summarises the results of the calculation in terms of volume balances.

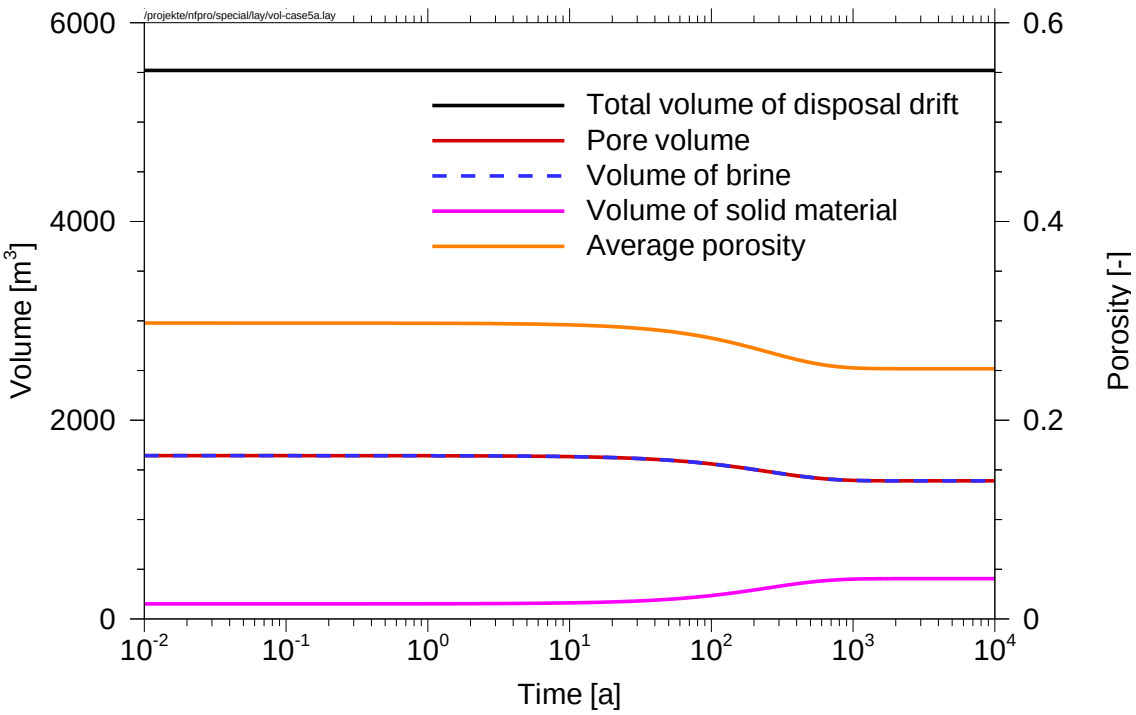

Fig. 2.18 Test case 5a: time evolution of volumes and porosity

Tab. 2.12 Results of test case 5a without gas storage

Time [a]	0.0		10 000
	Volume [m^3]		
Total volume of the disposal drift	5520		5520
Pore volume	1644		1390
Volume of gas	0.00		0.00
Volume of brine	1644		1390
Volume of brine squeezed out into the charging drift	0.00		0.00
Volume of brine replenished from the charging drift	0.00		336
Volume of brine used for corrosion			590
Increase of the volume of solid material			253
Volume of solid material	152		405

Fig. 2.19 shows the flow of brine between disposal drift and charging drift in m^3/a. This brine replaces the water consumed by corrosion. The flow of brine is initially approximately 1.3 m^3/a.

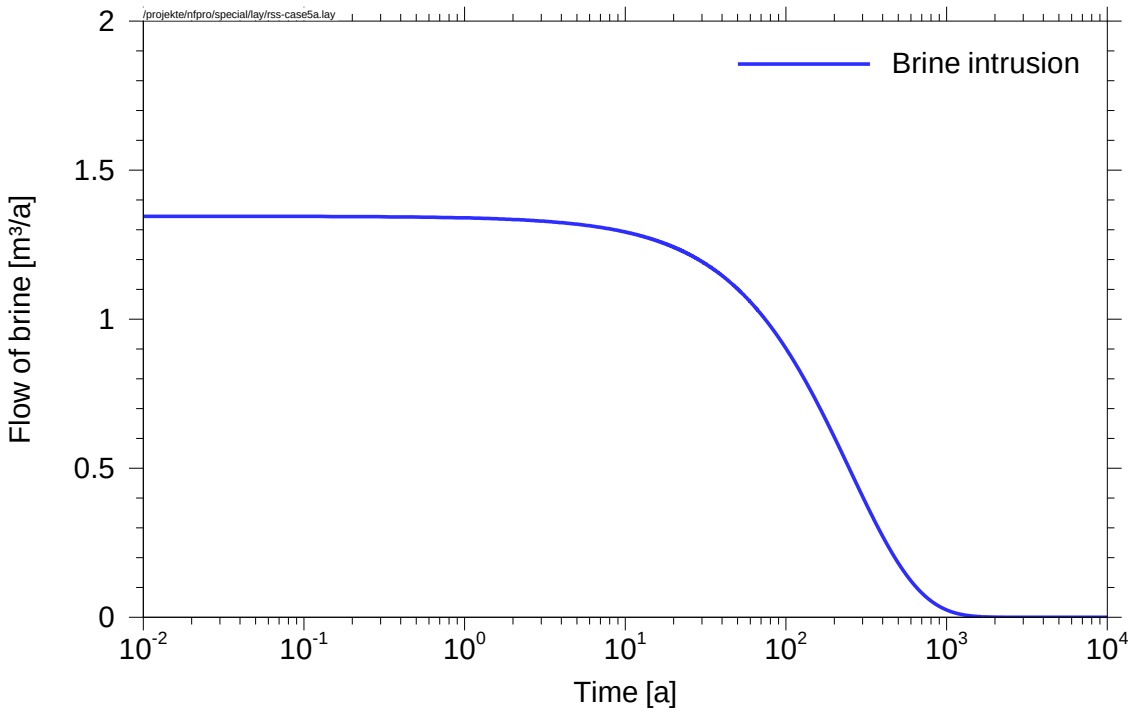

Fig. 2.19 Test case 5a: Flow of brine between disposal drift and charging drift

2.2.8 Test case 5b

In test case 5b, a gas-storage volume in the disposal drift is considered. The gas-storage volume is initially filled with air at atmospheric pressure. During the instantaneous flooding of the charging drift and the disposal drift with brine, the air trapped in the storage volume is compressed. As a result, after flooding of the drifts the gas storage in the disposal drift is no more completely filled with gas. The progressive gas generation tends to replenish the gas-storage volume, whereby brine is squeezed out of the disposal drift. Gas storage in the charging drift is not considered in the test cases.

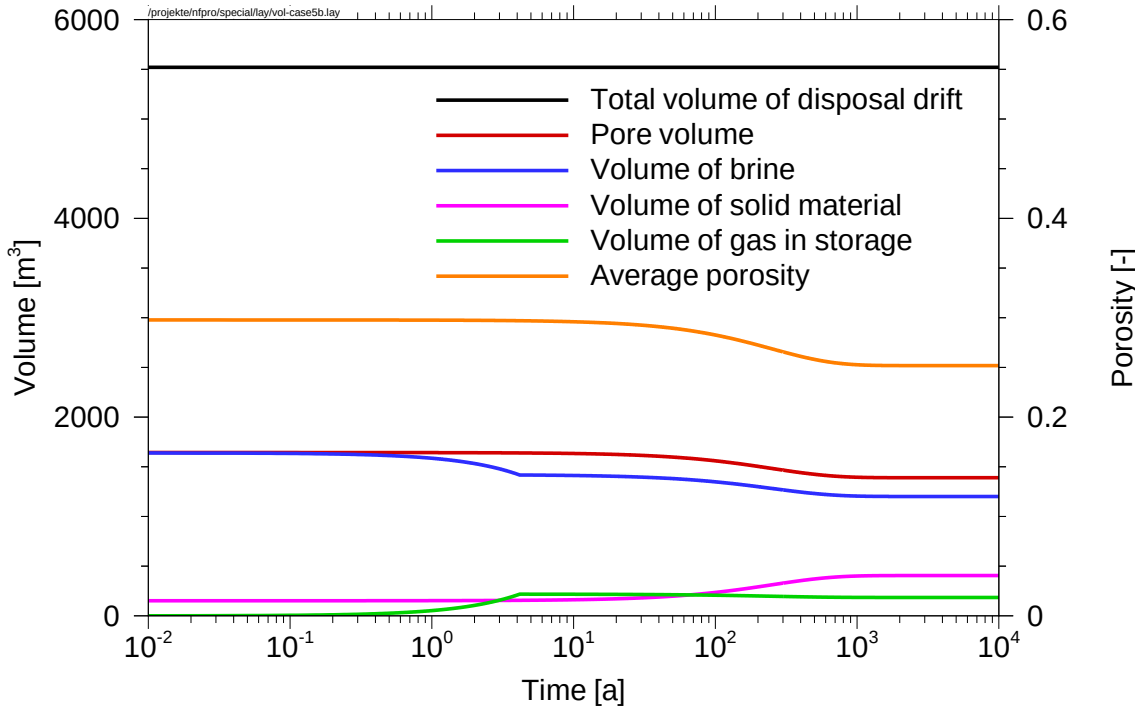

Fig. 2.20 Test case 5b: time evolution of volumes and porosity

After replenishment of the gas-storage volume, the further generated gas can escape from the disposal drift. The consumed water during corrosion of the iron is then replaced by brine from the neighbouring charging drift. The inflow is limited by the generated gas and increased volume of solid material.

Fig. 2.20 shows the time evolution of the volumes of the disposal drift, the pores, the brine, the gas in storage, the solid material in m^3 and of the average porosity. Table 2.13 summarises results of the calculation in terms of volume balances.

Tab. 2.13 Results of test case 5b with gas storage

Time [a]	0,0	4,0	10 000
	Volume [m^3]		
Total volume of the disposal drift	5520	5520	5520
Pore volume	1644	1640	1390
Volume of gas	5	218	185
Volume of brine	1639	1422	1205
Volume of brine squeezed out into the charging drift	0.00	208	208
Volume of brine replenished from the charging drift	0.00	0.00	364
Volume of brine used for corrosion		9	590
Increase of the volume of solid material		4	253
Volume of solid material	152	156	405

Fig. 2.21 shows the fluid pressure in the disposal drift in MPa, the gas production rate and the flow of gas from the disposal drift in mol/a. After approximately 4 years, the gas release from the disposal drift starts since the storage volume is filled with gas. The gas flow is somewhat greater than the gas production rate due to the volume increase of the solid material which causes gas extrusion.

In Fig. 2.22 the flow of brine between the disposal drift and charging drift is given in m^3/a. As long as the gas-storage volume is not completely filled, the displacement of brine by gas outbalances the water consumption. A flow of brine from the disposal drift of initially approximately 53 m^3/a is observed. After replenishment of the gas-storage volume, the further generated gas can escape. The consumed water is replaced by inflowing brine of about 1.5 m^3/a from the charging drift.

2.2.9 Test case 6a

Test case 6a corresponds to test case 5a, but convergence of the rock formation is considered. Fig. 2.23 shows the time evolution of the volumes of the disposal drift, the pores, the brine, the solid material in m^3 and of average porosity. In contrast to test case 5a, the total volume of the disposal drift changes by convergence.

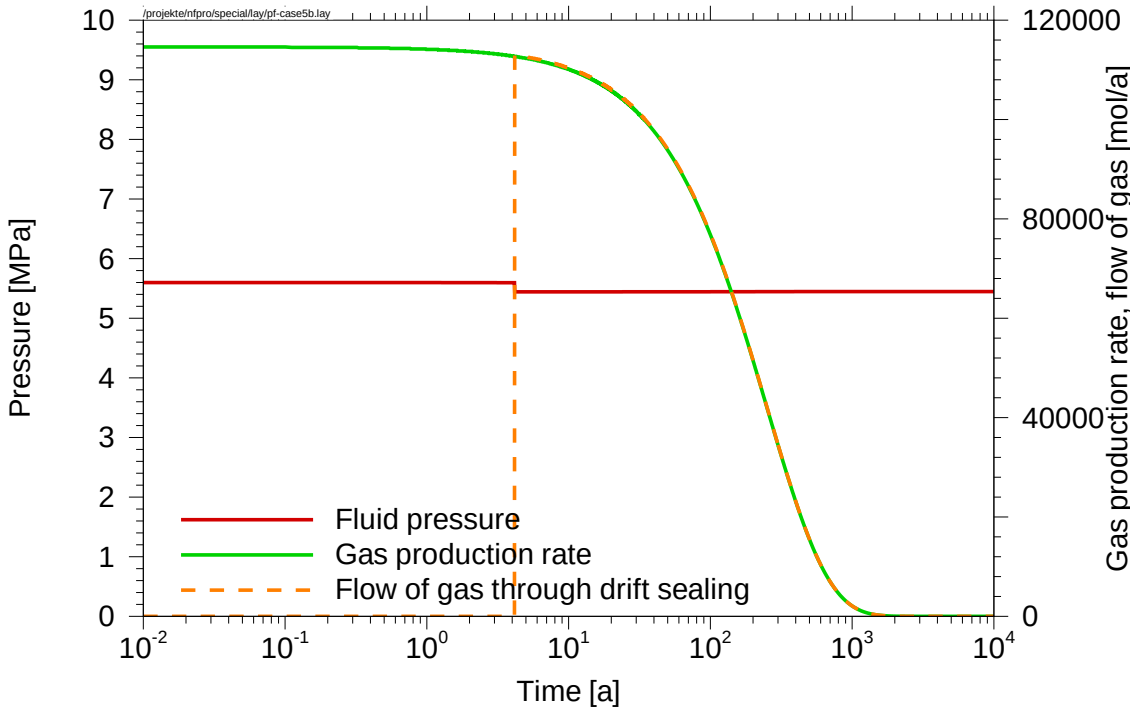

Fig. 2.21 Test case 5b: time evolution of fluid pressure and gas release

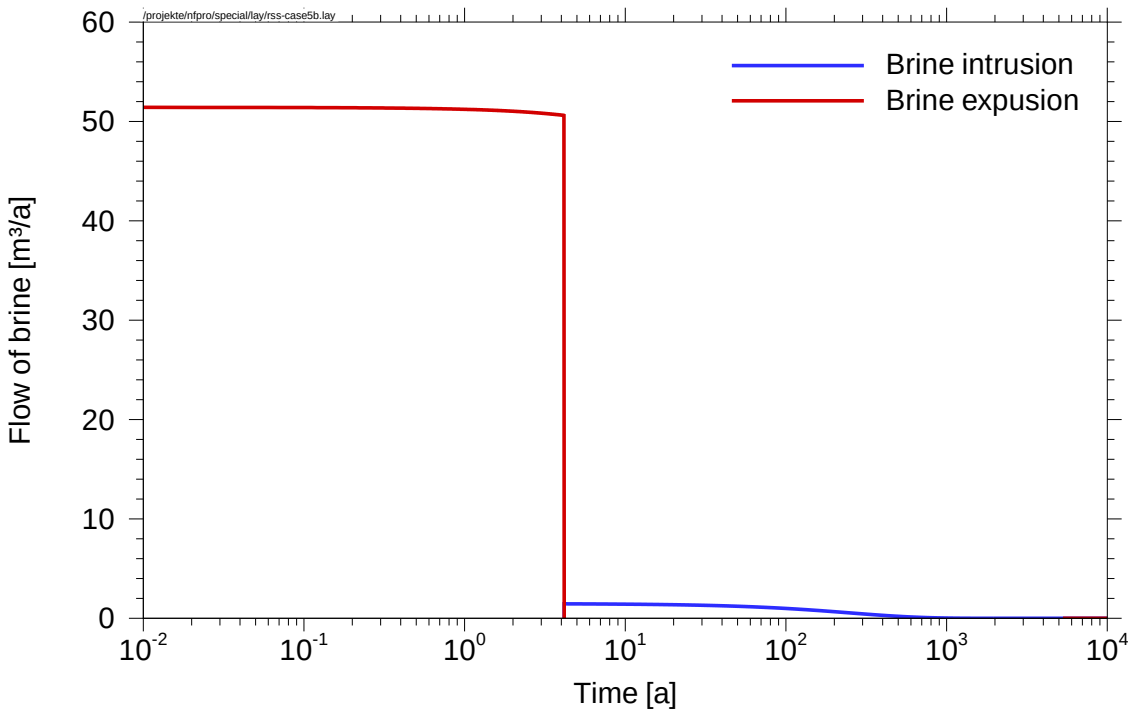

Fig. 2.22 Test case 5b: Flow of brine between disposal drift and charging drift

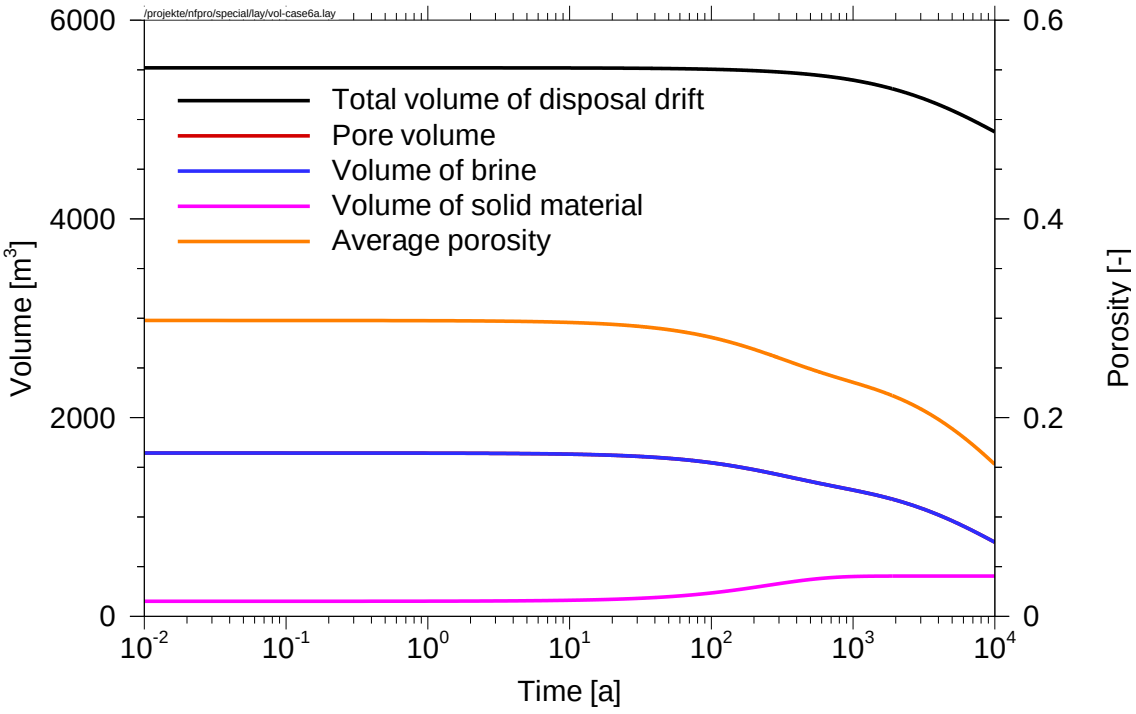

Fig. 2.23 Test case 6a: time evolution of volumes and porosity

Tab. 2.14 Results of test case 6a without gas storage

Time [a]	0.0	606	10 000
	Volume [m^3]		
Total volume of the disposal drift	5520	5440	4875
Pore volume	1644	1333	745
Volume of gas	0.00		0.00
Volume of brine	1644	1333	745
Volume of brine squeezed out into the charging drift	0.00	0.00	536
Volume of brine replenished from the charging drift	0.00	227	227
Volume of brine used for corrosion		538	590
Increase of the volume of solid material		231	253
Volume of solid material	152	383	405

Table 2.14 summarises the results of the calculation in terms of volume balances. The total volume is reduced by about 645 m^3 within 10 000 a by convergence. In comparison to test case 5a, less brine from the charging drift enters into the disposal drift. As a result, less brine is kept in the disposal drift at the end of the simulation. From approximately 606

to 10 000 a, an amount of liquid of approximately 536 m^3 in total is squeezed out of the disposal drift by convergence. Thus, less water is consumed by corrosion compared to what the reduction in pore volume can provide.

Fig. 2.24 shows the flow of brine between the drifts in m^3/a. The water consumed by corrosion is replaced by this inflowing brine from the charging drift.

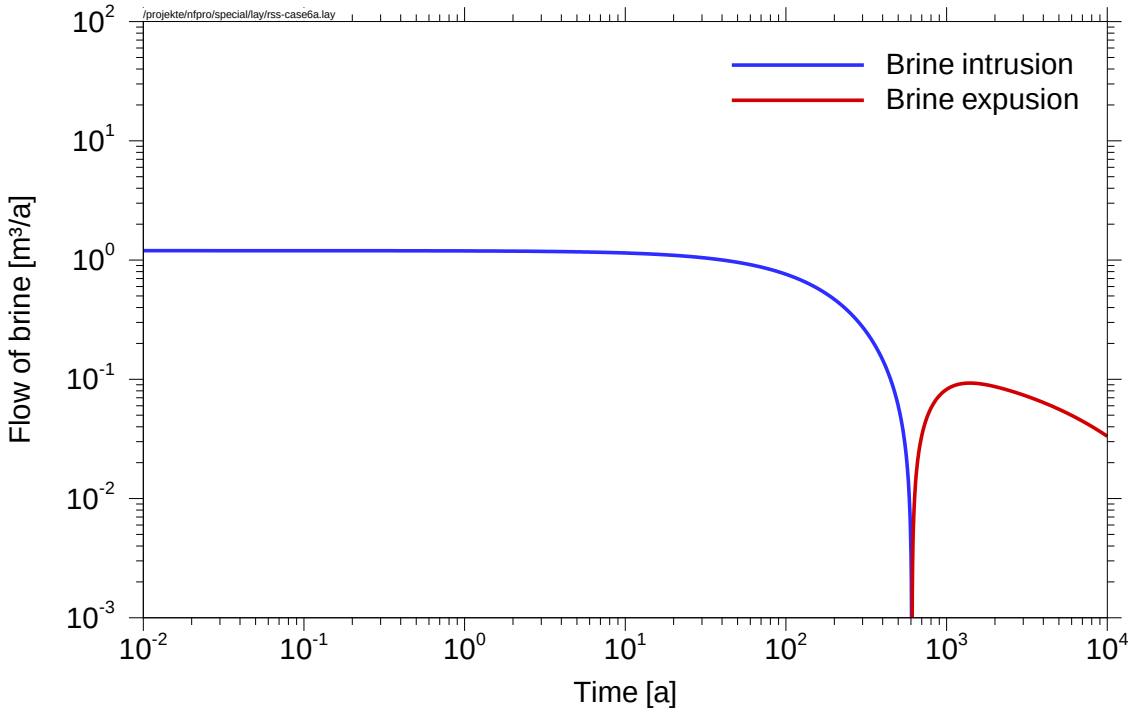

Fig. 2.24 Test case 6a: Flow of brine between disposal drift and charging drift

2.2.10 Test case 6b

Test case 6b corresponds of test case 5b, but the convergence of the salt formation is considered. Fig. 2.25 shows the time evolution of the volumes of the disposal drift, the pores, the brine, the gas in storage, the solid material in m^3 and of average porosity. In contrast to test case 5b, the total volume of the disposal drift changes by convergence.

Table 2.15 summarises the results of the calculation in terms of volume balances. The total volume is reduced by 645 m^3 after 10 000 a by convergence. Correspondingly smaller is the pore volume at the end of the simulation.

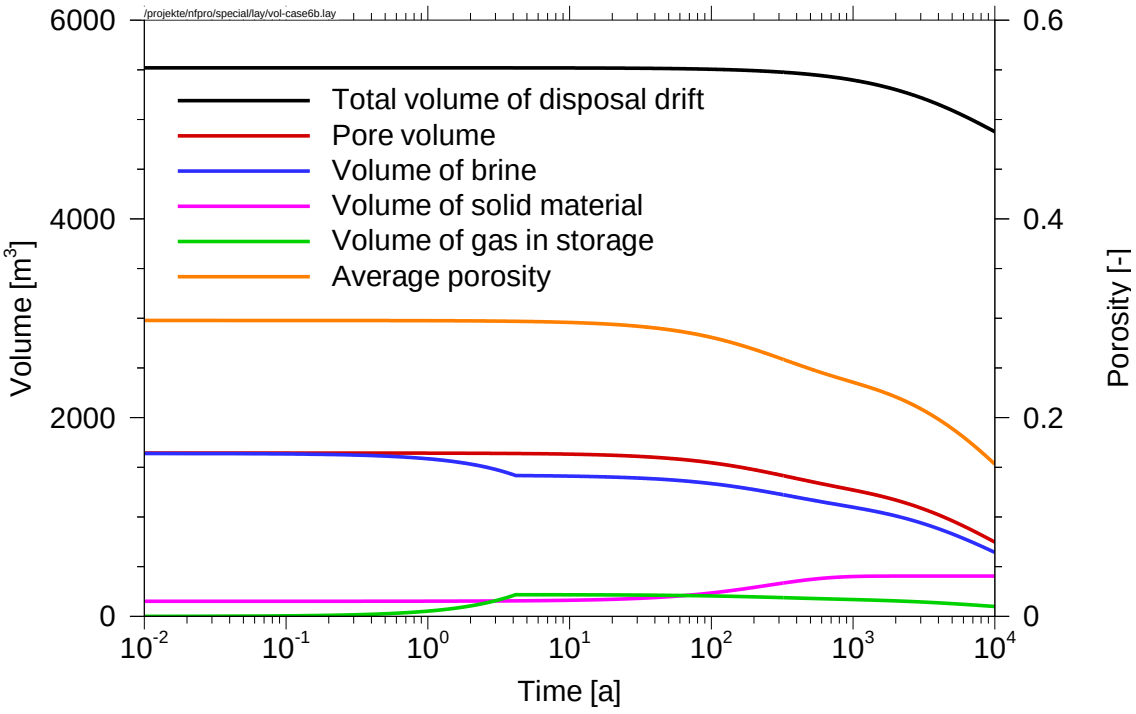

Fig. 2.25 Test case 6b: time evolution of volumes and porosity

Tab. 2.15 Results of test case 6b with gas storage

Time [a]	0.0	4	662	10 000
	Volume [m^3]			
Total volume of the disposal drift	5520	5519	5434	4875
Pore volume	1644	1639	1322	745.4
Volume of gas	5	218	176	99
Volume of brine	1639	1421	1146	646
Volume of brine squeezed out into the charging drift	0.00	209	209	667
Volume of brine replenished from the charging drift	0.00	0.00	264	264
Volume of brine used for corrosion		9	548	590
Increase of the volume of solid material		4	235	253
Volume of solid material	152	156	387	405

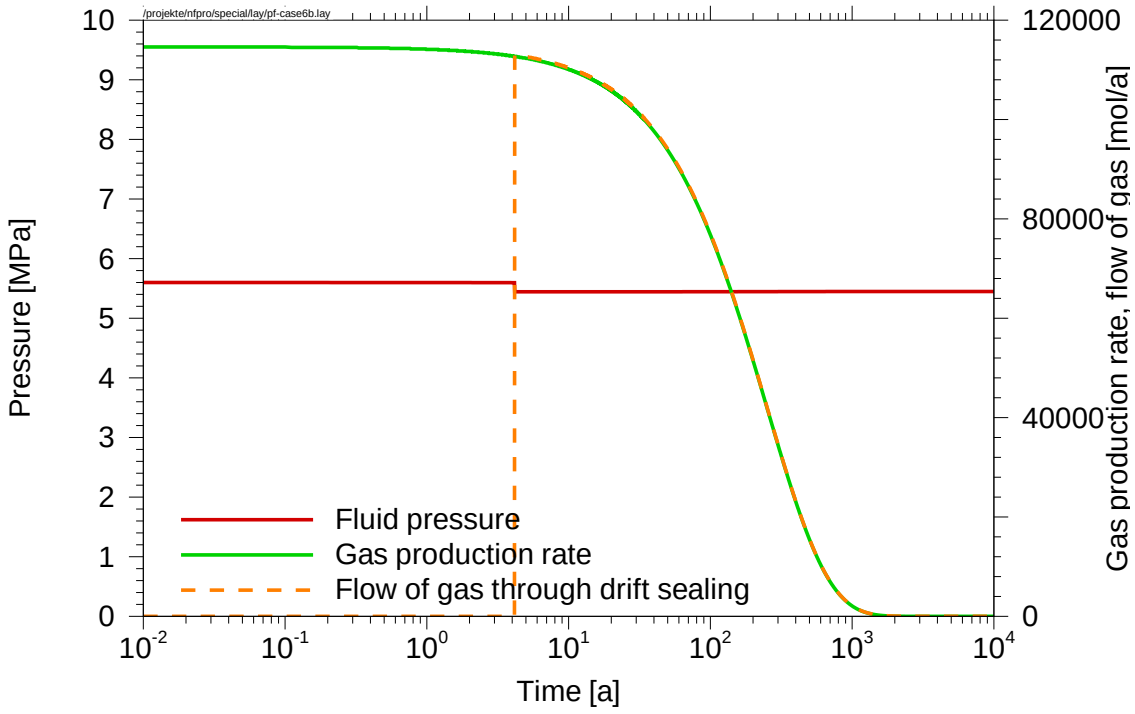

Fig. 2.26 Test case 6b: time evolution of fluid pressure and gas release

Fig. 2.26 shows the fluid pressure in the disposal drift in MPa, the gas production rate and the flow of gas out of the disposal drift in mol/a. After approximately 4 years, gas is released from the disposal drift because the gas-storage volume is replenished. The flow of gas is somewhat greater than the gas production rate due to increase of the volume of the solid material and convergence, which cause gas extrusion.

Fig. 2.27 shows the brine flow between the drifts in m^3/a. As long as the gas-storage volume is not completely filled, the displacement of brine by gas outbalances the water consumption. A brine flow from the disposal drift of about 53 m^3/a is observed. After replenishment of the gas-storage volume, the gas generated further can escape. The consumed water is replaced by inflowing brine from the charging drift of initially 1.3 m^3/a. Until replenishment of the gas storage, approximately 209 m^3 brine is squeezed out into the charging drift. After that, the water consumed by corrosion is replaced by inflowing brine from the charging drift. After approximately 662 to 10 000 a, about 667 m^3 brine is squeezed out of the disposal drift by convergence, i.e., significant less liquid is consumed by corrosion compared to what the reduction in pore volume can provide.

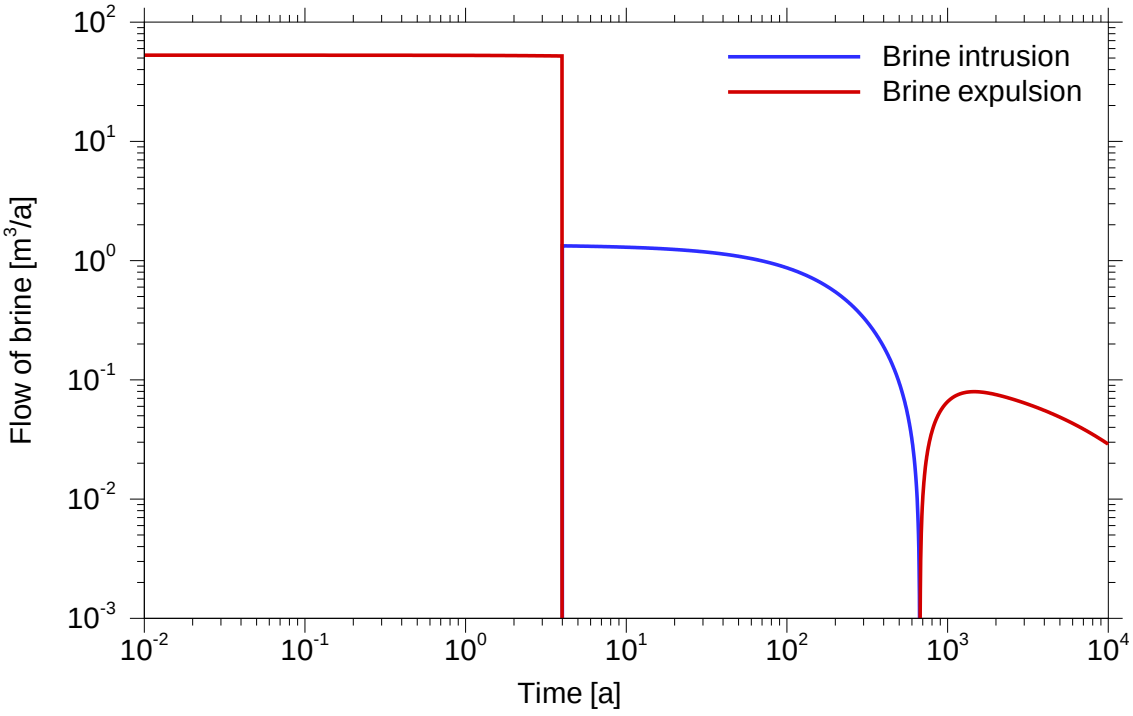

Fig. 2.27 Test case 6b: Flow of brine between disposal drift and charging drift

3 Model application to a more complex mine

In the following the near field module LOPOS of the EMOS code with the improved models of the disposal borehole and the disposal drift is applied to a more complex generic repository structure. This repository has all relevant components of a mine like drifts and disposal locations.

In general, with a intact shaft sealing with a permeability of at least 10^{-16} m^2 brine from the aquifer above the salt formation would need several thousand years to fill the infrastructure area. During this time the permeability of the backfilled drifts would decrease and it would be nearly impossible that brine enters the disposal drifts and boreholes. To study the behaviour of the disposal drifts and borehole during and after brine intrusion, thus, the shaft sealing failure scenario is investigated in the following. Here a permeability of the shaft sealing of 10^{-12} m^2 is assumed. Additionally, the permeability of drift sealings is increased to 10^{-15} m^2, each.

Time development of the pore volumes, the gas volumes and the volume of solid material in the disposal drifts and boreholes is calculated. Furthermore, the radionuclide release from the mine is calculated as radionuclide flow into the overburden and radionuclide exposition to men. The results are compared to those obtained under the assumption that no volume increase of metal and brine consumption would occur.

3.1 Input data

The model of the more complex mine and its division into segments is shown in Fig. 3.1, where CF represents the infrastructure area (central field), FD the flank drifts, CC the cross connections, CD the charging drifts, and DD the disposal drifts. The shaft and the disposal boreholes are perpendicular to the central field and to the charging drift, respectively. In a disposal drift 20 containers with spent fuel are disposed of, while a borehole (BH) takes 215 containers with vitrified waste.

Charging drift segments CD-M1, CD-M2 and CD-M3 represent 3 parallel drifts segments each, i.e. include the two neighbouring drift segments given in Fig. 3.1. Borehole segment BH-M1, thus, represents 3 boreholes, which are modelled as one borehole with a three

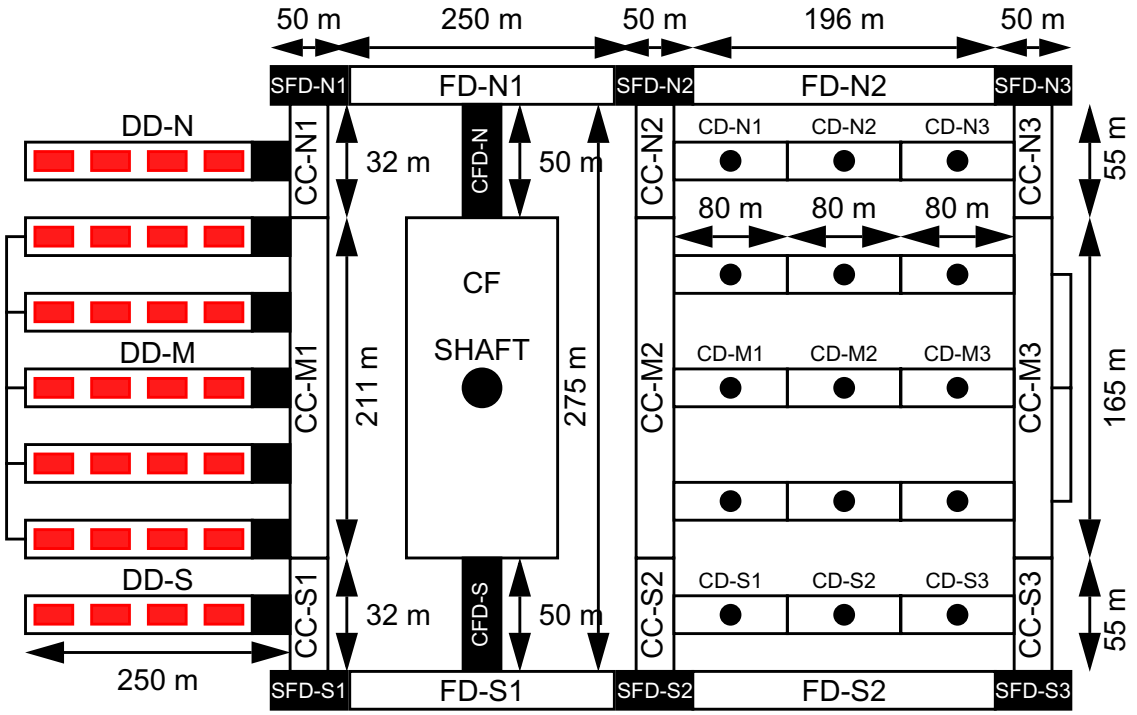

Fig. 3.1 Schematic representation of the mine

times larger cross section and three times more containers. The same holds for borehole segments BH-M2 and BH-M3. Disposal drift DD-M includes 4 neighbouring drifts and, thus, represents five disposal drifts with 100 containers in total.

Geometric data of the repository segments are listed in Tables 3.1, 3.2 and 3.3. General data used in models of physical and chemical effects, as far as not listed in Tables 2.1, 2.2 and 2.5, are given in Table 3.4.

Numbers of containers in disposal drifts and boreholes are given in Table 3.5. This Table also includes the mass of metal, the volume of the waste and the void volume in each container. The radionuclide inventory per container is listed in Table 3.6 and 3.7, respectively. Mobilisation models of radionuclides from vitrified waste (HLW) and from spent fuel (LWR) are the same as described in [2]. For simplicity, an instant container failure is assumed in all cases. Parameters of the waste mobilisation are given in Table 3.8. Inventory fractions of spent fuel are given in Table 3.9. Solubility limit of radionuclide in the disposal locations and other repository drifts are given in Table 3.10 and 3.11, respectively.

Tab. 3.1 Geometric data of the drift segments of the mine

Segment	Height [m]	Width [m]	Length [m]
SHAFT Sealing	6.65	6.65	50.00
CF infrastructure area	4.70	200.00	175.00
CFD-N dam north of CF	4.70	10.30	50.00
CFD-S dam south of CF	4.70	10.30	50.00
SFD-N1 flank drift sealing 1 north	4.70	10.30	50.00
SFD-N2 flank drift sealing 2 north	4.70	10.30	50.00
SFD-N3 flank drift sealing 3 north	4.70	10.30	50.00
SFD-S1 flank drift sealing 1 south	4.70	10.30	50.00
SFD-S2 flank drift sealing 2 south	4.70	10.30	50.00
SFD-S3 flank drift sealing 3 south	4.70	10.30	50.00
FD-N1 flank drift segment 1 north	4.70	10.30	250.00
FD-N2 flank drift segment 2 north	4.70	10.30	196.00
FD-S1 flank drift segment 1 south	4.70	10.30	250.00
FD-S2 flank drift segment 2 south	4.70	10.30	196.00
CC-N1 cross connection segment 1 north	4.70	6.00	32.00
CC-M1 cross connection mid segment 1	4.70	6.00	211.00
CC-S1 cross connection segment 1 south	4.70	6.00	32.00
CC-N2 cross connection segment 2 north	4.70	6.00	55.00
CC-M2 cross connection mid segment 2	4.70	6.00	165.00
CC-S2 cross connection segment 2 south	4.70	6.00	55.00
CC-N3 cross connection segment 3 north	4.70	6.00	55.00
CC-M3 cross connection mid segment 3	4.70	6.00	165.00
CC-S3 cross connection segment 3 south	4.70	6.00	55.00
CD-N1 charging drift north segment 1	4.70	6.00	80.00
CD-N2 charging drift north segment 2	4.70	6.00	80.00
CD-N3 charging drift north segment 3	4.70	6.00	80.00
CD-M1 charging drift mid segment 1	4.70	3×6.00	80.00
CD-M2 charging drift mid segment 2	4.70	3×6.00	80.00
CD-M3 charging drift mid segment 3	4.70	3×6.00	80.00
CD-S1 charging drift south segment 1	4.70	6.00	80.00
CD-S2 charging drift south segment 2	4.70	6.00	80.00
CD-S3 charging drift south segment 3	4.70	6.00	80.00

Tab. 3.2 Geometrical data of disposal drifts

Drift segment	Height [m]	Width [m]	Length [m]
DD-N disposal drift north	4.70	3.30	250.00
DD-N disposal drift middle	4.70	5×3.30	250.00
DD-N disposal drift south	4.70	3.30	250.00
Disposal drift sealings	4.70	3.30	15.00

Tab. 3.3 Geometrical data of disposal boreholes

Drift segment	Radius [m]	Length [m]
BH-N1 borehole 1 north	0.215	290.00
BH-N2 borehole 2 north	0.215	290.00
BH-N3 borehole 3 north	0.215	290.00
BH-M1 borehole 1 middle	$\sqrt{3} \times 0.215$	290.00
BH-M2 borehole 2 middle	$\sqrt{3} \times 0.215$	290.00
BH-M3 borehole 3 middle	$\sqrt{3} \times 0.215$	290.00
BH-S1 borehole 1 south	0.215	290.00
BH-S2 borehole 2 south	0.215	290.00
BH-S3 borehole 3 south	0.215	290.00
Borehole plugs north	0.215	10.00
Borehole plugs middle	$\sqrt{3} \times 0.215$	10.00
Borehole plugs south	0.215	10.00

To obtain a more convenient basis for comparing the different effects of the modified models of disposal boreholes and disposal drift the radionuclide exposure to men is shown. For this purpose transport though the geosphere and the biosphere to men is calculated. The radionuclide transport through the overburden is modelled as a 1-dimensional transport along a geosphere pathway. Data describing this pathway are listed in Table 3.12. Along the geosphere pathway sorption of radionuclides is considered. The sorption model uses Kd-concept with distribution coefficient given in Table 3.13.

Tab. 3.4 General data

Parameter	Dimension	Value
Reference level z_{ref}	m to surface	840
Rock pressure at reference level $p_{P,r}$	MPa	17.88
Hydrostatic pressure at reference level p_{hyd}	MPa	9.45
Permeability of shaft sealing	m^2	10^{-12}
Porosity of shaft sealing and dams	-	0.05
Permeability of dams and drift sealings	m^2	10^{-16}
Porosity of drift sealing	-	0.10
Initial porosity of backfill	-	0.30
Initial porosity of disposal drift sealing	-	0.30
Initial porosity of borehole plug	-	0.30
Fraction of gas storage f_{Gas} in disposal drift	% of the pore volume	13.3
Fraction of gas storage f_{Gas} in disposal boreholes	% of the pore volume	45.0
Diffusion coefficient	m^2/a	$3.1 \cdot 10^{-17}$
Dispersion length	m	5.0

Tab. 3.5 Waste and container specific data

	Disposal borehole	Disposal drift
Waste container	HLW canister	LWR POLLUX container
Number of containers per borehole or drift	215	20
Total volume of a container [m^3]	0.18	10.20
Void volume in a container [m^3]	0.03	0.766
Mass of metal (steel) [kg]	80.0	58 540
Mass of glass matrix [kg]	435.0	-

Tab. 3.6 Radionuclide inventory per HLW-container

Radionuclide	Inventory [Bq]	Radionuclide	Inventory [Bq]
^{14}C	-	^{248}Cm	$1.101 \cdot 10^{+05}$
^{60}Co	$3.322 \cdot 10^{+13}$	^{244}Pu	$1.119 \cdot 10^{+02}$
^{59}Ni	$7.000 \cdot 10^{+07}$	^{244}Cm	$1.126 \cdot 10^{+14}$
^{63}Ni	$9.504 \cdot 10^{+09}$	^{240}Pu	$7.611 \cdot 10^{+10}$
^{79}Se	$1.715 \cdot 10^{+10}$	^{236}U	$6.630 \cdot 10^{+07}$
^{87}Rb	$1.070 \cdot 10^{+06}$	^{232}Th	$5.652 \cdot 10^{+00}$
^{90}Sr	$3.232 \cdot 10^{+15}$	^{232}U	$1.109 \cdot 10^{+07}$
^{93}Zr	$8.928 \cdot 10^{+10}$	^{245}Cm	$1.105 \cdot 10^{+10}$
^{93}Mo	$6.467 \cdot 10^{+06}$	^{241}Pu	$1.273 \cdot 10^{+13}$
^{94}Nb	$8.182 \cdot 10^{+06}$	^{241}Am	$6.204 \cdot 10^{+13}$
^{99}Tc	$6.186 \cdot 10^{+11}$	^{237}Np	$1.662 \cdot 10^{+10}$
^{107}Pd	$4.647 \cdot 10^{+09}$	^{233}U	$1.834 \cdot 10^{+04}$
^{126}Sn	$2.427 \cdot 10^{+10}$	^{229}Th	$6.629 \cdot 10^{+03}$
^{129}I	$1.647 \cdot 10^{+04}$	^{246}Cm	$2.273 \cdot 10^{+10}$
^{135}Cs	$1.621 \cdot 10^{+10}$	^{242}Pu	$3.080 \cdot 10^{+08}$
^{137}Cs	$4.669 \cdot 10^{+15}$	^{242}Am	$1.547 \cdot 10^{+11}$
^{147}Sm	$2.221 \cdot 10^{+05}$	^{238}U	$6.673 \cdot 10^{+07}$
^{151}Sm	$1.525 \cdot 10^{+13}$	^{238}Pu	$4.277 \cdot 10^{+11}$
^{154}Eu	$3.898 \cdot 10^{+14}$	^{234}U	$2.102 \cdot 10^{+08}$
		^{230}Th	$3.166 \cdot 10^{+06}$
		^{226}Ra	$6.247 \cdot 10^{+03}$
		^{247}Cm	$4.215 \cdot 10^{+04}$
		^{253}Am	$1.054 \cdot 10^{+12}$
		^{239}Pu	$4.544 \cdot 10^{+10}$
		^{235}U	$3.506 \cdot 10^{+06}$
		^{231}Pa	$1.220 \cdot 10^{+06}$

Tab. 3.7 Radionuclide inventory per LWR-container

Radionuclide	Inventory [Bq]	Radionuclide	Inventory [Bq]
^{14}C	$1.964 \cdot 10^{+11}$	^{248}Cm	$1.243 \cdot 10^{+06}$
^{60}Co	$1.739 \cdot 10^{+15}$	^{244}Pu	$1.853 \cdot 10^{+05}$
^{59}Ni	$2.170 \cdot 10^{+12}$	^{244}Cm	$7.074 \cdot 10^{+14}$
^{63}Ni	$2.920 \cdot 10^{+14}$	^{240}Pu	$1.027 \cdot 10^{+14}$
^{79}Se	$7.870 \cdot 10^{+10}$	^{236}U	$5.101 \cdot 10^{+10}$
^{87}Rb	$4.340 \cdot 10^{+06}$	^{232}Th	$2.323 \cdot 10^{+01}$
^{90}Sr	$1.300 \cdot 10^{+16}$	^{232}U	$1.083 \cdot 10^{+10}$
^{93}Zr	$4.155 \cdot 10^{+11}$	^{245}Cm	$7.271 \cdot 10^{+10}$
^{93}Mo	$1.803 \cdot 10^{+10}$	^{241}Pu	$1.758 \cdot 10^{+16}$
^{94}Nb	$3.630 \cdot 10^{+11}$	^{241}Am	$2.609 \cdot 10^{+14}$
^{99}Tc	$2.683 \cdot 10^{+12}$	^{237}Np	$7.156 \cdot 10^{+10}$
^{107}Pd	$2.374 \cdot 10^{+10}$	^{233}U	$1.326 \cdot 10^{+07}$
^{126}Sn	$1.228 \cdot 10^{+11}$	^{229}Th	$4.169 \cdot 10^{+04}$
^{129}I	$6.835 \cdot 10^{+09}$	^{246}Cm	$1.816 \cdot 10^{+11}$
^{135}Cs	$7.647 \cdot 10^{+10}$	^{242}Pu	$4.926 \cdot 10^{+11}$
^{137}Cs	$1.935 \cdot 10^{+16}$	^{242}Am	$7.912 \cdot 10^{+11}$
^{147}Sm	$8.590 \cdot 10^{+05}$	^{238}U	$4.943 \cdot 10^{+10}$
^{151}Sm	$5.947 \cdot 10^{+13}$	^{238}Pu	$7.143 \cdot 10^{+14}$
^{154}Eu	$1.723 \cdot 10^{+15}$	^{234}U	$1.471 \cdot 10^{+11}$
		^{230}Th	$1.136 \cdot 10^{+07}$
		^{226}Ra	$2.422 \cdot 10^{+04}$
		^{247}Cm	$3.989 \cdot 10^{+05}$
		^{253}Am	$5.673 \cdot 10^{+12}$
		^{239}Pu	$5.669 \cdot 10^{+13}$
		^{235}U	$2.070 \cdot 10^{+09}$
		^{231}Pa	$5.605 \cdot 10^{+06}$

Tab. 3.8 Parameters of the mobilisation models

Parameter	Vitrified waste (HLW)	Spent fuel (LWR)
Reaction rate glass matrix [kg/(a m^2)]	0.365	-
Surface of waste matrix [m^2]	16.5	-
Activation energy [kJ/mol]	75.0	-
Mobilisation rate metal [1/a]	-	$3.6 \cdot 10^{-3}$
Mobilisation rate waste matrix [1/a]	-	$1.0 \cdot 10^{-6}$

Tab. 3.9 Inventory fractions of spent fuel

Element	Instant release fraction	Metal	Matrix	Element	Instant release fraction	Metal	Matrix
Am	0.0001	0.0000	0.9999	Pa	0.0001	0.0000	0.9999
C	0.0139	0.7220	0.2641	Pu	0.0001	0.0000	0.9999
Cm	0.0001	0.0000	0.9999	Ra	0.0001	0.0000	0.9999
Co	0.00025	0.9950	0.00475	Se	0.0300	0.0000	0.9700
Cs	0.0400	0.0000	0.9600	Sm	0.0100	0.0000	0.9900
Eu	0.0100	0.0000	0.9900	Sn	0.0200	0.0000	0.9800
I	0.0300	0.0000	0.9700	Sr	0.0010	0.0000	0.9990
Mo	0.00025	0.9950	0.00475	Tc	0.0001	0.0010	0.9989
Nb	0.00025	0.9950	0.00475	Th	0.0001	0.0000	0.9999
Ni	0.00025	0.9950	0.00475	U	0.0001	0.0000	0.9999
Np	0.0001	0.0000	0.9999	Zr	0.0453	0.0940	0.8607

Tab. 3.10 Solubility limits in the repository, disposal segments

Element	Solubility limit [mol/m^3]	Element	Solubility limit [mol/m^3]
Am	$1.0 \cdot 10^{-1}$	Pa	$1.0 \cdot 10^{-3}$
C	$1.0 \cdot 10^{+3}$	Pu	$1.0 \cdot 10^{-3}$
Cm	$1.0 \cdot 10^{-1}$	Ra	$1.0 \cdot 10^{-2}$
Co	$1.0 \cdot 10^{+1}$	Se	$1.0 \cdot 10^{-1}$
Cs	$1.0 \cdot 10^{+3}$	Sm	$1.0 \cdot 10^{+1}$
Eu	$1.0 \cdot 10^{+1}$	Sn	$1.0 \cdot 10^{+1}$
I	$1.0 \cdot 10^{+3}$	Sr	$1.0 \cdot 10^{+0}$
Mo	$1.0 \cdot 10^{+1}$	Tc	$1.0 \cdot 10^{-1}$
Nb	$1.0 \cdot 10^{+1}$	Th	$1.0 \cdot 10^{-3}$
Ni	$1.0 \cdot 10^{+1}$	U	$1.0 \cdot 10^{-1}$
Np	$1.0 \cdot 10^{-2}$	Zr	$1.0 \cdot 10^{-3}$

Tab. 3.11 Solubility limits in the repository, other segments

Element	Solubility limit [mol/m^3]	Element	Solubility limit [mol/m^3]
Am	$1.0 \cdot 10^{-2}$	Pa	$1.0 \cdot 10^{-4}$
C	$1.0 \cdot 10^{-1}$	Pu	$1.0 \cdot 10^{-4}$
Cm	$1.0 \cdot 10^{-2}$	Ra	$1.0 \cdot 10^{-2}$
Co	$1.0 \cdot 10^{-1}$	Se	$1.0 \cdot 10^{-1}$
Cs	$1.0 \cdot 10^{+3}$	Sm	$1.0 \cdot 10^{-1}$
Eu	$1.0 \cdot 10^{-1}$	Sn	$1.0 \cdot 10^{-1}$
I	$1.0 \cdot 10^{+3}$	Sr	$1.0 \cdot 10^{+0}$
Mo	$1.0 \cdot 10^{-1}$	Tc	$1.0 \cdot 10^{-1}$
Nb	$1.0 \cdot 10^{-1}$	Th	$1.0 \cdot 10^{-4}$
Ni	$1.0 \cdot 10^{-1}$	U	$1.0 \cdot 10^{-1}$
Np	$1.0 \cdot 10^{-3}$	Zr	$1.0 \cdot 10^{-4}$

Tab. 3.12 Data of the geosphere pathway

Parameter	Dimension	Value
Length of the pathway	m	9 394
Cross section of the pathway	m^2	36 900
Groundwater flow	m^3/a	48 000
Rock density	kg/m^3	2 500
Diffusion constant	m^2/a	10^{-20}
Dispersion length	m	65.0

Tab. 3.13 Distribution coefficients K_d at geosphere pathway

Element	K_d value [m^3/kg]	Element	K_d value [m^3/kg]
Ac	$4.0 \cdot 10^{-2}$	Pb	$1.0 \cdot 10^{+0}$
Am	$1.0 \cdot 10^{+0}$	Po	$1.0 \cdot 10^{+0}$
C	$5.0 \cdot 10^{-3}$	Pu	$1.0 \cdot 10^{+0}$
Cl	$1.0 \cdot 10^{+0}$	Ra	$9.0 \cdot 10^{-4}$
Cm	$1.0 \cdot 10^{+0}$	Se	$3.0 \cdot 10^{-4}$
Cs	$1.0 \cdot 10^{-3}$	Sm	$1.0 \cdot 10^{+0}$
I	$5.0 \cdot 10^{-4}$	Sn	$2.0 \cdot 10^{-1}$
Mo	$1.0 \cdot 10^{-3}$	Sr	$5.0 \cdot 10^{-4}$
Nb	$1.0 \cdot 10^{-1}$	Tc	$7.0 \cdot 10^{-3}$
Ni	$1.0 \cdot 10^{-2}$	Th	$3.0 \cdot 10^{-1}$
Np	$3.0 \cdot 10^{-2}$	U	$2.0 \cdot 10^{-3}$
Pa	$1.0 \cdot 10^{+0}$	Zr	$1.0 \cdot 10^{-1}$

3.2 Results

The program package EMOS with its near field, far field and biosphere modules is used to calculated the release rates of radionuclides from the repository mine, their transport through the overburden and the radiation exposure to men, taking into account the different biosphere pathways by using dose conversion factors. The calculation is performed in two ways:

- First the volume increase of solid material and the water consumption during metal corrosion is considered. This case is called the reference case.
- Second, the volume increase of solid material and the water consumption is neglected. This case is called the comparison variant.

Fig. 3.2 shows the brine flow through the shaft of the mine. Here, negative flow means intruding brine while a positive flow shows that brine is extruded from the mine. The infrastructure area CF is already filled after about 0,37 a. This results from the very low flow resistance of the shaft sealing assumed for the considered scenario of shaft sealing failure. Whenever another segment of the mine is filled with brine the flow resistance for the intruding brine increases. This increase is shown by a stepwise reduction of the brine flow into the mine. In the present LOPOS code this is a model artifact, instead of a continuous increase of the flow resistance during brine intrusion, the complete resistance of a repository segment is added whenever a segment is filled with brine. This model artifact will be deleted during the PAMINA project in WP 4.1.

At that moment, when the mine is filled, the sudden increase of the hydrostatic pressure yields a compaction of the gas stored in the boreholes and drifts. The following refill of the gas storage and the extrusion of the brine is responsible for the peaks of the brine flow through the shaft at 89a and 138 a in the reference case and 85 a and 135 a in the comparison variant, shown in Fig. 3.2.

In the reference case brine is consumed by metal corrosion. Therefore, the fill-up of the mine is delayed by about 3 a compared to the variant with no brine consumption. Additionally, a small negative flow, i.e. a flow into the mine, occurs for about 60 a, showing that brine consumption in the disposal segments is still going on in the reference case, while in the comparison variant a continuous brine release from the mine can be observed.

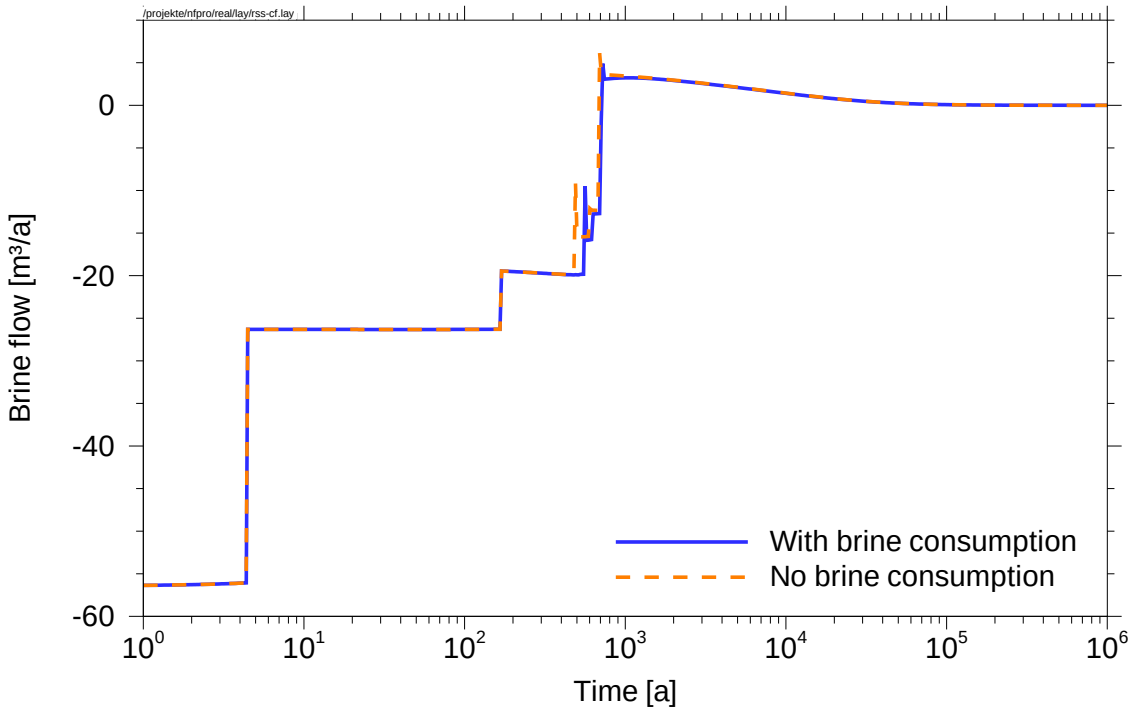

Fig. 3.2 Brine flow through the shaft

Figs. 3.3 to 3.6 show the time evolution of the pore volume and volumes of brine, gas and solid material in a representative borehole (BH-N1) and a representative drift (DD-N) for both, the reference case and the comparison variant. In the reference case the borehole is filled with brine at t = 26.9 a, only 0.6 a later than in the comparison variant. However, the time span during which the brine volume increased is shorter since at the beginning all the brine which enters the borehole is consumed by metal corrosion.

Due to the much greater pore volume and the greater amount of metal the delay in filling the segments is more pronounced in the disposal drift. In the reference case the disposal drift DD-N is filled at t = 83.2 a, while in the comparison variant the disposal drift DD-N is filled at t = 79.4 a. The amount of brine, which the disposal drift can take, is 698 m^3 in the reference case and 747 m^3 in the comparison variant. The smaller amount of brine result from the volume increase of the solid material, but also from the continuing faster convergence during the delay of about four years, before brine pressure rises to the hydrostatic value corresponding to the depth of the mine.

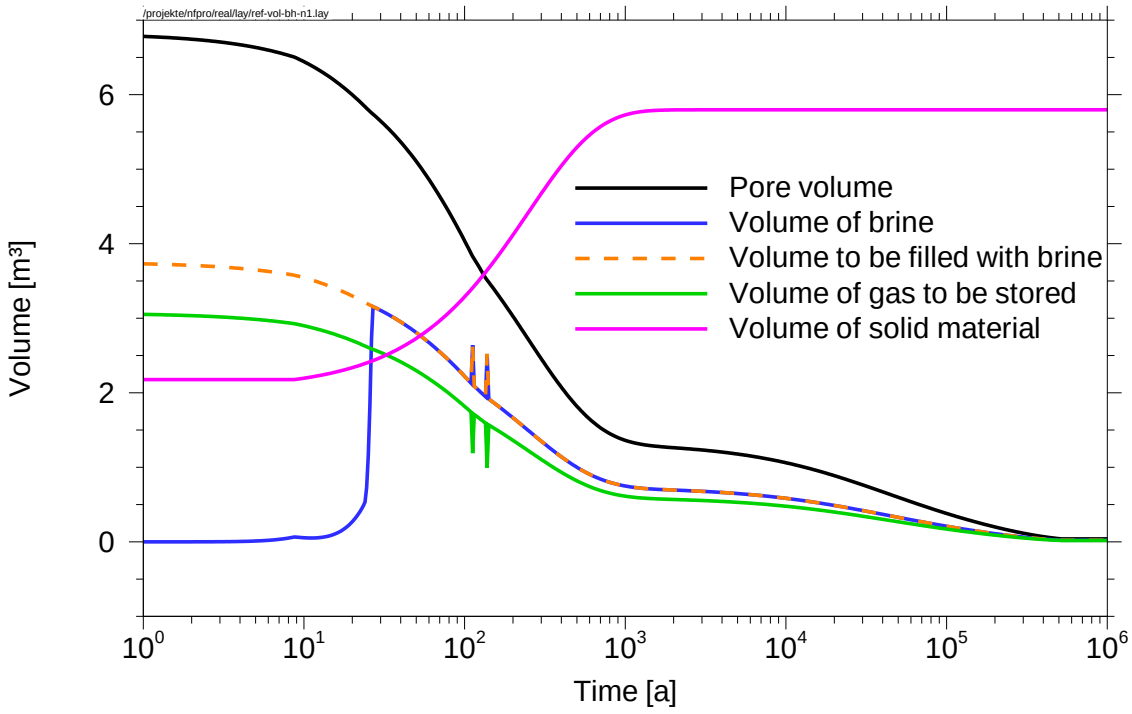

Fig. 3.3 Reference case: time evolution of volumes of BH-N1

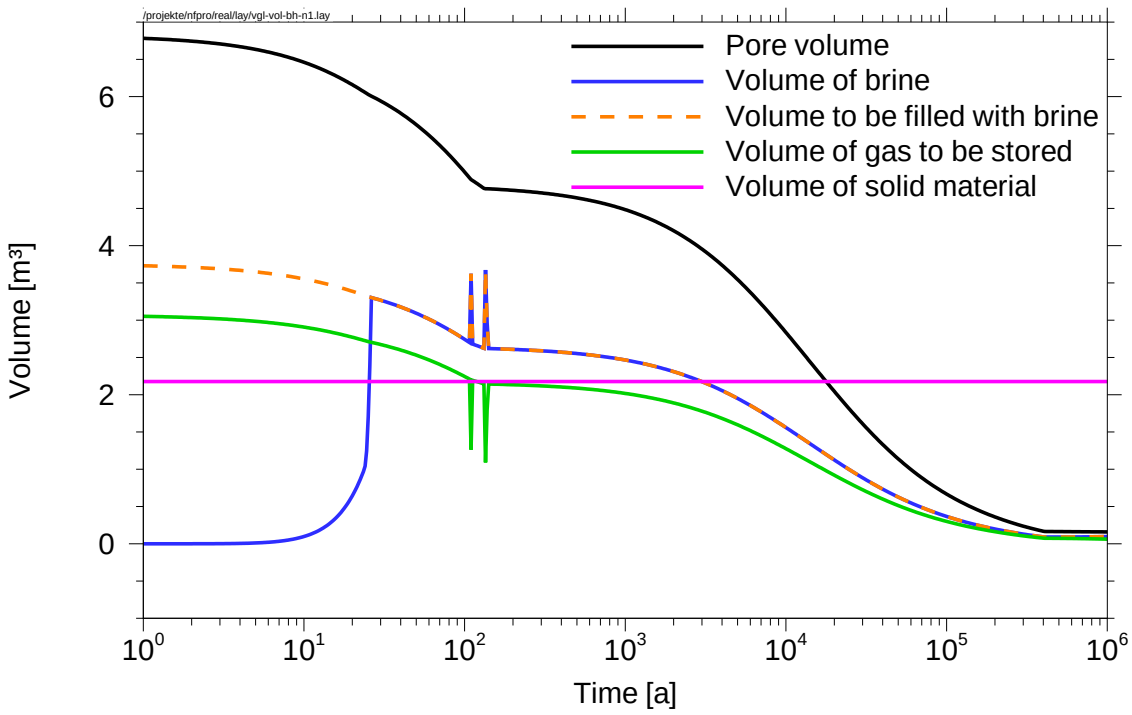

Fig. 3.4 Comparison variant: time evolution of volumes of BH-N1

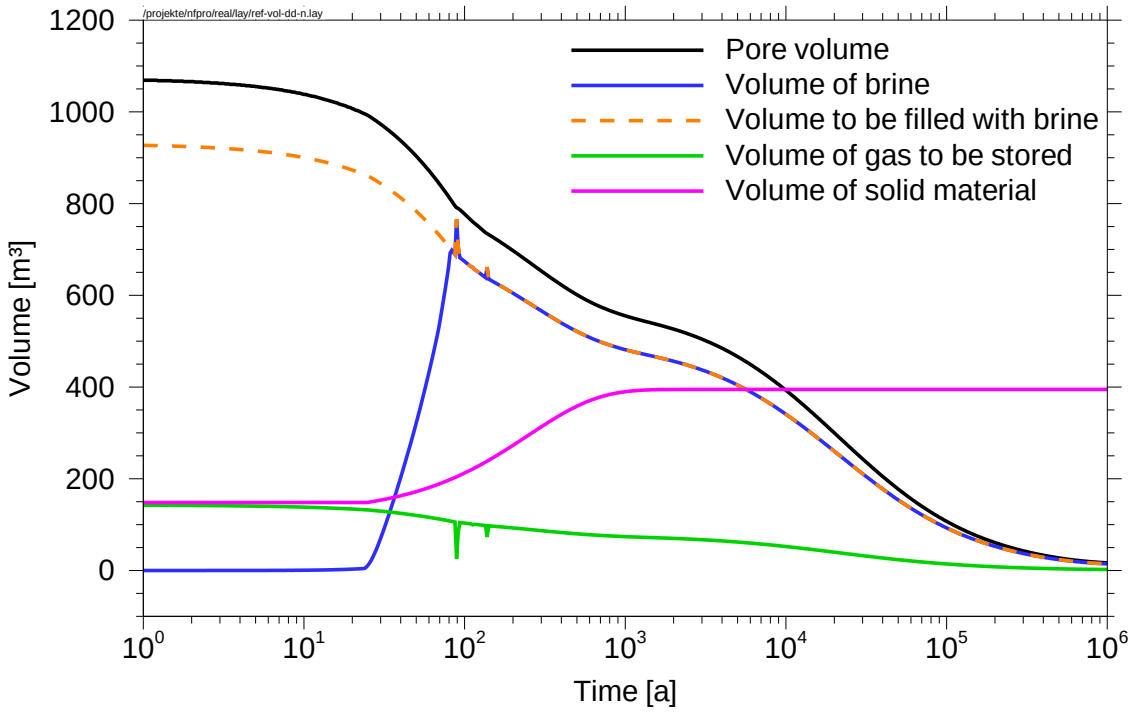

Fig. 3.5 Reference case: time evolution of volumes of DD-N

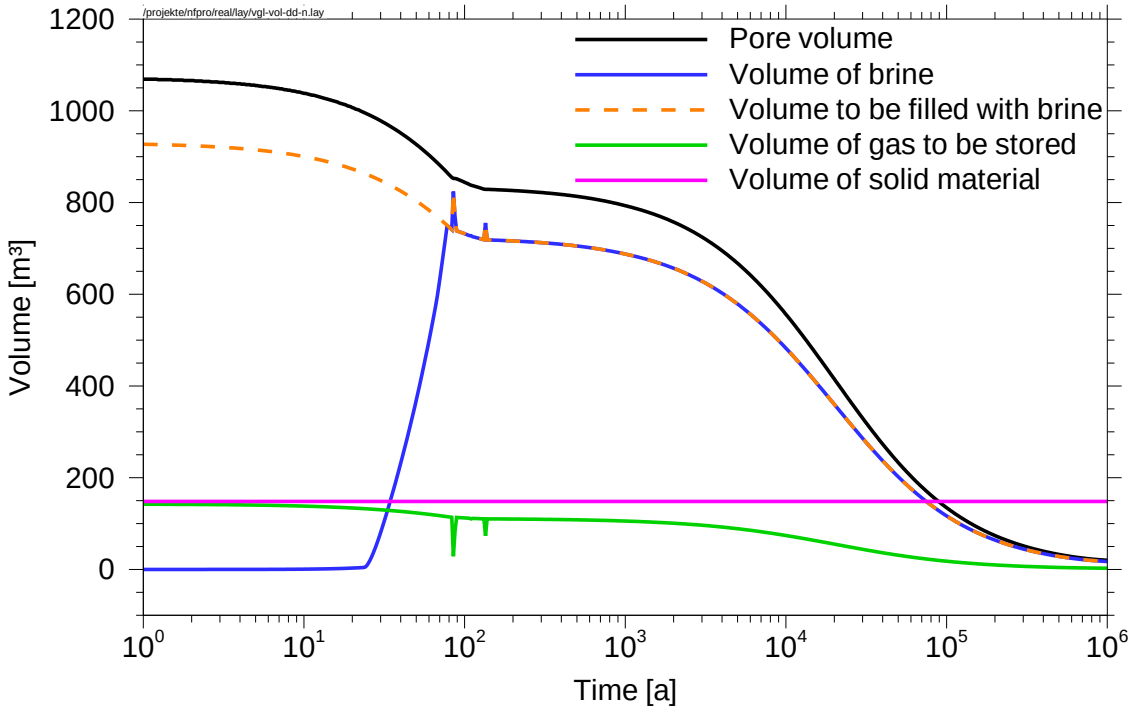

Fig. 3.6 Comparison variant: time evolution of volumes of DD-N

The peaks in gas and brine volumes reflect the compression of gas and the refill of the segments when the fluid pressure increases. Figs. 3.3 and 3.5 also show the increase of the volume of solid material by the increase factor g_c of 2.668 (cf. Table 2.2), almost completed during the first 1000 a.

Fig. 3.7 shows the radionuclide flow of some release relevant fission and activation products leaving the mine. The radionuclide flow is dominated by the release of ^{59}Ni. At late times the maximum contribution results from ^{79}Se. Comparison between the reference case and the variant reflects the delay of brine extrusion from the disposal locations by a later release of radionuclide in the reference case and a decline of the flow maxima.

Fig. 3.8 shows the radionuclide flow of some release-relevant radionuclides from the decay chains leaving the mine. At times smaller than 20 000 a the flow is dominated by the Cm isotopes while at later times the main contribution comes from ^{233}U and ^{237}Np. Comparison between the reference case and the variant again reflects the delay of brine extrusion from the disposal locations by a later release of radionuclides in the reference case and a decline of the flow maxima.

However, the maxima of ^{79}Se and ^{246}Cm, shown in the figures, are higher in the reference case. These radionuclides have a relative small inventory in a disposal drifts which is of the same order of magnitude as that in a disposal borehole. This clearly shows, that the delay in release is mainly due to the delay of brine extrusion from the disposal drifts.

In Fig. 3.9 the annual exposure to men is shown for the reference case as well as for the comparison variant. Here, the reference case gives an increase of radiation exposure clearly delayed more than 1500 a. The maximum exposure, however, lies at $2.1 \cdot 10^{-4}$ Sv/a at about 46 000 a in the reference case, while in the comparison variant the maximum is shifted to about 57 000 a but the maximum value of $2.2 \cdot 10^{-4}$ Sv/a is almost unchanged.

For completeness, Fig. 3.10 gives the contribution of the most relevant radionuclides to the annual exposure for the reference case as well as for the comparison variant. Here, at the beginning the exposure is made by ^{79}Se in both cases.The maximum is made by ^{135}Cs, which is higher in the reference case. However, the comparison variant shows a larger contribution from ^{226}Ra, which is responsible for the shift and increase of the maximum exposure in the comparison variant.

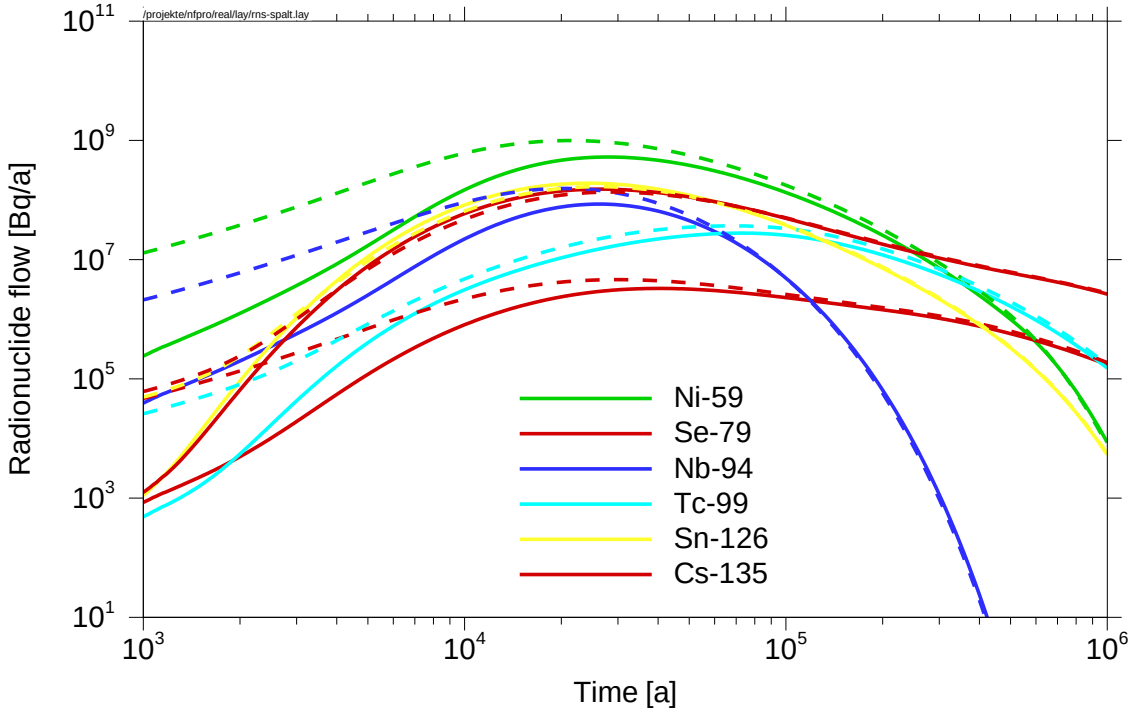

Fig. 3.7 Radionuclide flow through the shaft (solid: reference, dashed: variant)

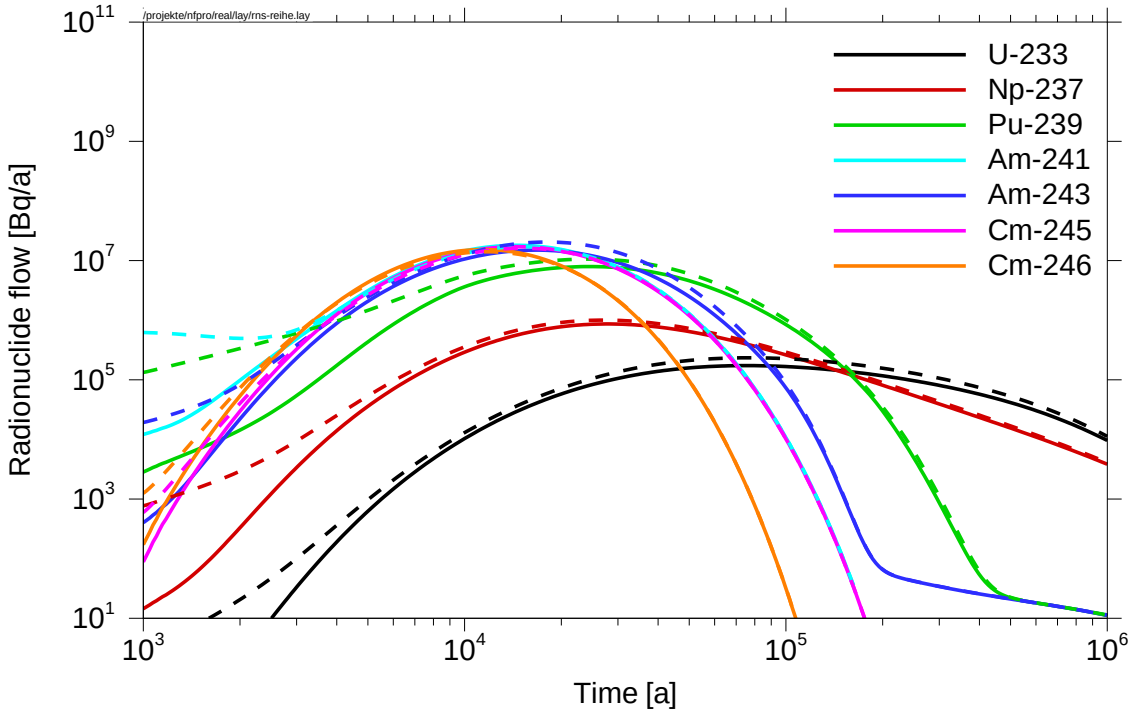

Fig. 3.8 Radionuclide flow through the shaft (solid: reference, dashed: variant)

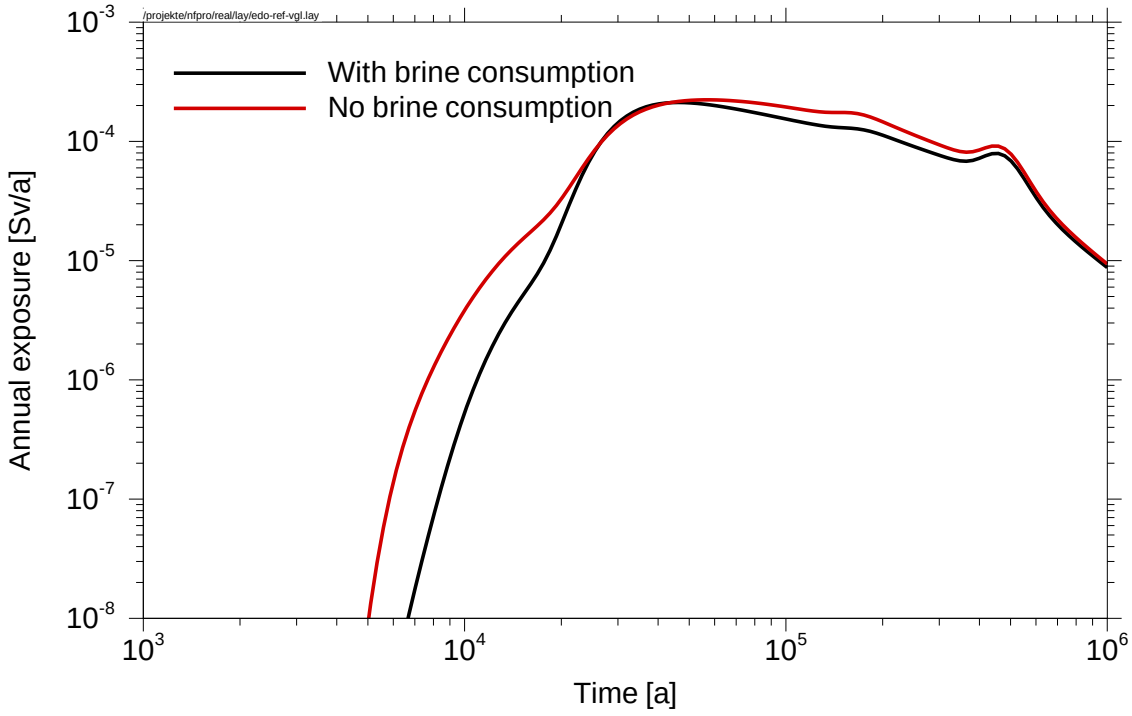

Fig. 3.9 Comparison of the annual exposure

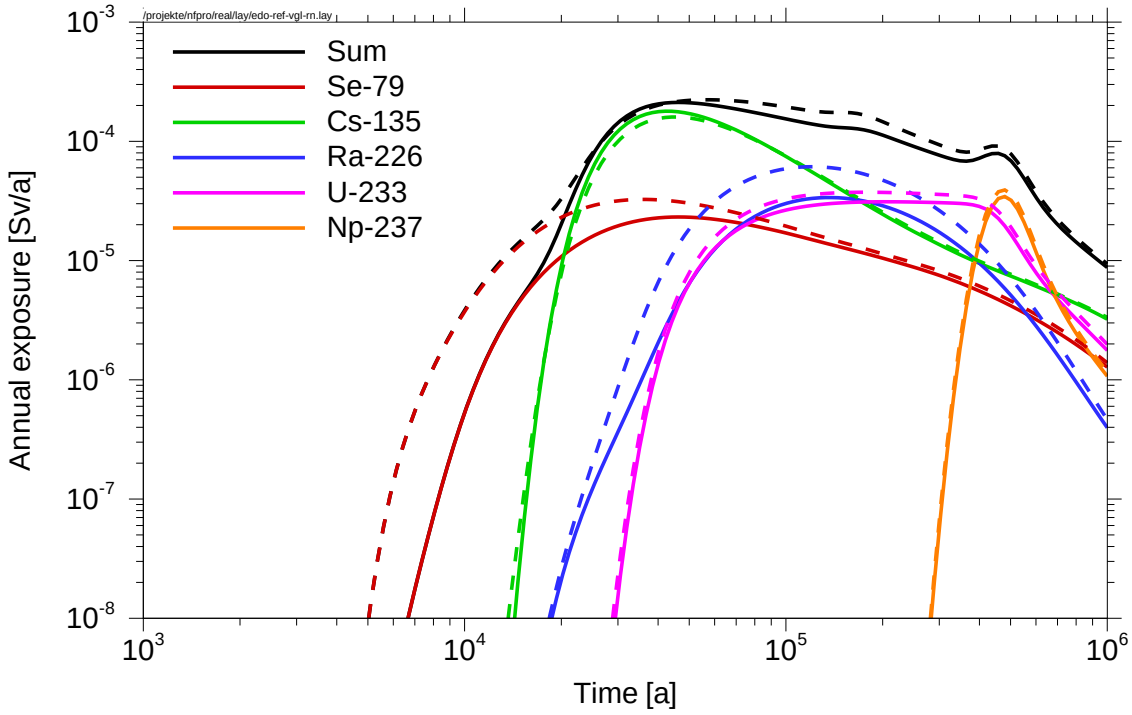

Fig. 3.10 Contribution of relevant radionuclides to the annual exposure (solid: reference, dashed: variant)

4 Summary

It could be shown that the modifications of the models of disposal segments work correctly. Brine consumption yields a time delay with respect to filling up the disposal segments and thus a later release of brine and radionuclides from disposal locations.

Additionally, there is a reduction of maximum amount of brine which the disposal locations can take. This is, on one hand, related to the pore volume reduction due to volume increase of solid material, on the other hand by the ongoing faster convergence due to time delay of the fill-up phase of the mine and, hence, a somewhat later pressure increase. This smaller volume of brine may also have influence on the radionuclide concentration in the disposal locations, if there is low solubility of the respective radionuclide. This effect is expected to take place in boreholes where one has a rather small pore volume from the beginning.

The effect time delay is more pronounced in disposal drifts where one has a larger amount of metal, but also more pore volume. Thus, the volume increase of solid material and the large amount of brine consumed during corrosion have a stronger delay in brine and radionuclide release. Therefore, radionuclide with a high inventory in disposal drift show a more pronounced effect on release.

In general, taking into account the volume increase of solid material and the brine consumption during corrosion has a benefit on the isolation potential of the repository. However, not the increase of solid material but rather the brine consumption is responsible for this effect.

5 References

[1] Noseck, U.; et al.: Wissenschaftliche Grundlagen zum Nachweis der Langzeitsicherheit von Endlagern. Gesellschaft für Anlagen- und Reaktorsicherheit (GRS) mbH, GRS-204, Braunschweig, Juli 2005

[2] Hirsekorn, R.-P.; et al.: LOPOS: Programm zur Berechnung der Schadstofffreisetzung aus netzwerkartigen Grubengebäuden. Gesellschaft für Anlagen- und Reaktorsicherheit (GRS) mbH, GRS-157, Braunschweig, Juni 1999

Appendix: Numerical method

To make the system of equations more easy to survey, the following substitutions are made:

$$x_i = 1 - \frac{p_i(z)}{p_{P,r}}, \qquad (5.1)$$

$$A_{i,j} = R_{i,j}^{-1} \cdot p_{P,r}, \qquad (5.2)$$

$$p_P(z_i) = p_{P,r} - \Delta z_i \cdot \rho_S \cdot g. \qquad (5.3)$$

Moreover, for the pressure function [1] holds

$$f_p(p_i) = \left(\frac{p_P(z_i) - p_i(z_i)}{p_{P,r}} \right)^m. \qquad (5.4)$$

Using the above equations, individual terms in eq. 2.37 can be rearranged to

$$f_p(p_i) = \left(1 - \frac{p_i}{p_{P,r}} - \frac{\Delta z_i \cdot \rho_S \cdot g}{p_{P,r}} \right)^m = \left(x_i - \frac{\Delta z_i \cdot \rho_S \cdot g}{p_{P,r}} \right)^m, \qquad (5.5)$$

$$\frac{\dot{p}_i(t) / p_{P,r}}{(p_i(t) / p_{P,r})^2} = -\frac{\mathrm{d}}{\mathrm{d}t}\left(\frac{p_{P,r}}{p_i(t)} \right) \Rightarrow \frac{-1}{\Delta t} \cdot \left(\frac{p_{P,r}}{p_i(t)} - \frac{p_{P,r}}{p_i(t - \Delta t)} \right). \qquad (5.6)$$

With the additional substitutions

$$x_i^0 = 1 - \frac{p(t - \Delta t)}{p_{P,r}}, \qquad (5.7)$$

$$\Theta_i = \frac{\Delta z_i \cdot \rho_S \cdot g}{p_{P,r}} \qquad (5.8)$$

finally the following system of equations results

$$\beta_i \cdot (x_i - \Theta_i)^m + \sum_j A_{i,j} \cdot (x_i - x_j - \Delta_{i,j} \cdot \rho_L \cdot g) \qquad (5.9)$$
$$-(\Omega_{L,i} - \Omega_{F,i}) \cdot \dot{n}_{G,i} + \frac{\tilde{\gamma}_i}{1 - x_i} + \frac{\tilde{\delta}_i}{\Delta t} \cdot \frac{x_i - x_0}{(1 - x_i) \cdot (1 - x_i^0)} = 0 = F_i .$$

This system of nonlinear equations is solved by Newton method at any time *t*. The iterative solution of

$$F_i([x_l]) = 0 \qquad (5.10)$$

provides

$$x_i^{(n+1)} = x_i^{(n)} - D_{i,k}^{-1}([x_l^{(n)}]) \cdot F_k([x_l^{(n)}]) \qquad (5.11)$$

with

$$D_{i,k}([x_l]) = \frac{\partial}{\partial x_i} F_k([x_l]) \qquad (5.12)$$

where $F_k([x_l])$ is given in equation 5.9 and $x_i^{(n)}$ describes the results of the *n*-iteration.

List of Figures

List of Tables

Gesellschaft für Anlagen- und Reaktorsicherheit (GRS) mbH

Schwertnergasse 1
50667 Köln
Telefon +49 221 2068-0
Telefax +49 221 2068-888

Forschungsinstitute
85748 Garching b. München
Telefon +49 89 32004-0
Telefax +49 89 32004-300

Kurfürstendamm 200
10719 Berlin
Telefon +49 30 88589-0
Telefax +49 30 88589-111

Theodor-Heuss-Straße 4
38122 Braunschweig
Telefon +49 531 8012-0
Telefax +49 531 8012-200

www.grs.de

ISBN 978-3-939355-06-9